Design and Analysis of Heteronunlear Dipolar Decoupling Schemes in Solid-State Nuclear Magnetic Resonance

A Thesis

Submitted to the
Tata Institute of Fundamental Research, Mumbai
for the degree of Doctor of Philosophy
in Chemistry

by
Rajendra Singh Thakur

School of Natural Sciences
Tata Institute of Fundamental Research
Mumbai
October, 2008

DECLARATION

This thesis is a presentation of my original research work. Wherever contributions of others are involved, every effort is made to indicate this clearly, with due reference to the literature, and acknowledgement of collaborative research and discussions.

The work was done under the guidance of Dr. P. K. Madhu, at the Tata Institute of Fundamental Research, Mumbai.

[Rajendra Singh Thakur]

In my capacity as supervisor of the candidate's thesis, I certify that the above statements are true to the best of my knowledge.

[Dr. P. K. Madhu]
Date:

Acknowledgements

I would like to use this opportunity to thank a large number of people who helped me to shape this work in present form. Their help was indispensable to finish this work.

First of all I would like to acknowledge Dr. P. K. Madhu, the supervisor in this thesis work. His involvement as a project leader was the impetus for results. His writing and linguistic skills were utilised for presenting the work at various platforms. His knowledge of the research field gave the good starting points for various investigations. A special mention of holidays allowed has to be made, as often they are availed in large number to regain energy after exhausting periods.

Prof. N. D. Kurur is another person who contributed throughout the work. His understanding of various concepts and intuitive arguments were the main source of understanding in the initial period of my work. Various discussions with him can be remembered for the straightforward opinions presented with admirable levels of polishing.

A special thanks to Prof. Shimon Vega from Weizmann Institute of Science, Israel. During a period of nearly two months spent in his lab, various discussions were made to learn theoretical aspects of solid-state NMR. These discussions were used to shape few results in the later stages. His style of interacting with fellow coworkers and a constant pursuit of practising science was worth learning.

A combined acknowledgment for Prof. Malcolm Levitt, Prof. Anil Kumar, Prof. K. V. Ramanathan, Prof. Detlef Reichert, Prof. Angelica Sebald, Dr. Thomas Brauniger, and Dr. T. G. Ajith Kumar has to be made, as few discussions with them during various meetings were made. These discussions were a great source of knowledge and understanding of the field. Another thank to Dr. P. K. Madhu for arranging many of these meetings.

Prof G. Krishnamoorthy is another person to be acknowledged. I worked under his supervision on a project for a scheduled period of six month. The period was memorable for many stimulating discussions with him and his insightful thinking was worth following.

I have to offer special thanks to members of National Facility for High Field NMR, namely Manoj Naik, Devidas Jadhav, Mamta Joshi, and Mohan Dabholkar. They had promptly offered their excellent technical assistance at the time of need. The use of 500 MHz solid-state NMR facilities at the National Facility for High Field NMR, TIFR, Mumbai, and NMR Research Centre, IISc, Bangalore, is acknowledged.

Various funding agencies have to be acknowledged as journeys made with the sponsorships led to discussions with many eminent scientists, hence enhancing the productivity. Sarojini Damodaran International Fellowship Program offered the travel expenses to Israel and Weizmann Institute of Science arranged the local expenses and accommodation. Nuclear Magnetic Resonance Society, India kindly offered the expenses to attend 5^{th} Alpine Conference in Solid State NMR. Department of Chemical Sciences, TIFR offered partial support for Israel trip and complete expenses for visit to NMR Research Centre, Indian Institute of Science, Bangalore.

I am indebted to my innumerous friends in TIFR as well as at other places. Mentioning all of them is not possible as it alone can form a Chapter of this report. Their company made my stay in TIFR, a pleasure.

Table of Contents

List of Figures

List of Tables

Statement regarding new facts

- Improved decoupling methods in solid-state NMR

    1. Robust methods for heteronuclear dipolar decoupling have been designed under Magic-Angle Spinning (MAS). These methods are insensitive to experimental parameters like pulse length, phase difference, and ^{1}H off-resonance.
    2. Improved methods for heteronuclear dipolar decoupling were demonstrated under static conditions. These methods are more tolerant to ^{1}H off-resonance than earlier standard method, resulting in spectral enhancement.
    3. A robust method for heteronuclear dipolar decoupling was demonstrated for quadrupolar nuclei under Multiple-Quantum Magic-Angle Spinning (MQ-MAS) experiments.
    4. Decoupling sequences were compared for High-Resolution Magic-Angle Spinning (HRMAS) experiments and the sample was found to be insensitive to phase modulated decoupling methods.
    5. The strategy for designing robust decoupling sequences under Magic-Angle Spinning was successfully adapted to high frequencies.
    6. Additional modification to our approach resulted in enhanced bandwidth for ^{1}H off-resonance.

- Understanding decoupling methods in solid-state NMR

    1. Theoretical analysis of heteronuclear dipolar decoupling was done under MAS which has shown adiabatic sweep as the route to robustness.

- Work in progress

    1. Theoretical analysis of decoupling is being done for static condition.
    2. Theoretical analysis of off-resonance behavior of decoupling is under way.

Synopsis

Statutory Declarations

Name of the Candidate	:	*Rajendra Singh Thakur*
Title of the Thesis	:	*Design and Analysis of Heteronunlear Dipolar Decoupling Schemes in Solid-State Nuclear Magnetic Resonance*
Degree	:	*Doctor of Philosophy (Ph. D.)*
Subject	:	*Chemistry*
Name of the Guide	:	*Dr. P. K. Madhu*
Registration No.	:	*CHEM - 024*
Date of Registration	:	*28^{th} March 2006*
Place of Research	:	*Department of Chemical Sciences Tata Institute of Fundamental Research, Homi Bhabha Road, Colaba, Mumbai - 400005*

Introduction

Interactions in NMR: Rigid vs dynamic phase

Interactions in NMR are inherently anisotropic, having different values in different directions. This can be understood from the example of chemical shift anisotropy (CSA). Chemical shift arises from shielding of magnetic field felt at nucleus by electron distribution. Anisotropic electron density around the nuclei leads to CSA. Large CSA values are associated with groups having highly anisotropic electon distribution making carbonyl groups to have larger CSA compared to aliphatic groups. The orientation dependence leads to a term of the form ($3\cos^2\theta$-1) associated with CSA. The orientation dependence is common to all NMR interactions with similar behavior. Anisotropic interaction causes line broadening in powdered sample having random orientation of crystallites. Some other interactions relevant for later sections will be introduced now.

Spins are magetic dipoles and influence each other by through-space dipolar interactions. Dipolar coupling is termed homonuclear or heteronuclear when spins involved belong to same or different nuclei. The pair of coupled spins have different relative orientation with respect to external magnetic field resulting in anisotropy of the form ($3\cos^2\theta$-1) associated with dipolar coupling. Homonuclear and heteronuclear couplings behave differently as few terms are negligible under heteronuclear condition.

Quadrupolar interactions occur with nuclei having spin angular momentum (I) larger than $\frac{1}{2}$, as the nucleus no longer remains spherical. The electric quadrupole moment possessed by non-spherical nuclei interacts with electric field gradient generated by electrons. The description of quadrupole involves various terms of different nature and only one among them has ($3\cos^2\theta$-1) associated with it.

The presence of molecular tumbling (of GHz order) in isotropic liquids leads to averaging of anisotropic interactions whereas rigidity in solids allow anisotropy to appear with full vigor. The anisotropic interactions in solids are orders of magnitude larger than

isotropic counterparts in solution phase, demanding different set of principles and methods for solid and solution state. Stronger anisotropic interactions in solids lead to broad spectra with width defined by the strongest interaction.

One of the essential techniques in solid-state NMR for resolution enhancement is Magic-Angle Spinning (MAS) which involves mechanical spinning of sample at an angle of 54.74° with respect to external magnetic field [1, 2]. The origin of the technique can be understood on general presence of the term ($3\cos^2\theta$-1) in various interactions, which becomes zero when θ is 54.74°. Under influence of MAS, anisotropic interactions are averaged to zero, leaving narrow isotropic spectrum in favorable cases. Often additional methods are employed for resolution enhancement of spectra, mostly by means of radiofrequency (RF) pulses. With a suitable RF modulation scheme, interactions can be made to disappear from spectrum and this modulation scheme is called decoupling sequence. Decoupling results in sensitivity and resolution enhancement in case of anisotropic interactions.

Current work is focussed upon improving and understanding methods for heteronuclear dipolar decoupling. Pulse sequences existed for heteronuclear dipolar decoupling but their mechanism was elusive. Attempts are made to design methods with robust as well as improved performance. Work is also done to understand mechanism of heteronuclear dipolar decoupling.

Heteronuclear dipolar decoupling in solid-state NMR

Heteronuclear dipolar coupling is the dominant spin interaction in solids of rare nuclei coupled to abundant nuclei and decides the resolution of spectrum. Such a situation represents large number of systems which can be studied by NMR. ^{13}C coupled to ^{1}H is one of such spin system and it alone covers a large number of biological and medicinal systems, highlighting the importance of heteronuclear dipolar decoupling for resolution enhancement. Better decoupling methods improve resolution as spectral lines become

narrower and is naturally accompanied by gain in sensitivity.

Heteronuclear dipolar decoupling involve irradiation of abundant nuclei to enhance resolution in the spectra of rare spins. Application of unmodulated RF field, known as Continuous Wave (CW) method was tested in 1955 by Bloom et al. [3] and the work demonstrated the significance of decoupling. However, a study of Ernst et al. revealed many shortcomings of CW [4]. Most noticeable shortcoming of CW was the deterioration of efficiency with increasing MAS frequency. CW was also found sensitive to the off-resonance, resulting in inferior spectrum. Many methods were designed to obtain enhanced resolution over CW, but success was not achieved for a long time.

A breakthrough method in this field, Two Pulse Phase Modulation (TPPM) was reported only after four decades in 1995 [5]. Linewidth reduction over CW by a factor of two or higher was demonstrated with application of TPPM. TPPM consists of a pair of pulses having equal length (denoted by τ) differing by small phase (denoted by 2ϕ). TPPM is less sensitive to off-resonance compared to CW and delivers uniform resolution with MAS frequency. Effectiveness of TPPM prompted many groups to design modifications for improved performance.

Fung et al. desgined SPINAL by modulating phase difference of the TPPM pair. This method was found to give improved performance over TPPM leading to its wide acceptance [6]. In an alternative approach by Gan et al; amplitude of RF field of TPPM pulses were modulated, called as AMTPPM (Amplitude Modulated TPPM). With the lack of improvement over TPPM, the study was only of academic interest but of no practical use [7].

A different scheme consisting of two pulses of 180° phase difference was experimentally found by Ernst and coworkers [8]. The method was named XiX, and it was found to work at high values of RF field strength (over 100 kHz) and MAS frequency of around 30 kHz. Such MAS frequencies were not common and high RF field strength required is unsuitable for sensitive samples, thus the method could find limited applications.

A conceptually different appraoch of symmetry was also considered to design decoupling sequences [9]. The symmtery approach developed by Levitt treats spin interactions on the basis of rotational properties exhibited under MAS and RF [10]. Using symmetry approach, one can decide the fate of various interactions and design pulse sequences accordingly. However this approach has not been able to deliver improved method for heteronuclear dipolar decoupling. Comprehensive account of the work in heteronuclear dipolar decoupling has been covered in recent reviews [11, 12].

Numerical analysis of the heteronuclear dipolar decoupling suggested influence of other interactions, like CSA and homonuclear dipolar coupling [4]. Thus description of problem is complex and it is difficult to get insight into it. Complexity of the problem along with limited success with various attempts made enhancement of even 10-20 % significant. A need to design methods with improved performance exists but robustness is also advantageous as it leads to ready to use methods. Robust methods are insensitive to instrumental fluctuations and thus take care of an uncontrollable factor. Methods suitable for higher MAS frequencies are also getting attention with increasing field of the spectrometers.

A decoupling method was designed by sweeping pulse length of TPPM pairs. The pulse length is varied tangentially, having slower variation in the middle and faster towards the end. Thus, modulation frequency is swept tangentially and the method is named SW$_f$-TPPM (SWept-*f*requency TPPM) [13]. For spin $\frac{1}{2}$ systems, SW$_f$-TPPM offered robust performance under MAS [13, 14] and spectral enhancement is achieved under static conditions with SW$_f$-TPPM [14, 15]. SW$_f$-TPPM also offered intensity enhancement and robust performance for quadrupolar nuclei (spin $> \frac{1}{2}$) under MQMAS scheme) [16]. Later on it was found that simultaneously varying the phase hyperbolic-tangentially alongwith tangential variation of pulse length leads to further spectral enhancement. The method designed along this line is called SW$_{fp}$-TPPM (SWept-(frequency & phase) TPPM) [17] and this method is more suitable for intermediate MAS frequen-

cies.

Various spin systems are found with ^{13}C and ^{1}H nuclei and there has been discussions over the ideal spin-system for evaluation of decoupling. It was known that CH_2 is stronger coupled system compared to CH_1, owing to presence of more ^{1}H nuclei, while even strongly coupled CH_3 displays methyl-rotation which leads to averaging of interactions. Thus, CH_2 is the most challenging system and methods which work on this system have universal acceptance. Decoupling efficiency is always evaluated on CH_2 systems in our studies. CH_1 systems are studied additionally in a few cases.

The design of decoupling sequences

TPPM can be represented as $[\tau_{\phi}\ \tau_{-\phi}]$ with τ and ϕ representing pulse length and phase of the pulses. SPINAL was designed by modulating phase of the TPPM and basic SPINAL-8 is of the form $[\tau_{10}\ \tau_{-10}]\ [\tau_{15}\ \tau_{-15}]\ [\tau_{20}\ \tau_{-20}]\ [\tau_{15}\ \tau_{-15}]$ with higher versions like SPINAL-16, SPINAL-32, SPINAL-64 etc. designed by supercycling the basic SPINAL-8 block.

SW_f-TPPM consists of eleven TPPM pairs with pulse length varied tangentially and can be represented as $[0.78\tau_{\phi}\ 0.78\tau_{-\phi}]\ [0.86\tau_{\phi}\ 0.86\tau_{-\phi}]\ [0.94\tau_{\phi}\ 0.94\tau_{-\phi}]\ [0.96\tau_{\phi}\ 0.96\tau_{-\phi}]\ [0.98\tau_{\phi}\ 0.98\tau_{-\phi}]\ [1.00\tau_{\phi}\ 1.00\tau_{-\phi}]\ [1.02\tau_{\phi}\ 1.02\tau_{-\phi}]\ [1.04\tau_{\phi}\ 1.04\tau_{-\phi}]\ [1.06\tau_{\phi}\ 1.06\tau_{-\phi}]\ [1.14\tau_{\phi}\ 1.14\tau_{-\phi}]\ [1.22\tau_{\phi}\ 1.22\tau_{-\phi}]$. Pulse length of the middle pair (τ) is optimised for performance and sweep is achieved by the multiplicative factors. The design was inspired by adiabatic slow passage of the Continuous Wave NMR, popular before Fourier transform.

Performance of SW_f-TPPM under magic-angle spinning

Decoupling efficiency of SW_f-TPPM was compared with TPPM and SPINAL-64 at various RF field strength and MAS frequencies. Intensity of CH_2 peak of U-^{13}C-tyrosine was taken

as the measure of decoupling efficiency. It was found that SW_f-TPPM is on par with other methods if not better. The robustness comparison of various methods as a function of pulse length, phase difference and ^{1}H off-resonance was done where SW_f-TPPM was found to be the least affected by variation of parameters. This comparison was done at 14 kHz of MAS frequency and 100 kHz of RF field strength [13].

Extensive theoretical analysis was done in collaboration with Prof. Shimon Vega using Bimodal-Floquet approach to understand efficiency of TPPM and robustness of SW_f-TPPM [18]. Small phase modulation (in TPPM) can be split into two field components, a large field same as CW irradiation and an additional small perpendicular field. The efficiency of TPPM was shown to be arising from the small perpendicular field. Theoretical study of spin system having heteronculear dipolar coupling under MAS suggested spins to be pointing in all directions of space. CW field can average components perpendicular to it while those lying along CW can only be averaged by small perpendicular field. Decoupling is most effective when the amplitude of perpendicular field matches that of spin component lying along CW field. This was defined as the decoupling condition. Optimum performance by TPPM involves a careful setting of pulse length and phase difference to satisfy the decoupling condition. Tangential sweep of pulse length leads to adibatic sweep through the decoupling condition which imparts robustness to SW_f-TPPM. Adiabatic sweep through a resonance condition was known to be efficient [19].

It was experimentally found that sweep profiles other than tangential are equally effective. Many possible profiles were found experimentally to be effective in decoupling, and this fact can be used as a strategy for designing robust decoupling sequences.

Later on it was found that robustness with respect to ^{1}H off-resonance ($\Delta\nu(^1\mathrm{H})$) under adiabatic sweep is realised when cycle time of the modulation is shorter than rotor period. It makes SW_f-TPPM ineffective at high MAS frequency when modulation time exceeds rotor period. As SW_f-TPPM consists of 11 TPPM pairs, modulation period is 11 times that of a single TPPM pair. Modulation cycle can be made short by either

reducing pulse length or number of TPPM pairs. Reduced pulse length can be achieved with high RF field strength which has known deleterious effects on the sample. SW_f-TPPM variants with reduced number of pulses were designed for high MAS frequencies and were found to be effective.

Performance of SW_f-TPPM under static condition

Performance of SW_f-TPPM and analogues were compared to the established method on MBBA, a liquid-crystal sample, under static conditions. Liquid crystals are organic molecules with such a structure that the molecules are arranged in ordered manner with restricted motion. Limited motion results in spectral broadening, and NMR of this phase is similar to that of the solid state. Presence of motion in this state renders partial averaging of orientation dependent interactions (chemical shift anisotropy, dipolar coupling etc.), thus reducing the strength of interactions and smaller RF field strength is needed for heteronuclear dipolar decoupling. The nature of phase also restricts the amplitude of RF field as associated heating effect can destroy the system. Liquid crystal is a model system for membrane proteins and better decoupling methods are needed to study these macromolecules. Prior to our study, SPINAL-64 was considered as the best method for this phase.

Decoupling efficiency of SW_f-TPPM and analogs and SPINAL-64 at RF field strength of 25 kHz was compared on various peaks of MBBA. Swept-frequency methods demonstrated improved ^{1}H off-resonance behavior over SPINAL-64 [15]. ^{13}C resonances separated by large chemical shift were found to possess widely different ^{1}H on-resonance frequencies. This observation can be explained by chemical shift difference in ^{13}C and ^{1}H spins for bonded groups owing to similar chemical environment. Improved off-resonance charcteristics of SW_f-TPPM and analogs have resulted in overall spectral improvement.

Evaluation of SW$_f$-TPPM for static case

Study was done in order to understand ^{1}H off-resonance behavior of heteronuclear dipolar decoupling sequences under static conditions. Efficiency of various decoupling sequences was compared, and it was found that TPPM yields improved line width over CW and is on par with modulated TPPM methods at ^{1}H on-resonance. Owing to acute dependence on ^{1}H off-resonance, TPPM delivers overall inferior spectra. Under static conditions, performance of modulated TPPM methods depends acutely on pulse length. SW$_f$-TPPM and analogs deliver improved ^{1}H off-resonance behavior leading to improved spectra.

Performance of SW$_f$-TPPM under MQMAS scheme for quadrupolar nuclei

Multiple-Quantum MAS (MQMAS) is a technique for obtaining high resolution spectra from half-integer spin quadrupolar nuclei (I = $\frac{2n+1}{2}$, n > 0) under MAS [20]. This technique relies upon absence of 1^{st} order quadrupolar couplings owing to symmetry of energy states and 2^{nd} order quadrupolar couplings are averaged by combination of MAS and RF pulses. Thus, spectra obtained with MQMAS schemes are free from quadrupolar effects and are called isotropic spectrum. MQMAS involves evolution of multiple-quantum coherences and corresponding variants, 3QMAS, 5QMAS etc. exists. Feasilbilty of a particular variant of MQMAS for a nuclei is decided by its spin quantum number.

Presence of heteronuclear dipolar couplings by the virtue of molecular composition also contributes to line broadening and use of decoupling sequences becomes necessary. This is often the case when ^{1}H is constituent of organic and inorganic materials. It was proposed that heteronuclear coupling evolves p-fold during p-quantum evolution in MQMAS scheme [21]. This makes it even more important to use efficient decoupling sequences in such systems.

CW was applied succesfully in these systems to obtain improved resolution and further enhancement was demonstrated with application of TPPM. More sophisticated schemes, like SPINAL-64 and SW_f-TPPM were not applied in such systems although they have shown better performances over TPPM elsewhere. We have studied SPINAL-64 and SW_f-TPPM on a sample of gibbsite for 3QMAS and 5QMAS schemes and compared the performance with CW and TPPM. Gibbsite is a mineral of ^{27}Al ($I = \frac{5}{2}$), having layered structure of basic-aluminum hydroxide, $Al(OH)_3$ having large number ^{1}H nuclei around ^{27}Al nuclei.

In our study TPPM offered approximately 100% intensity enhancement over CW method in all cases. SPINAL-64 and SW_f-TPPM have shown further enhancement of 20% over TPPM in isotropic spectra under 3QMAS scheme. These methods, especially SW_f-TPPM were found to be robust with respect to various experimental parameters to avail this advantage. In 5QMAS scheme, SPINAL-64 performed comparable to TPPM and only SW_f-TPPM offered intensity enhancement of 8% over TPPM [16].

Study of decoupling sequences for HRMAS experiments

A comparative study of various decoupling sequences was done for High-Resolution MAS (HRMAS) experiments. This class of experiments is gaining in popularity as it covers a wide range of soft condensed matter ranging from tissues on one hand to synthetic polymers on the other. These materials are spun at low spinning frequencies ($\sim$ 5 kHz) and do not tolerate high RF field strengths. Presence of internal motion makes decoupling to be realised at smaller RF field strength compared to that in rigid solids.

A block copolymer of ethylene oxide (EtO) and propylene oxide (PrO), called F-127 was studied. F-127 has composition of $(EtO)_{100}$-$(PrO)_{65}$-$(EtO)_{100}$ with molecular weight of 12,600 daltons. The sample was spun at 4 kHz and various methods were applied at RF field strength of 20 kHz to effect heteronuclear dipolar decoupling. The study shows that the sample was sensitive to decoupling as lack of it yields broad featureless lines

in the spectrum. However all decoupling methods produce comparable effect on the spectrum and no appreciable advantage over CW was obtained with more sophisticated methods. It was concluded that CW is a method of choice for this system as sophisticated methods do not offer advantage compared to the effort required for implementation [16].

Improved adiabatic sweep for enhanced decoupling efficiency

Adiabatic sweep was known in NMR before Fourier-transform was introduced as it was extensively used to obtain improved spectrum with frequency sweep. In adiabatic sweep, detection of a resonance was done by fast frequency sweep away from resonance and slow passage was employed close to resonance. Fourier-transform introduced pulsed NMR and its wide adoption made frequency sweep obsolete. Adiabaticity was used in pulsed NMR to design efficient inversion and J-decoupling methods and explored heavily in the process [19, 22]. The adiabtaic sweep (in SW_f-TPPM) was found to improve decoupling efficiency of TPPM, making it a robust method and thus improved adiabatic methods were expected to further enhance decoupling efficiency. Enhanced performance was realised with sequences of improved adiabaticity.

Tangent function was an intuitive approach for adiabatic sweep and it was used to design SW_f-TPPM. One of the improved adiabatic function known was tanh/tan, where amplitude and frequency was varied in the form of hyperbolic tangent and tangent respectively [22]. Frequency was swept tangentially in SW_f-TPPM by varying pulse length while amplitude can be swept by varying phase difference hyperbolic tangentially. A method was designed on this principle and called SW_{fp}-TPPM [17]. According to previous notation, it can be denoted as $[1.22\tau_{2}\ 1.22\tau_{-2}]\ [1.14\tau_{3}\ 1.14\tau_{-3}]\ [1.06\tau_{4}\ 1.06\tau_{-4}]\ [1.04\tau_{5}\ 1.04\tau_{-5}]\ [1.02\tau_{7}\ 1.02\tau_{-7}]\ [\tau_{10}\ \tau_{-10}]\ [0.98\tau_{13}\ 0.98\tau_{-13}]\ [0.96\tau_{15}\ 0.96\tau_{-15}]\ [0.94\tau_{16}$

$0.94\tau_{-16}$] [$0.86\tau_{17}$ $0.86\tau_{-17}$] [$0.78\tau_{18}$ $0.78\tau_{-18}$]. SW_{fp}-TPPM demonstrated improved off-resonance over TPPM, SPINAL-64 and SW_f-TPPM at various MAS frequencies and RF field strength studied. It was found to be the method of choice at intermediate MAS frequencies.

SW_{fp}-TPPM demonstrates acute dependence on pulse length together with improved ^{1}H off-resonance. Pulse length can be set precisely for optimum performance while the ^{1}H off-resonance can only be addressed by suitable modulation schemes. Improved ^{1}H off-resonance leads to spectral enhancement and thus SW_{fp}-TPPM is a better method than SW_f-TPPM.

Bibliography

[1] E. R. Andrew, A. Bradbury, and R. G. Eades, Nature. **182**, 1659 (1958).

[2] I. J. Lowe, Phys. Rev. Lett. **2**, 285 (1958).

[3] A. L. Bloom and J. N. Shoolery, Phy. Rev. **97**, 1261 (1955).

[4] M. Ernst, H. Zimmermann, and B. H. Meier, Chem. Phys. Lett. **317**, 581 (2000).

[5] A. E. Bennett, C. M. Rienstra, M. Auger, K. V. Lakshmi, and R. G. Griffin, J. Chem. Phys. **103**, 6951 (1995).

[6] B. M. Fung, A. K. Khitrin, and K. Ermolaev, J. Magn. Reson. **142**, 97 (2000).

[7] Z. Gan and R. R. Ernst, Solid State Nucl. Magn. Reson. **8**, 153 (1997).

[8] A. Detken, E. H. Hardy, M. Ernst, and B. H. Meier, Chem. Phys. Lett. **356**, 298 (2002).

[9] K. Riedel, C. Herbst, J. Leppert, O. Ohlenschläger, M. Görlach, and R. Ramachandran, Chem. Phys. Lett. **429**, 590 (2006).

[10] M. H. Levitt, *Encyclopedia of NMR*, edited by D. M. Grant and R. K. Harris (Wiley, Chichester, 1996), Vol. 9, p. 165.

[11] M. Ernst, J. Magn. Reson. **162**, 1 (2003).

[12] P. Hodgkinson, Prog. Nucl. Magn. Reson. Spectrosc. **46**, 159 (2005).

[13] R. S. Thakur, N. D. Kurur, and P. K. Madhu, Chem. Phys. Lett. **426**, 459 (2006).

[14] R. S. Thakur, N. D. Kurur, and P. K. Madhu, J. Magn. Reson. **193**, 77 (2008).

[15] R. S. Thakur, N. D. Kurur, and P. K. Madhu, J. Magn. Reson. **185**, 264 (2007).

[16] R. S. Thakur, N. D. Kurur, and P. K. Madhu, Magn. Reson. Chem. **46**, 166 (2008).

[17] R. S. Thakur, N. D. Kurur, and P. K. Madhu, Manuscript in preparation.

[18] M. Leskes, R. S. Thakur, P. K. Madhu, N. D. Kurur, and S. Vega, J. Chem. Phys. **127**, 024501 (2007).

[19] E. Kupče and R. Freemann, J. Magn. Reson. A **117**, 246 (1995).

[20] L. Frydman and J. S. Harwood, J. Am. Chem. Soc. **117**, 5367 (1995).

[21] M. J. Duer, Chem. Phys. Lett. **277**, 167 (1997).

[22] K. Uğurbil, M. Garwood, A. R. Rath, and M. R. Bendall, J. Magn. Reson. **78**, 472 (1998).

List of publications

1. R. S. Thakur, N. D. Kurur, and P. K. Madhu, Swept-frequency two-pulse phase modulation for heteronuclear dipolar decoupling in solid-state NMR, Chem. Phys. Lett. **426**, 459 (2006).

2. R. S. Thakur, N. D. Kurur, and P. K. Madhu, Improved heteronuclear dipolar decoupling sequences for liquid-crystal NMR, J. Magn. Reson. **185**, 264 (2007).

3. M. Leskes, R. S. Thakur, P. K. Madhu, N. D. Kurur, and S. Vega, A bimodal Floquet description of heteronuclear decoupling in solid-state nuclear magnetic resonance, J. Chem. Phys. **127**, 024501 (2007).

4. R. S. Thakur, N. D. Kurur, and P. K. Madhu, An experimental study of decoupling sequences for multiple-quantum and high-resolution MAS experiments in solid-state NMR, Magn. Reson. Chem. **46**, 166 (2008).

5. R. S. Thakur, N. D. Kurur, and P. K. Madhu, An analysis of phase-modulated heteronuclear dipolar decoupling sequences in solid-state nuclear magnetic resonance, J. Magn. Reson. **193**, 77 (2008).

6. R. S. Thakur, N. D. Kurur, and P. K. Madhu, Improving off-resonance behavior of heteronuclear dipolar decoupling sequences in solid-state NMR, Manuscript in preparation.

7. R. S. Thakur, N. D. Kurur, and P. K. Madhu, Implementation of phase modulated heteronuclear dipolar decoupling sequences in liquid-crystal NMR, Manuscript in preparation.

8. S. Paul, R. S. Thakur, and P. K. Madhu, ^{1}H Homonuclear dipolar decoupling at high magic-angle spinning frequencies with rotor-synchronised symmetry sequences, Chem. Phys. Lett. **456**, 253 (2008).

9. S. Paul, R. S. Thakur, M. Goswami, A. C. Sauerwein, S. Mamone, M. Concistrè, H. Förster, M. H. Levitt, and P. K. Madhu, Supercycled homonuclear dipolar decoupling sequences in solid-state NMR, Submitted to J. Magn. Reson.

10. S. Paul, R. S. Thakur, M. H. Levitt, and P. K. Madhu, Improved rotor-synchronised symmetry sequences for ^{1}H homonuclear dipolar decoupling, Manuscript in preparation

Chapter 1

Introduction

Nuclear Magnetic Resonance (NMR) [1, 2] is a branch of spectroscopy involving transitions between energy levels of a nucleus arising from its spin angular momentum, where the degeneracy between these levels is lifted by a static magnetic field. The transitions between these energy levels are normally induced by the appplication of a magnetic field modulating in a plane perpendicular to the static magnetic field [3, 4].

NMR is a versatile spectroscopic tool to study local environment and dynamics of the nucleus involved. The information content of an NMR spectrum is often obtained selectively by suitable experiments. Selective information of local environment and dynamics makes NMR a versatile tool despite the deficiency in sensitivity [3, 4].

The energy levels corresponding to angular momentum levels of a spin is coupled to its local environment in various ways [5, 6]. This form of spectroscopy, NMR, is sensitive to the local environment and as different phases of matter behave in a different way, mobility of the phase decides the resolution of the resulting NMR spectrum. While isotropic liquids yield narrow lines in their NMR spectrum allowing the number of chemical sites to be counted, solids often yield broad and featureless spectra. Thus, rigid solids and isotropic liquids behave in contrasting ways and intermediate phases such as liquid crystals, bicelles, and soft condensed matter, behave in a composite fashion. Various techniques have been developed to narrow down the NMR spectra of solids [5–10].

This thesis addresses improvement of resolution in spectral lines of rotating rigid solids and static liquid crystals, i.e. motionally restricted phases. Robust and improved methods for resolution enhancement have been developed and demonstrated on spinning solids and static liquid crystals. A general introduction of NMR is presented in this Chapter on the basis of which the thesis work will be explained in later Chapters. A description of the thesis work is presented towards the end of this Chapter.

1.1 Principles of NMR

NMR involves resonance absorption of energy by nuclear magnetic moments. A nucleus possessing the quantum mechanical property called spin (spin quantum number I) by virtue of its composition, is amenable to NMR spectroscopy. These nuclei behave as magnets and their magnetic moments are given by

$$\overrightarrow{\mu} = -\gamma \overrightarrow{I} \tag{1.1}$$

where γ is the gyromagnetic ratio of the nucleus, which decides the strength alongwith the relative direction of the magnetic moment of nucleus with respect to its angular momentum.

A nucleus of spin quantum number I has $2I + 1$ angular momentum projections which are degenerate in the absence of a magnetic or electric field. Under the influence of magnetic field, the energy levels of these projections are given by $\overrightarrow{\mu}.\overrightarrow{B}$ i.e. $\gamma \overrightarrow{I}.\overrightarrow{B}$, and thus degeneracy is lifted. These energy levels are called Zeeman energy levels.

The energy levels of an isolated spin $\frac{1}{2}$ nucleus, in the presence of a static magnetic field B_0, splits into two Zeeman energy levels. The separation between these levels, ΔE is given by,

$$\Delta E = \hbar(-\gamma B_0) = \hbar\omega_0 \tag{1.2}$$

where $\hbar$ is the universal Planck's constant. Energy difference between these states increases with magnetic field (B_0), which in turn decides the population difference between the levels. Thus, sensitivity of an NMR experiment depends upon the magnetic field applied.

The resonance frequency, ω_0, is a characteristic of the nucleus. It is also called the Larmor precession frequency, as the same value is obtained for precession of spin in a magnetic field of strength B_0,

$$\omega_0 = -\gamma B_0 \tag{1.3}$$

The resonance frequency of a nucleus is linearly proportional to the magnetic field and any inhomogeneity in the magnetic field appears in the spectrum. Thus, homogeneity of magnetic field affects the spectral resolution. The achievability of homogeneity puts an upper bound on the magnitude of Zeeman field and hence limits the sensitivity of NMR experiments.

Measurement of Zeeman frequencies involves resonant interaction with a photon belonging to radiofrequency range owing to the achievable homogeneous magnetic field. Conventional detection of Larmmor frequencies involved sweeping across the resonance by varying the magnetic field keeping irradiation frequency constant. This method of detection is called frequency-swept NMR or continuous-wave NMR [4] and is obsolete.

Modern NMR spectrometers record spectra in a better but slightly complicated way, called Fourier Transform NMR (FTNMR) [11]. It involves a steady magnetic field and simultaneous application of all frequencies by an RF pulse.

1.2 Interactions in NMR

A nucleus with spin angular momentum behaves like a quantum-mechanical object, and when perturbed by a coherent RF irradiation, the response follows the simple rules of rotation of angular momentum. Physical basis of quantum mechanical behavior will be

explored in Section 1.3.

NMR experiments can be understood based upon a quantum-mechanical formulation. In this formalism, interactions affecting the spin system and their associated Hamiltonians are classified in two categories: external and internal. External Hamiltonians include Zeeman and RF fields which are directly controlled by the spectroscopist while internal Hamiltonians include interactions of a spin with magnetic field via local environment (chemical shift), with another spin (dipolar and scalar coupling), and with electric field gradient (quadrupolar coupling). Internal interactions are manipulated by imposing modulations using external interactions. As nuclear spins precess rapidly under Zeeman field, the internal spin interactions are truncated to the angular momentum terms evolving with the Larmor frequency. This approximation is called "secular approximation" [6].

Two representations are popular to characterise Hamiltonians in NMR, cartesian and spherical. Cartesian representation, based upon three mutually perpendical axis system is intuitive while spherical representation, based upon the rotational behavior of objects, although difficult to visualise, is more relevant for understanding purposes. NMR interactions and their couplings to the local environment are thoroughly described by Mehring [5, 6]. Hamiltonians in NMR will be explained after a brief introduction of spherical tensor operator formalism.

1.2.1 Rotational properties of NMR Hamiltonians

A variety of multiple pulse experiments (RF schemes) exists in the realm of solid-state NMR to manipulate the spins. Magic-angle spinning (MAS) is a universally applicable technique (involving mechanical modulation of sample) in solid state which is explained in a later Section. In a large number of experiments, MAS and RF schemes are applied in a combined way. Rotation of spins in real space (MAS) or in spin space (RF schemes) modulates the spin interactions and hence it is useful to study rotational properties of

NMR Hamiltonians. The rotational properties are used extensively to understand solid-state NMR. A spherical tensor of rank l is a set of $2l+1$ (denoted by m) objects (T_{lm}) such that when any of them is rotated ($R(\Theta)$ representing the operator for rotation through angle Θ) in 3 dimensions, the result is a linear superposition of the same set of objects:

$$R(\Theta)T_{lm}R(\Theta)^{-1} = \sum_{m'=-l}^{+l} T_{lm}D^{l}_{m'm}(\Theta) \tag{1.4}$$

where $D^{l}_{m'm}(\Theta)$ are the elements of Wigner matrix. Tensors of different rank differ in their behavior under rotation. Scalars are tensors of rank 0 as they are invariant under rotation and vectors are tensor of rank 1. Tensors of rank 2 are simply called tensors. Rank 0 tensors are unaffected by rotation in the corresponding frames. Vectors are tensors of rank 1 with intuitive rotational properties. Rank 2 tensors are difficult to picturise owing to complex rotation properties, d-orbitals of an atom being an example.

Interactions in NMR possess rotational properties in their spin and space components and both components behave as 2^{nd} rank tensors (T_{2m}) in general. Under secular pproximation, higher values of m do not survive in the internal spin interactions [6]. Defining A_{20} and T_{20} as the space and spin part of a tensorial interaction, a typical spin interaction in the laboratory frame under high-field approximation can be written as,

$$H = [A_{20}]^{L}[T_{20}]^{L} \tag{1.5}$$

where L denotes the representation in the Laboratory frame.

The spatial part is modulated by mechanical modulation under MAS, and is defined by the frame of rotor:

$$H_{MAS} = \sum_{m=-2}^{+2} [A_{2m}]^{R}[T_{20}]^{L} \tag{1.6}$$

where R denotes the representation in the rotating frame, defined by MAS for the spatial component. m represents the components of spatial tensor.

RF modulates the spin components and under combined influence of MAS and RF pulses, the spatial and spin components are modulated and the Hamiltonian becomes,

$$H_{MAS,RF} = \sum_{\mu=-2}^{+2} \sum_{m=-2}^{+2} [A_{2m}]^R [T_{2\mu}]^R \tag{1.7}$$

where R denotes the representation in the rotating frame, defined by RF for the spin component. μ represents the components of spin tensor.

Various interactions differ upon the rank of spin or space component and this property of interactions was used by the group of Levitt to design a series of sequences [12]. In this notation, various interactions are represented by their ranks. Various spin interactions will be revisited now, and their rotational properties will be presented.

1.2.2 Zeeman interaction

This is the most important Hamiltonian as the presence of magnetic field qualifies an experiment as magnetic resonance. It simply represents the splitting of energy levels of a spin in static magnetic field. For representation purposes, the static magnetic field is chosen to point along z, the azimuthal axis. Thus, Zeeman Hamiltonian may be written as,

$$H_z = \gamma B_z I_z = \omega_0 I_z \tag{1.8}$$

Zeeman interaction is the basis of NMR as it creates energy eigenstates. Each nucleus has a characteristic value of γ which makes them resonate at distinct frequencies.

1.2.3 Radiofrequency field

This is the most important tool in the hand of an NMR spectroscopist. It refers to an oscillating magnetic field applied perpendicular to the Zeeman field which induces tran-

sitions between Zeeman levels. The form of the RF interaction is given by,

$$H_{rf} = B_1 \sin(\omega t + \phi) \tag{1.9}$$

where B_1 denotes the amplitude of RF field and is often represented in frequency units (denoted by ω_1) according to the following relation. It is based upon the nutation of spins induced by RF field. The nutation frequency ω_{nut} is equal to ω_1 at on-resonance, i.e. when the irradiation frequency matches with that of nuclear precession.

$$\omega_1 = \frac{1}{2}\gamma B_1 = \omega_{nut}^{on-resonance} \tag{1.10}$$

This expression represents the strength of RF field in angular frequency with units of radians per second. In NMR, often RF field strength is expressed in rotations per second (in Hz) after dividing ω_1 by 2π. Thus, RF field is often presented in the units of kHz and denoted by ν_1. In accordance with this notation, the off-resonance of RF irradiation is also presented in the units of Hz and denoted by $\Delta\nu$.

It will be discussed in Section 1.3 that pulses of various characteristics can be produced in radiofrequency regime which paves the way for various NMR applications.

1.2.4 Chemical shift

Electrons circulating around a nucleus in a diamagnetic molecule, when placed in a magnetic field, induce a small magnetic field in the opposite direction. This effect leads to the reduction of magnetic field felt by, and a reduction in resonance frequency of the nucleus. This shift is governed by the electronic environment, and hence called chemical shift. This interaction makes NMR a tool for chemical site identification and molecular structure determination, with the corresponding Hamiltonian represented by,

$$H_{cs} = \delta^{iso}(-\gamma B_0)I_z = \delta^{iso}\omega_0 I_z$$

$$H_{cs} = [A_{00}]^L [T_{10}]^L = \delta^{iso} \omega_0 I_z \tag{1.11}$$

This shift, $\delta^{iso}\omega_0$ is linearly proportional to Zeeman field and is often represented in parts per million (δ^{iso}) after normalisation with respect to the applied field. The frequency and ppm scales follow opposite sign conventions in the representation of NMR spectrum.

1.2.4.1 Chemical shift anisotropy

Chemical shift arises from shielding of magnetic field by electrons. The distribution of electron density around a nucleus is not necessarily isotropic and anisotropy is often associated with chemical shift. This interaction is called chemical shift anisotropy (CSA) and is represented by,

$$H_{csa} = \delta^{aniso} \omega_0 I_z \tag{1.12}$$

$$H_{csa} = [A_{20}]^L [T_{10}]^L = [A_{20}]^L B_0 I_z \tag{1.13}$$

The anisotropy is represented by $\Delta\omega_{aniso}$ and is a function of the spin orientation with respect to the magnetic field. Like the isotropic chemical shift, chemical shift anisotropy is also linearly proportional to the Zeeman field. Thus, anisotropy is naturally associated with chemical shift and is a good example to understand difference between rigid solids and isotropic liquids, and this distinction is presented in Section 1.4. It is averaged to zero in isotropic liquids by rapid isotropic tumbling of molecules, which are of GHz frequency.

1.2.5 Direct dipolar couplings

Spins are naturally magnetic dipoles and influence each other by through space dipolar couplings. The dipolar coupling between a pair of spins $\overrightarrow{I_1}$ and $\overrightarrow{I_2}$ with γ_1 and γ_2 as

their respective gyromagnetic ratio, is given by the expression,

$$H_{12}^{dd,full} = \frac{\mu_0}{4\pi}\frac{\hbar\gamma_1\gamma_2}{r_{12}^3}\left\{\overrightarrow{I_1}.\overrightarrow{I_2} - 3(\overrightarrow{I_1}.\hat{e}_{12})(\overrightarrow{I_2}.\hat{e}_{12})\right\} \tag{1.14}$$

where $\hat{e}_{12}$ denotes the unit vector in the direction of line joining the centres of the two nuclei and r_{12} represents the internuclear distance. μ_0 is the factor deciding the role of medium, known as permittivity.

Different forms for homonuclear and heteronuclear dipolar couplings arise under secular aproximation, which are as follows:

$$H_{dd}^{homo}(\Theta_{12}) = \frac{\mu_0}{4\pi}\frac{\hbar\gamma_1\gamma_2}{r_{12}^3}(3\cos^2\Theta_{12} - 1)(\overrightarrow{I_1}.\overrightarrow{I_2} - 3\hat{I}_{1z}.\hat{I}_{2z}) \tag{1.15}$$

$$H_{dd}^{hetero}(\Theta_{12}) = \frac{\mu_0}{4\pi}\frac{\hbar\gamma_1\gamma_2}{r_{12}^3}(3\cos^2\Theta_{12} - 1)(-2\hat{I}_{1z}.\hat{I}_{2z}) \tag{1.16}$$

where Θ represents the orientation dependence of spin pair with respect to the applied magnetic field. The dipolar coupling does not possess the isotropic component, i.e. it does not shift the position of spectral lines. It is only a source of line broadening. The interaction is symmetric, giving rise to a particular lineshape. The dipolar couplings are represented in spherical tensor notation as

$$H_{dd,homo}^{ii} = [A_{20}]^L[T_{20}]^L \tag{1.17}$$

$$H_{dd,hetero}^{ij} = [A_{20}]^L[T_{10}]^{L,i}[T_{10}]^{L,j} \tag{1.18}$$

It can be noticed that homonuclear and heteronuclear dipolar couplings have different forms, and deserve separate treatments. Separate class of experiments and approaches have been designed to deal with heteronuclear and homonuclear dipolar couplings [5–10].

Non-secular terms of dipolar couplings have the forms like $I_i^{\pm}I_j$, $I_i^{\pm}I_j^{\mp}$, and $I_i^{\pm}I_j^{\pm}$

which are responsible for polarisation transfer, explained in Section 1.5.2.

1.2.6 Indirect spin couplings

Scalar coupling is the coupling between two nuclei mediated by surrounding electrons. It is thus an indirect coupling and hence does not depend upon the spatial distance between the two nuclei. Contrary to direct dipolar coupling, it is neither symmetric nor traceless in the general case. The isotropic part of this interaction can be written as,

$$H_J^{ij} = \hbar \sum_{j<k} J_{j,k} \overrightarrow{I_j} . \overrightarrow{I_k} \tag{1.19}$$

The anisotropic part of this interaction is similar in form to the dipolar coupling and is of much smaller magnitude to be observed in solids.

1.2.7 Quadrupolar interaction

A nucleus in an atom or molecule is surrounded by electrons which are capable of inducing large electric fields. Gradient of this electric field can affect nuclear energy levels if the nucleus is not spherical. The electric quadrupole moment is associated with a non-spherical nucleus that interacts with electric field gradient (EFG) and this interaction is called quadrupolar interaction. Nuclei with spin angular momentum $\frac{1}{2}$ are spherical and free of quadrupolar interaction. The electric origin of quadrupolar interaction makes it the strongest interaction for nuclei having spin angular momentum greater than $\frac{1}{2}$. The form of the quadrupolar Hamiltonian is given by,

$$H_Q = \frac{1}{6}\hbar\nu_Q \left[(3I_z^2 - I(I+1) + \eta(I_x^2 - I_y^2) \right] \tag{1.20}$$

where η is the assymetry parameter and the quadrupolar frequency, ν_Q, a measure of the strength of quadrupole is governed by charge of electron (e), electric quadrupole

moment of the nucleus (Q) and the component of electric field gradient (V_{zz}) along the direction of Zeeman field. It is defined as

$$\nu_Q = \frac{3eQ}{2I(2I-1)\hbar} V_{zz} \tag{1.21}$$

The general form of the quadrupolar Hamiltonian in the notation of irreducible tensor operators is given as

$$H = \frac{\nu_Q}{3} \sum_{k=-2}^{2} (-1)^k T_q^2 V_{-q}^2 \tag{1.22}$$

In the laboratory frame the quadrupolar interaction can be treated as a perturbation to the Zeeman field, and can be expressed as a sum of first- and second-order terms.

$$H_Q \equiv H_Q^{(1)} + H_Q^{(2)} \tag{1.23}$$

The first-order quadrupolar coupling is sufficient for the description of the quadrupoles having strength significantly smaller than the Zeeman field. It is given by

$$H_Q^1 = \frac{\nu_Q}{3} T_0^2 V_0^2 = \frac{\hbar \nu_Q'}{6} \left[3I_z^2 - I(I+1) \right] \tag{1.24}$$

where ν_Q' the quadrupolar frequency (ν_Q), expressed as a function of the orientation (α and β) of the nuclear spin and asymmetry (η) of the environment, is given by

$$\nu_Q' = \nu_Q \left(\frac{3\cos^2\beta - 1}{2} + \frac{\eta}{2} \sin^2\beta \cos 2\alpha \right) \tag{1.25}$$

This first-order quadrupolar coupling causes the splitting of $2I$ lines of quadrupolar nuclei into equally spaced lines separated by $\Delta\nu_Q$. $\Delta\nu_Q$ is a function of the polar angles θ and ϕ which relate the Zeeman field to the EFG principal axis system. This term is a second-rank Legendre polynomial and vanishes under MAS. The first-order frequency

shifts $\Delta\nu_{m,m+1}$ of the allowed transitions ($m \longleftrightarrow m+1$) are given by

$$\Delta\nu_{m,m+1} = \Delta\nu(\theta,\phi)\left(m+\frac{1}{2}\right) \tag{1.26}$$

The orientation dependence of the first-order term causes broadening of the individual transitions. Central transition (-$\frac{1}{2} \longleftrightarrow \frac{1}{2}$) of half-integer spins does not experience this broadening as m = $\frac{1}{2}$. This broadening is again absent for other (directly) non-observable symmetric transitions ($m \longleftrightarrow -m$) in a quadrupolar nucleus.

In the case of a strong quadrupole, first-order perturbation theory is not sufficient and second-order terms are employed as correction. Second-order terms possess both isotropic and anisotropic parts. The second-order quadrupolar interaction is given by,

$$H_Q^2 = \frac{\hbar\nu_Q^2}{9\nu_0}\left\{2I_z[2I_z^2 - I(I+1) + \frac{1}{4}]V_{-1}^2V_1^2 + I_z[I_z^2 - I(I+1) + \frac{1}{2}]V_{-2}^2V_2^2\right\} \tag{1.27}$$

A more complete description of quadrupoles is presented in Chapter 5, in the context of work involving a quadrupolar system.

1.2.8 Relative magnitude of anisotropic interactions in solids

A large number of nuclei (and isotopes) in the periodic table is amenable to NMR spectroscopy and their presence in various molecular environment gives rise to different combination of interactions. Linewidth of their solid-state NMR spectrum is governed by the strongest interaction in the situation, few of the situations will be discussed here.

The anisotropic interactions impart broadening in the NMR spectrum of solids and the strongest interaction determines the width of the spectrum. For nuclei having spin angular momentum > $\frac{1}{2}$, quadrupolar interaction is the stongest interaction and for spin $\frac{1}{2}$ nuclei with large gyromagnetic ratio such as ^{1}H and ^{19}F, the spectral resolution is determined by homonuclear dipolar couplings. For lighter spin $\frac{1}{2}$ rare nuclei with small gyromagnetic ratio (γ), heteronuclear dipolar coupling is larger than chemical

shift anisotropy and dominates their spectrum whereas heavy nuclei have large chemical shift anisotropy which sometimes surpasses heteronuclear dipolar coupling.

1.3 Dominance of coherence in NMR

Spectroscopy is interaction between light and matter. A quantum of electromagnetic radiation interacts with resonant energy levels of an atom or molecule. This is a microscopic picture, however, if all the photons in a bundle are in phase with the same direction of propagation, they are called coherent. When a coherent beam of photons interacts with an uncoupled system, coherent states are generated. Coherence generated in radiofrequency region survives for longer times, and can be further manipulated by RF pulses. This is typically the case in NMR, and this form of spectroscopy rests upon the dominance of coherence. The physical basis for dominance of coherence in NMR and its effects will be explored now.

The nature of spectroscopy changes with the frequency involved, thus RF spectroscopy (10^8 Hz frequency) is different from the more commonly encountered UV-Visible spectroscopy (10^{21} Hz frequency) and so on towards X-rays. NMR occurs in the RF regime and its description is significantly different from spectroscopy at higher frequencies. The origin of this difference can be seen in the Einstein's equation governing rate of stimulated (denoted by A_{fi}) and spontaneous emission (denoted by B_{fi}) between the energy levels separated by ν, in frequency units [15].

$$A_{fi} = \frac{8\pi\hbar\nu_{fi}^3}{c^3} B_{fi} \tag{1.28}$$

where $\hbar$ and c represent the Planck's constant and the velocity of light in vacuum respectively.

In low-frequency region, this equation predicts higher propensity for stimulated emission. This allows for efficient generation of RF pulses on the one hand and restricts

spontaneous emission of spins on the other hand, allowing coherence to dominate in the behavior of the system.

In the low frequency region, where the difference between the energy levels of nuclear spin falls, the frequencies are generated with negligible spread. This allows one to express the RF field as a single photon with a large amplitude,

$$H_{rf} = A\sin(\omega t + \phi) \tag{1.29}$$

where A is the amplitude of the RF field and is a measure of its strength as it determines the influence of RF pulse on an interaction. ω and ϕ represent the frequency and phase of the waveform respectively. Equation 1.28 also implies the longer lifetime of coherent states in the low-frequency region, explaining the longer dephasing time (T_2) for coherent states in the absence of other factors.

Interactions in NMR are manipulated by pulses, which are easy to generate in low-frequency region. An interaction can be removed from a spectrum with suitably designed pulse schemes, an example being J-decoupling in solution-state NMR [13]. In another extreme, interactions getting averaged (by mechanical averaging) can be brought back by means of pulses, termed as recoupling [14]. This behavior is different from other forms of spectroscopy. It is possible due to combination of the following facts:

1. Internal interactions are weak compared to external interactions. Zeeman and RF terms are much stronger than the internal interactions. Except quadrupolar, all internal interactions are magnetic in nature and hence orders of magnitude smaller than electric interactions.

2. The nature of irradiation is also cooperative. Lack of spontaneous emisson and high efficiency of photon generation in low frequency region make large amplitudes of RF field achievable.

3. The phase of the coherent RF field is under control and is produced virtually free

from noise. The phase of the RF field becomes important as the wavelength (in metres) is much longer than the sample volume. The control over the phase allows various ways of manipulating the spins.

In the context of NMR, coherent RF irradiation interacts with energy levels of nuclear spins, and converts population difference into coherence. The small difference between the energy levels of nuclear spins allows longer survival of coherence which can be further manipulated by RF modulation schemes. Thus, multiple-pulse NMR relies upon the dominance of coherence in the low frequency region. The purely quantum mechanical behavior of nuclear spins appears as bulk properties due to dominance of coherence. This feature makes NMR a unique form of spectroscopy, having knitted co-existence of experiments and theory. Experimental results can be understood on theoretical basis upto first order and theoretical deductions can also be rigorously verified experimentally. This has also led to interesting applications like "quantum-computing in NMR" [16, 17] as NMR offers generation and manipulation of "pure-quantum states" in the bulk magnetisation. A recent trend is the optimisation of perturbation scheme to achieve a target state from the initial state in the most optimal way, known as optimal control theory [18, 19].

1.4 NMR: Solids vs liquids

Solution-state NMR spectra of molecules consist of narrow lines, as many broadening mechanisms are averaged (removed from spectra) by rapid isotropic tumbling in GHz frequencies. This leaves only the isotropic chemical shift and the scalar coupling (J-coupling) yielding narrow linewidths determined by residual broadening and field inhomogeneity.

The chemical shift anisotropy of a nucleus is a reflection of its surrounding electronic environment. All other spin interactions are also anisotropic in nature [6] and

this anisotropy is averaged by molecular motion in solution but not in rigid solids. Thus, solids and spatially oriented samples (liquid crystals, bicelles, and cell membranes) have different NMR properties than isotropic solutions which often complicate the study of rigid systems. The unavailability of molecular motions makes anisotropic effect of interactions to appear in full glory, rendering the spectra broad and uninterpretable (if more than one interaction is present which is often the case). Broadening of spectrum in solids appears in shorter T_2, the dephasing time of coherence. The lack of molecular motion reduces the local fluctuations of local field which results in longer T_1, the relaxation time of population. To summarise, signals decay faster in rigid systems to give broad spectrum and population distribution attains equillibrium in longer times, making signal averaging a tedious process.

1.5 Improving the spectrum of solids

The lack of resolution and sensitivity in solids are circumvented through various methods for specific purposes and situations. Two most general methods are described here, one dealing with resolution enhancement and another with sensitivity enhancement.

1.5.1 Magic-angle spinning: MAS

Magic-angle spinning refers to physical rotation of sample at an angle of 54.74° with respect to Zeeman field. It was discovered independently by Andrew [20] and Lowe [21] in 1959 that spinning the sample along this axis has narrowing effect on the spectra. Andrew et al. studied ^{23}Na in a single crystal of NaCl having static linewidth of about 2 kHz. Calculations suggested that isotropic spectra for dipolar coupled systems under MAS can be obtained when spinning frequency surpasses the static width of the spectrum and this technique was only useful for favorable samples having weak dipolar couplings. Dipolar coupling for realistic samples containing ^{1}H and ^{19}F nuclei are quiet strong, and

line narrowing by MAS needed high frequencies which were not achievable at that time. Thus, MAS was not implemented commercially for a long time. In 1971, demonstration on samples having spectra broadened due to CSA revealed isotropic spectrum with spinning sidebands upon application of MAS [22]. Line narrowing was achieved at MAS frequencies lower than the strength of the interaction [22], establishing the effectiveness of MAS, and commercial implementation followed. The different behavior under MAS led to a new classification of spin interactions: homogeneous and inhomogeneous [23].

MAS frequencies are presented in units of kHz in this thesis and denoted by ν_r. The remarkable effect of MAS is shown on the ^{13}C spectrum of histidine in Figure 1.1. The static spectrum is broad and featureless although only 6 resonances are present. Presence of aromatic resonances with large CSA made static spectrum featureless and hence uninterpretable. For smaller number of resonances, interpretable spectrum with sharp features is obtained for samples like glycine. Upon the introduction of MAS, the isotropic spectrum flanked by spinning sidebands but free from CSA broadening results. The position of sidebands from the isotropic peak is given by integral multiple of MAS frequency and they disappear for MAS frequencies higher than the strength of CSA. Larger number of spinning sidebands are obtained at lower spinning frequencies, and the number reduces at higher MAS frequencies. Thus higher MAS frequencies are needed for enhanced resolution. As the strength of CSA is linearly proportional to Zeeman field, higher MAS frequencies are needed on spectrometers with higher fields.

MAS averages the spatial (anisotropic) part of the interaction, the line broadening component. It can again be understood with the example of chemical shift anisotropy. In a powdered sample, the vector of spin angular momentum points in every possible orientation in space, it samples full volume of electron cloud to give rise to chemical shift anisotropy. The axis of MAS makes equal angle with all the three axis of the Cartesian system, and CSA implies unequal components along the three mutually perpendicular axes. Upon spinning the sample along the magic angle, the unequal components of CSA

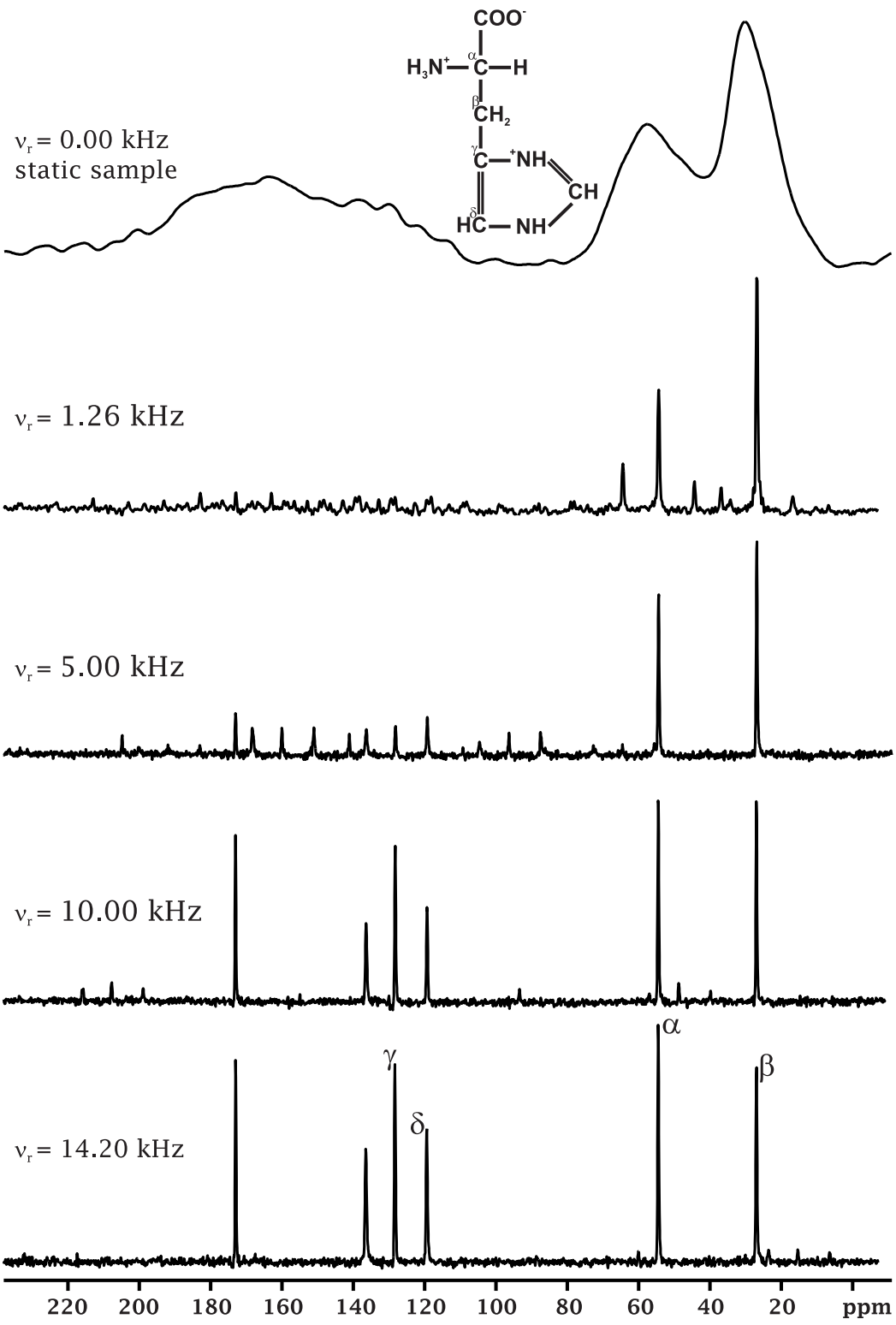

Figure 1.1: Effect of Magic-Angle Spinning on ^{13}C spectrum of histidine. The cross-polarised ^{1}H decoupled ^{13}C spectrum of histidine is acquired with spinning frequencies mentioned in the figure itself. These experiments are performed on a Bruker Avance 500 MHz spectrometer, using a 4 mm triple-resonance probe. The spinning sidebands in these spectrum can be identified by variation of their position with MAS frequency.

interconvert and the average value (isotropic chemical shift) is obtained.

Mathematically, narrowing effect of MAS can be understood on the basis of transformation of interactions of tensorial nature. All anisotropic interactions possess 2^{nd} rank tensorial characteristics in spatial component. The interactions are defined in their Principal-Axis System (PAS), where interactions are diagonal and when transformed to Molecular-Axis System (MAS), they acquire orientation dependence. When tensorial interactions with 2^{nd} rank on spatial part are transformed to Rotor-Axis System (RAS), they acquire $3\cos^2\Theta - 1$ dependence where Θ is the angle of transformation. For an angle of $54.74°$, $3\cos^2\Theta - 1 = 0$ leading to complete averaging of anisotropic interactions.

MAS is limited to interactions of 2^{nd} rank tensors and is ineffective on tensors of higher rank, like 4^{th} rank tensor of 2^{nd} order quadrupolar interaction. As another limitation of the technique, narrowing under MAS for rates smaller than interaction strength is realised when crystallites are not coupled.

1.5.2 Cross polarisation: CP

In the year 1948, Hartmann and Hahn found that when two different nuclei are locked with RF field of same amplitude, polarisation transfers from abundant (high γ) to rare (low γ) nuclei [24]. They called this phenomena as "Nuclear Double Resonance", and later on Waugh's group established it for enhancing sensitivity of rare spins [25, 26].

The energy difference between Zeeman levels and in turn polarisation (population difference) of a nucleus depends upon its gyromagnetic ratio (γ). Thus nuclei having large gyromagnetic ratios (γ_I), like ^{1}H and ^{19}F are more sensitive nuclei while nuclei with smaller gyromagnetic ratios (γ_S), like ^{13}C and ^{15}N, are less sensitive. In accordance with this criteria, ^{1}H and ^{19}F nuclei fall under abundant spins while ^{13}C and ^{15}N are considered rare spins.

The transfer of polarisation takes place through flip-flop terms of the heteronuclear dipolar coupling. These terms are truncated under Zeeman field owing to large separa-

tion in the precession frequency of the two nuclei. When both nuclei are made to evolve with same frequency under RF field, flip-flop terms become active which transfer energy between nuclei. Typical sensitivity enhancement for rare nuclei is given by the order of their gyromagnetic ratios i.e. $\frac{\gamma_I}{\gamma_S}$.

The condition for Hartmann-Hahn match under static condition and MAS is given by the following expressions

$$\nu_{1I} = \nu_{1S}$$

$$\nu_{1I} = \nu_{1S} \pm n\nu_r \tag{1.30}$$

where ν_{1I} and ν_{1S} represent the strength of the applied RF field on the abundant (I) and the rare (S) nuclei. ν_r represents MAS frequency and n is an integer. Thus, "CP-fingers" are obtained under MAS, with their position and separation defined by MAS frequency. Metz et al. discovered that the method becomes more usable under MAS by applying ramp on one of the amplitudes [27].

Besides sensitivity enhancement, another advantage associated with CP is the decay of transferred polarisation to rare spin with the rate constant of abundant nuclei. Flip-flop terms are present for homonuclear dipolar couplings in abundant nuclei which cause fluctuations in local magnetic field to spread among all spins. Thus, abundant spins have smaller rate constant for decay of population. With smaller population decay time, signal averaging can be carried out in a relatively short time.

1.6 Heteronuclear dipolar decoupling in solid-state NMR

Dipolar coupling to the abundant nuclei, heteronuclear dipolar coupling, is the principal contributor to the line width of rare spins in solid state. As this interaction is entirely anisotropic and inhomogeneous, MAS should, in principle average it completely. How-

ever, only spinning the sample does not lead to high-resolution spectrum for rare spins. For spinning samples, a respectable line width is often achieved by RF modulation of the abundant spins, and the modulation scheme is addressed as a heteronuclear dipolar decoupling sequence. A continuous burst of irradiation, called CW scheme, was routinely applied as heteronuclear dipolar decoupling scheme [28].

Figure 1.2 shows the resolution enhancement with CW scheme under MAS for a sample of natural abundance histidine. These experiments are done a Bruker Avance 500 MHz spectrometer, using a 4 mm triple-resonance probe. The spectrum marked with (A) is recorded without RF decoupling on ^{1}H channel and the other spectra (marked with B, C, and D) are acquired with CW decoupling at an RF field of 100 kHz. The MAS frequencies were 14.2 kHz for (A) and (B) spectra which were 10.0 and 5.0 kHz respectively for (C) and (D) spectra.

Even at the MAS frequency of 14.2 kHz, the resolution obtained without decoupling in (A) spectrum (compared to the static spectrum shown in Figure 1.1) is discouraging. A significant enhancement is obtained with CW decoupling, as seen in the (B) spectrum. The resolution enhancement under CW scheme improves with decrease in MAS frequency as evident from the (C) and (D) spectrum, a phenomena which was observed and explained by Ernst et al. [32]. The resonances at 25, 55, 120, and 135 ppm broaden with increasing MAS frequencies. The other two resonances belong to ^{13}C sites not directly bonded to ^{1}H and weaker heteronuclear dipolar coupling arises from spatially distant ^{1}H nuclei. These resonances are not sensitive to ^{1}H decoupling. Resonances appearing at smaller chemical shifts (20-60 ppm) correspond to aliphatic ^{13}C sites which are strongly coupled to directly bonded ^{1}H nuclei, at smallest interatomic distance. A larger dipolar broadening can be observed in the CH_2 system (C_β resonance) owing to the characteristically stronger dipolar coupling and efficiency of decoupling schemes is normally evaluated on these systems. The broadening of the carbonyl and the C_γ resonances arises mainly from their large CSA values which is completely averaged under

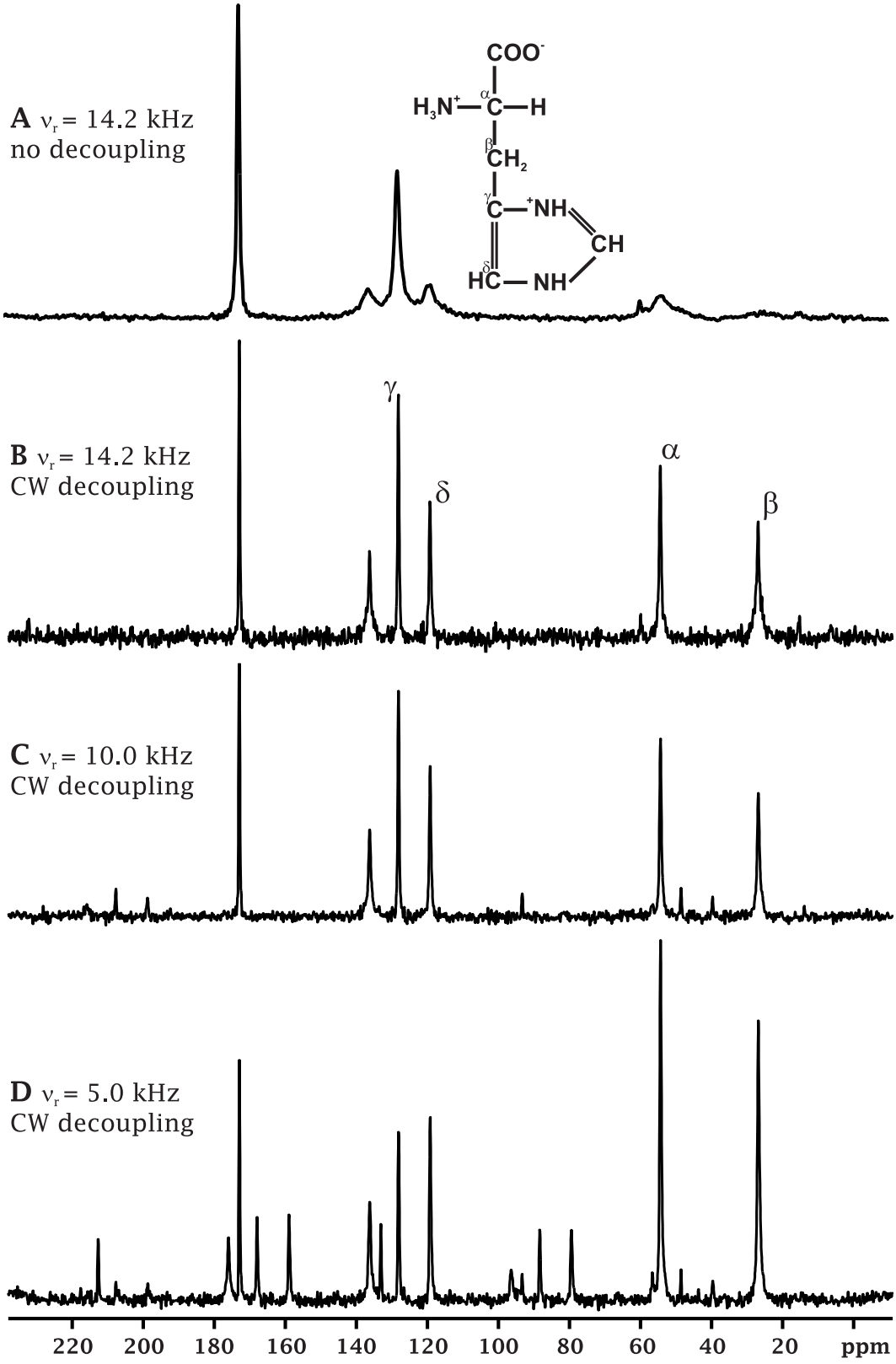

Figure 1.2: Cross-polarised MAS spectrum of histidine showing the resolution enhancement by CW decoupling. The deterioration of efficiency of CW scheme with increase in MAS frequency. The spinning sidebands in these spectrum can be identified by variation of their position with MAS frequency. These experiments are performed on a Bruker Avance 500 MHz spectrometer, using a 4 mm triple-resonance probe.

MAS.

A broader linewidth for CH_2 system compared to that of CH is worth noticing in this set of spectrum. For CH and CH_2 groups having equal bond length, the stronger dipolar coupling for CH_2 system was known for a long time. Dipolar oscillation for CH systems were observed by the group of Ernst [29] and Waugh [30]. Dipolar oscillation frequency of $\sqrt{2}\omega_D$ for CH_2 systems was predicted by group of Waugh [30], where ω_D is oscillation frequency of CH systems. Values confirming these predictions for CH, CH_2, and CH_3 was experimentally observed by Rybaczewski et al. [31]. Thus, CH_3 is more strongly dipolar coupled system than CH and CH_2, but often the anisotropic interactions are partially averaged by prominent methyl rotation. This leaves CH_2 as the most challenging system and decoupling efficiency is evaluated in these systems.

The deterioration of spectral resolution with increase in MAS frequency is a serious disadvantage of the CW scheme as higher MAS frequencies are needed for unambiguous (free from spinning sidebands) and resolved (MAS averages all 2^{nd} rank interactions) spectrum. These advantages of high MAS frequency can be seen in the histidine spectrum (Figure 1.2), where a small number of spinning sidebands appear in the A and B spectra along with the significant resolution enhancement for ^{13}C resonances of the Carbonyl site and another marked with C_γ. A clear demand for efficient decoupling sequences suitable for higher MAS frequencies hence existed, and a breakthrough came from the group of Griffin [33]. They demonstrated linewidth reduction of rare spins by a factor of two or more with a scheme involving two pulses of equal duration and a small phase difference between them. The scheme was called two-pulse phase modulation, TPPM [33].

1.6.1 TPPM scheme

The TPPM scheme consists of two pulses of equal length with a small phase difference and efficient performance of the method involves careful optimisation of both these parameters. This feature of TPPM was outlined in the original report where the optimum

pulse length is generally a range of values around a flip angle of $\approx 180^\circ$ while the general range of optimum phase difference is from 10° to 60°. During the course of work presented in this thesis, the optimum flip angle came out to be $\leq 180^\circ$ while 10°-40° of phase difference was found for optimum performance of TPPM.

Although the optimum performance of TPPM demands accurate setting of experimental parameters, the gain in resolution qualifies it to be the first dedicated method for heteronuclear dipolar decoupling. The CW scheme was demonstrated for J-decoupling [28] and hence it was also attempted for heteronuclear dipolar decoupling. More remarkably, the line width under TPPM decoupling remains reasonably constant with MAS frequency and it was a better choice at higher MAS frequencies. Many heteronuclear dipolar decoupling schemes have been designed by taking TPPM as the building block [34–37, 41].

1.6.2 A survey of heteronuclear dipolar decoupling sequences

TPPM was the first sequence to offer considerable improvement in decoupling efficiency over CW. This scheme consists of two pulses of equal lengths having a phase difference.

Some of the decoupling sequences introduced after TPPM that deserve merit are the following. Gan et al. modulated the amplitude of pulses in TPPM resulting in a scheme called AMTPPM (Amplitude Modulated TPPM) [34]. The study gave some insight into the mechanism of TPPM but AMTPPM did not demonstrate improved performance over TPPM. An improvement of TPPM was introduced by Fung et al. which consisted of TPPM blocks with discretely incremented phases and called small phase incremental alteration, SPINAL [36]. The sequence was originally designed for liquid crystals but it also performed admirably for rigid solids under MAS. Another modification of TPPM with continuous phase modulation termed as Cosine Modulation, CM, was proposed by Paëpe et al. [43–46]. In this approach, square wave pulses in TPPM were replaced by cosine profile with different initial values and time periods generated by automated iteration for

optimum performance. This study was partly successful in unravelling the mechanism of decoupling, but experimental implementation is involved. Gerbaud et al. designed decoupling schemes by convoluting a Gaussian with cosine modulation leading to certain degree of robust performance [47]. Khitrin et al. convoluted many cosine modulations to to enhance the performance of heteronuclear dipolar decoupling [48]. This approach was based on their semi-quantitaive arguments which suggested the need for additional modulations on TPPM for improved heteronuclear dipolar decoupling [48].

An altogether different strategy of symmetry was adopted by Levitt et al. to design heteronuclear dipolar decoupling sequences. Principles of symmetry treats various NMR interactions on the basis of rotational properties exhibited under MAS and RF [12]. As various interactions can be distinguished on the basis of "rotational signatures", pulse sequences can be designed to selectively remove or retain any of them. A set of C-symmtery sequences was demonstrated for heteronuclear dipolar decoupling, but improvement over TPPM was not realised [49]. Riedel et al. attempted incorporation of adiabatic pulses in C-sequences which demonstrated improvement in performance. The performance with this approach is comparable to that of TPPM [50, 51].

A conceptually distinct approach for heteronuclear dipolar decoupling was taken by the group of Ernst. It was demonstrated that a pair of 180° shifted pulses of duration defined by rotor period, named XiX, is effective over TPPM for MAS frequencies over 25 kHz at RF field of 100 kHz [52]. The origin of this sequence could be traced to an attempt by Tekely et al. [53].

A perpetual desire of narrowing the width of resonance in NMR exists and it becomes more relevant in the solid state. A demand for more efficient heteronuclear decoupling schemes than SPINAL exists but the features of easy implementation, consistent performance with MAS frequencies, and immunity to RF inhomogeneity are also desired. Modifications of TPPM with these set of guidelines are presented in this thesis which will be shown to be comparable or more efficient to SPINAL in the range of lower and

intermediate MAS frequencies and XiX in the higher MAS frequencies.

An understanding of heteronuclear dipolar decoupling is necessary to design schemes with improved performance and ease of implementation. The status of understanding of heteronuclear dipolar decoupling in solid-state NMR will be presented now. A brief discussion of the factors hindering development of this area will also be made.

1.6.3 Understanding heteronuclear dipolar decoupling

An interaction is decoupled in NMR when its influence from the evolution of the spin system is removed. Hahn demonstrated the refocussing of chemical shift by a 180° pulse. The phenomenon of refocussing can be understood on the definitive role of external interaction which can force the reversal of evolution of spin system under internal interaction. The sign of spin coefficient is inverted by 180° rotation along the appropriate axis, i.e. $\pm I_z/I_x$ change to $\mp I_z/I_x$ by a 180° pulse applied along y axis. Thus, an echo is formed as if the spin system has not evolved under the chemical shift. Decoupling is thus achieved by repetitive refocussing of corresponding interaction. After refocussing of chemical shift was discovered, variety of schemes has been devised to decouple various internal interactions.

MAS alone is capable of refocussing all 2^{nd} rank tensorial anisotropic interactions. It refocusses CSA completely, giving isotropic spectrum along with spinning sidebands. The form of heteronuclear dipolar coupling Hamiltonian is similar to that of CSA and it should also be averaged under MAS. However, isotropic spectrum with sidebands is not obtained for heteronuclear dipolar coupled systems suggesting that the simple first-order picture of heteronuclear dipolar coupling is not sufficient. Inclusion of higher orders of perturbation treatment was shown to be necessary to understand certain aspects of heteronuclear dipolar decoupling [54].

Isotropic spectrum along with spinning sidebands for a heteronuclear dipolar coupled system was experimentally observed on a sample having isolated pair of ^{15}N nuclei

coupled to ^{1}H spins. The compound was specially synthesized for this purpose where the heteronuclear dipolar coupled pairs were separated from each other by placing them in between a large number of ^{2}H nuclei [32]. This suggested a strong influence of homonuclear dipolar coupling on the heteronuclear interaction. Higher-order terms of heteronuclear dipolar coupling and its cross terms with other interactions, like CSA and homonuclear dipolar coupling, are also present in the spin system and they were proved to be a source of the line broadening [32,55]. Additionally, the presence of homonuclear dipolar coupling poses difficulty in the numerical analysis of the problem [55].

Heteronuclear dipolar decoupling via RF is attained by modulating the spins. Modulation of spins causes their rapid rotation which is capable of averaging the orientation dependent interaction. This was the motivation of applying CW, a continuous burst of RF irradiation on abundant spins to enhance the resolution of rare spins and line narrowing to a certain degree was achieved [28].

1.6.3.1 Difficulty in understanding heteronuclear dipolar decoupling

The development of heteronuclear dipolar decoupling in solid-state NMR is hampered by the inherent difficulty and the interplay of various spin interactions. The shortcomings in the way of understanding the heteronuclear dipolar decoupling will be sketched in this Section.

Heteronuclear dipolar coupled systems under the influence of MAS alone do not give isotropic spectrum, and the resolution achieved is insufficient to resolve and identify even a small number of chemical sites. This can be observed in the histidine spectrum (Figure 1.2) with only 6 chemical shifted ^{13}C resonances. Ineffectiveness of MAS alone on heteronuclear dipolar coupled systems suggested the coupling with other internal interactions. Under CW decoupling scheme, the presence of cross term of CSA with heteronuclear dipolar coupling was shown to be the principal contributor to the line width of rare spins in solids [32,55].

With emergence of TPPM and other sophisticated schemes, several drawbacks of CW decoupling scheme were also noticed. Contrary to expectation, a broadening of spectral lines was observed with increase in MAS frequencies (shown in Figure 1.2), which was explained by the reduction in the rate of spin diffusion which averages the cross terms of heteronuclear dipolar coupling with CSA of the abundant spins [32]. Under XiX decoupling scheme, the cross term of heteronuclear and homonuclear dipolar coupling was found to be the factor determining the line width of rare spins [56]. An understanding of heteronuclear dipolar decoupling is hence involved.

To summarise, a rigorous understanding of spin interactions with higher-order terms and cross terms among various interactions is needed to unravel the mechanism of heteronuclear dipolar decoupling. Results from bimodal Floquet analysis will be presented in the next Chapter which also suggest cross terms of CSA and heteronuclear dipolar coupling contributing to the line width of rare spins in solids.

1.6.4 Interference of MAS and RF field

MAS modulates spatial part of the NMR interactions and application of heteronuclear dipolar decoupling scheme perturbs the spin part of the interaction. Both the techniques introduce time dependence in the system and simultaneous application of both the techniques is expected to cause interference, producing constructive or destructive effect on the spectrum. Dipolar couplings and CSA are averaged under MAS but with suitable RF modulation schemes, they can be reverted in spectrum. This phenomenon is called recoupling which allows estimation of distance and orientation but results in loss of spetral resolution.

The application of CW decoupling scheme at an RF fields strength of ν_1 under MAS at a frequency ν_r can lead to recoupling of dipolar couplings when $\nu_1 = n\nu_r$ with n equal to $\frac{1}{2}$ or 1 [54]. The case of $n = \frac{1}{2}$ leads to homonuclear rotational recoupling (HORROR) [57] and $n = 1$ to rotary resonance recoupling (R^3) [58] which recouples

heteronuclear dipolar couplings.

The HORROR condition is indicated to be good for heteronuclear dipolar decoupling [55]. It is advisable to avoid the later resonance condition by suitably choosing the strength of RF field and the MAS frequency.

1.7 Conclusions

A brief introduction of NMR was presented with an emphasis on the spectroscopy of the rigid solids. Various spin interactions were revisited and their dominance in different circumstances were stated. A physical basis of salient features of NMR was also presented. A universally applicable technique for resolution enhancement, magic-angle spinning and another widely used technique for sensitivity enhancement, cross-polarisation, pertinent to solid-state NMR, were discussed.

In the later half of this Chapter, the factors enhancing the resolution of rare spins dipolar coupled to abundant spins in the rigid solids were outlined. The particular emphasis was on the irradiation schemes applied on the abundant spins, heteronuclear dipolar decoupling sequences. A summary of the existing schemes with their performance was presented.

1.8 Description of this thesis

The existing heteronuclear decoupling sequences and their performance can be summarised in the following lines in order to state the context of this work.

- The efficiency of the classical method, CW scheme, deteriorates with MAS frequency and it becomes largely ineffective at higher MAS frequencies, $\nu_r \geq 15$ kHz.

- TPPM delivers resolution enhancement over CW scheme by a factor of two and the resulting linewidth remains unaffected with MAS frequency. The optimum perfor-

mance under TPPM scheme is realised after careful optimsation of experimental parameters. Thus, its implementation is demanding.

- SPINAL scheme was designed by taking TPPM as the building block and incorporating phase modulation over it. This method was shown to deliver an enhanced performance over TPPM. It was also known to be insensitive to certain experimental parameters, facilitating its implementation [45]. The design principle of this method was based upon the irradiation spectrum. The underlying principle of the incorporation of supercycling in the design is not clear.

- XiX scheme was shown to be far superior to TPPM at higher MAS frequencies, ν_r $>$ 25 kHz, but the RF field strength required is usually much larger than 100 kHz, making it less useful, especially for heat-sensitive samples.

For heteronuclear dipolar decoupling, schemes delivering enhanced performance and a ready to use implementation protocol are desired. Another desired feature is the effective performance at high MAS frequencies. Effectiveness of decoupling schemes at low RF field strength is desired for sensitive samples.

This thesis presents improved heteronuclear dipolar decoupling sequences for applications in solid-state NMR. These sequences will be shown better than or equally efficient to SPINAL in the lower and intermediate MAS frequencies and to XiX, at higher MAS frequencies. Additionally, these sequences are robust with respect to various experimental parameters facilitating an easy implementation. The design principle of these sequences will be explained in the next Chapter and their experimental demonstrations will follow the later Chapters of this thesis. The outline of this thesis is as follows:

- **Chapter 2** presents design principle of the new schemes for heteronuclear dipolar decoupling. An intuitive picture derived from a thorough theoretical analysis [55] is also presented.

- **Chapter 3** covers experimental investigation of efficiency of these schemes on spin $\frac{1}{2}$ nuclei in rigid solids. It also presents the investigation of regions of good performance for these schemes and influence of MAS frequency and homonuclear coupling on their performance. An investigation of SPINAL series is also presented which correlates the design with the performance. A study of heteronuclear dipolar schemes for J-decoupling in isotropic solutions is also presented.

- **Chapter 4** consists of experimental investigation of the newly designed heteronuclear dipolar decoupling schemes on spin $\frac{1}{2}$ nuclei in liquid crystal phase.

- **Chapter 5** contains experimental demonstration of new schemes for heteronuclear dipolar decoupling on abundant spin $\frac{1}{2}$ nuclei to enhance the resolution in the spectrum of a half-integer spin quadrupolar nucleus.

- **Chapter 6** presents a study of heteronuclear dipolar decoupling schemes on spin $\frac{1}{2}$ nuclei in soft condensed matter systems.

Chapter 2

Improved sequences for heteronuclear dipolar decoupling in solid-state NMR

High-resolution spectrum of rare spins in solid-state NMR is routinely obtained with the combined use of MAS and suitable RF modulation scheme on the abundant nuclei. An appropriate RF modulation scheme is applied to decouple the dipolar couplings to the abundant nuclei and is called heteronuclear dipolar decoupling sequence. Decoupling improves the resolution of rare-spin spectrum as resonances appear with narrower frequency distribution which is naturally followed by enhanced sensitivity. Efficient heteronuclear dipolar decoupling sequences are needed to obtain resolved spectrum of ^{13}C, ^{15}N, and ^{31}P nuclei when they are coupled to the omnipresent ^{1}H nuclei in biomolecules, drugs, and many other systems.

Many decoupling sequences have been designed and investigated over the years, among them mention of CW [28], TPPM [33], SPARC [35], SPINAL [36], and XiX [52] has to be made to sketch the progress in this area. A brief description of development in the area of heteronuclear dipolar decoupling is presented in Chapter 1 and more comprehensive coverage can be found in the recent reviews [59, 60].

A demand for heteronuclear dipolar decoupling schemes with features of easy implementation and robustness exists, the efficiency of which can be comparable to SPINAL at

lower MAS frequencies or XiX at higher MAS frequencies. With this set of requirements, improved sequences are designed and their experimental demonstrations are presented in this thesis.

This Chapter presents improved heteronuclear dipolar decoupling sequences for enhancing the spectral resolution in the NMR of rare spins in rigid systems. Their improved performance under various experimental conditions constitutes the rest of this thesis. The methods designed are modifications of TPPM.

2.1 Design of new decoupling sequences

The design principles of the various new decoupling schemes will be outlined in this Section to frame the discussion in later parts of this thesis. To facilitate this, design of a few of the existing methods will be outlined.

CW decoupling involves application of a continuous burst of RF on abundant nuclei. TPPM was the first sequence dedicated for heteronuclear dipolar decoupling. The sequence consists of two pulses of equal length (denoted by τ) having a small phase difference (denoted by ϕ). This schematic can be represented as $[\tau_{\phi}\ \tau_{-\phi}]$.

Many effective schemes for heteronuclear dipolar decoupling were designed by modifying the basic TPPM block. Fung et al. designed SPARC series of decoupling sequences by cycling the phase of TPPM pair. Notating the TPPM block as Q and defining $\overline{Q}$ as $[\tau_{-\phi}\ \tau_{\phi}]$, SPARC-2, SPARC-4, and SPARC-8 are obtained as $Q\overline{Q}$, $Q\overline{Q}\overline{Q}Q$, and $Q\overline{Q}\overline{Q}QQ\overline{Q}QQ\overline{Q}$ respectively. These cycling schemes were inspired from the work on J-decoupling in solution state NMR by Levitt et al. [42]. In liquid crystals, SPARC series yielded certain degree of spectral enhancement over TPPM.

SPINAL is another scheme designed by Fung et al. and is designed by incrementing the phase of TPPM pairs followed by supercycling. The basic SPINAL-8 scheme can be notated as $[\tau_{10}\ \tau_{-10}]\ [\tau_{15}\ \tau_{-15}]\ [\tau_{20}\ \tau_{-20}]\ [\tau_{15}\ \tau_{-15}]$. Taking phase vs the occurrence in the series, this profile would resemble three-quarter of a Gaussian. Taking SPINAL-8

block as Q and defining $\overline{Q}$ as $[\tau_{-10}\ \tau_{10}]\ [\tau_{-15}\ \tau_{15}]\ [\tau_{-20}\ \tau_{20}]\ [\tau_{-15}\ \tau_{15}]$, higher members of SPINAL series were designed by cycling the phase in the same way as was done for SPARC series, and this cycling was called supercycling. For liquid crystal sample, SPINAL series of sequences delivered spectral enhancement over SPARC, and although this series was designed for liquid crystals, it was also found efficient for spinning samples. Efficient performance and ease of use over TPPM led to the widespread popularity of SPINAL-64 [55].

XiX is another scheme of two pulses, but phase difference is set to 180° and optimum pulse length is a function of rotor period. Thus, it can be notated as $[\tau_0^r\ \tau_{180}^r]$, where "r" in the superscript denotes the rotor period dependence of pulse length.

2.1.1 Improved sequences for heteronuclear dipolar decoupling: SW$_f$-TPPM

This thesis introduces improved methods for heteronuclear dipolar decoupling in solid-state NMR. The first method was designed by tangentially sweeping the pulse length (defining the frequency of phase modulation) of TPPM, and the method was named SWept-frequency TPPM, SW$_f$-TPPM. SW$_f$-TPPM consists of eleven TPPM pairs with pulse length varied tangentially and can be represented as $[0.78\tau_\phi\ 0.78\tau_{-\phi}]\ [0.86\tau_\phi\ 0.86\tau_{-\phi}]\ [0.94\tau_\phi\ 0.94\tau_{-\phi}]\ [0.96\tau_\phi\ 0.96\tau_{-\phi}]\ [0.98\tau_\phi\ 0.98\tau_{-\phi}]\ [1.00\tau_\phi\ 1.00\tau_{-\phi}]\ [1.02\tau_\phi\ 1.02\tau_{-\phi}]\ [1.04\tau_\phi\ 1.04\tau_{-\phi}]\ [1.06\tau_\phi\ 1.06\tau_{-\phi}]\ [1.14\tau_\phi\ 1.14\tau_{-\phi}]\ [1.22\tau_\phi\ 1.22\tau_{-\phi}]$. The duration of the central pulse pair (τ) is defined and the tangential frequency sweep is achieved by the multiplicative factor to τ. A schematic of the design is presented in Figure 2.1.

For spin $\frac{1}{2}$ rare nuclei, SW$_f$-TPPM offers robust performance under MAS [37, 39] which is presented in Chapter 3. Spectral enhancement of liquid crystal samples is achieved under static conditions with SW$_f$-TPPM scheme [38, 39] and these studies are presented in Chapter 4. SW$_f$-TPPM also offers intensity enhancement and robust

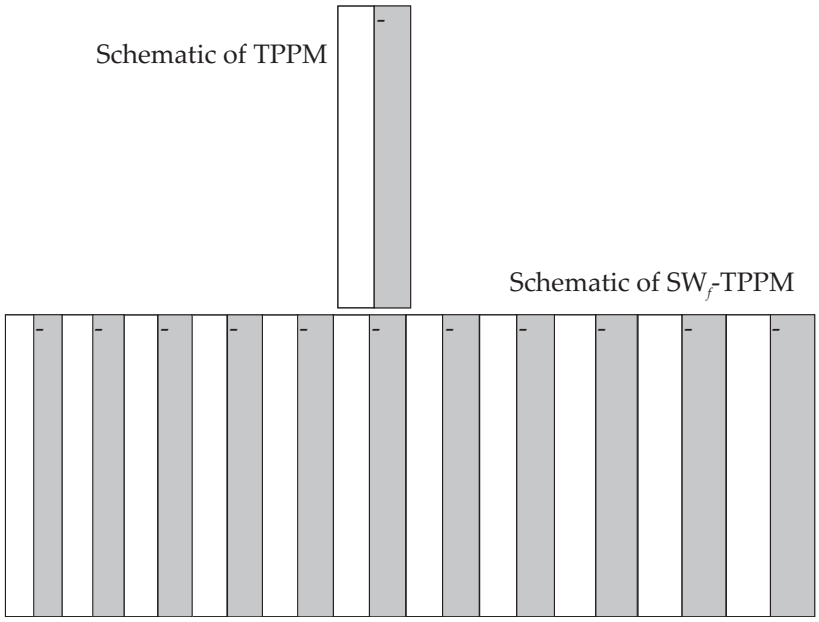

Figure 2.1: TPPM scheme, two pulses of equal duration with a small phase difference is shown on the top. The SW$_f$-TPPM decoupling scheme consists of 11 TPPM blocks with pulse length increased tangentially. Pulse durations are mentioned as a multiplying factor to the central TPPM block and the tangential profile is maintained by these factors.

performance for half-integer spin quadrupolar nuclei under MQMAS scheme [40], which will be covered in Chapter 5.

A pulse length corresponding to flip angle of 180° normally delivers optimum performance under SW$_f$-TPPM decoupling scheme. The optimum value of phase difference (2ϕ) lies in the region of 10°-50°.

The motivation for the incorporation of tangential frequency sweep to enhance the performance of TPPM will be explained after presenting a semi-quatitative understanding of its efficiency.

2.1.2 A semi-quantitative understanding of TPPM

An understanding of reason(s) of decoupling efficiency of TPPM is a primary requirement to improve its performance. With a completely numerical approach, group of Emsley earlier derived the cosine modulation of phase as a means to improved decoupling [46].

The first term in the Fourier expansion of phase modulation (in TPPM) is $\frac{4}{\pi}\sin(\omega_c t)$. In the rotating frame of phase-modulated sequences, the RF Hamiltonian is given by

$$H_{rf} = \omega_1 \left\{ \sum_i I_x^i \cos(\phi(t)) + \sum_i I_y^i \sin(\phi(t)) \right\} \tag{2.1}$$

An analysis of the case where the RF phase $\phi(t)$ is $a\cos(\omega_c t)$ will be done, a and $\omega_c(t)$ respectively representing the modulation depth and frequency of the phase modulation. The analysis for other sinusoidal modulation patterns will only differ slightly. The spin system Hamiltonian consisting of chemical shift of an S spin and many I spins, the heteronuclear ($I_i S$) and homonuclear ($I_i I_j$) terms is given by

$$H_{sys} = \omega_s S_z + \sum_i \omega_i(t) I_z^i + \sum_i \omega_{iS}(t) 2 S_z I_z^i + \sum_{i,j} \omega_{I,j}(t)[I_z^i I_z^j - (I_x^i I_x^j + I_y^i I_y^j)] \tag{2.2}$$

where the time dependence is arising from MAS, the period of which is given by τ_r.

The RF Hamiltonian becomes time independent, $\omega_1 I_x$, in a frequency-modulated frame defined by $T = \exp(-i\phi(t)\sum_i I_z^i t)$, but the I spin offset becomes $(\omega_i(t) - \dot{\phi}(t))$. Often in heteronuclear decoupling of rotating solids, the RF Hamiltonian is large relative to its offset which allows transformation into the frame defined by the large term, given by $T' = \exp(-i\omega_1 \sum_i I_z^i t)$. The heteronuclear decoupling by phase modulation happens in this frequency-modulated interaction frame. Excluding this frequency modulation, the analysis thus, far is identical to CW decoupling [32]. In this frame, the only difference from CW case is shown by the I spin offsets, which are given by

$$\left(\omega_i(t) - \dot{\phi}(t)\right)\left(I_z^i \cos(\omega_1 t) + I_y^i \sin(\omega_1 t)\right) \tag{2.3}$$

For cosine modulation, $\dot{\phi}(t) = -a\omega_c \sin(\omega_c t)$ where the modulation frequency is often close, if not equal to ω_1. When the equality holds at resonance, the average Hamiltonian over the nutation period $\tau_1 = \frac{2\pi}{\omega_1}$ is of the form $-\frac{a\omega_c}{2} I_y$, which looks like an

additional RF term. The amplitude of this term is defined by $-\frac{a\omega_c}{2}$ and will be referred to as ω_1^p.

A second averaging about this term will be performed which is justified by the large time scale separation between τ_r and τ_1 (corresponding to ω_1^p) given by $\tau_r \gg \tau_1$. The case of $\omega_1^p = \frac{1}{2}\omega_r$ leads to recoupling of homonuclear dipolar coupling under MAS by the HORROR condition [57] which leads to efficient spectral diffusion. Earlier studies established the connection between enhanced spectral diffusion over the network of abundant spins and improved efficiency of heteronuclear dipolar decoupling [46, 54]. Efficiency of all phase-modulated schemes over CW decoupling can be accounted by the reintroduction of the homonuclear dipolar coupling among abundant spins at the HORROR conditions.

The improvement in the decoupling efficiency of TPPM can be made by making the HORROR condition broadbanded. The conventional HORROR condition was made broadbanded in the DREAM (Dipolar Recoupling Enhancement through Amplitude Modulation) sequence by amplitude modulation [61]. A simple approach of sweeping though the HORROR condition in the most efficient manner was borrowed from adiabatic methods. Adiabaticity is known in NMR before the advent of Fourier transform in NMR. In other words it was known before the birth of pulsed NMR. Before the discovery of Fourier transform, a resonance was detected by sweeping the frequency through it. The adiabatic sweep through the resonance was found to be most efficient way of acquiring the spectrum, where the rate of frequency sweep was faster away from the resonance and slower passage was adopted close to the resonance. Tangential variation was found to be the intuitive adiabatic function.

Variation of modulation depth a or the modulation frequency ω_c can achieve adiabatic sweep in TPPM. SPINAL series of sequences was designed by varying a [36], the other parameter, ω_c, was swept tangentially to design SW_f-TPPM. The justification of adiabatic sweep was deduced by Leskes et al. [55] in a theoretical analysis using bimodal

Floquet theory. At a later stage, decoupling schemes were designed with enhanced adiabatic sweep, which will be presented towards the last Section.

A clarification about HORROR as the decoupling condition has to be made. The HORROR condition was proposed to be accountable for improved decoupling efficiency, the efficient performance of phase modulated decoupling schemes is often realised away from the HORROR condition [55]. The quantitative analysis by Leskes et al. using bimodal Floquet approach lead to the general decoupling condition for phase modulated decoupling schemes, but the adiabatic sweep through this decoupling condition was also achieved by SW_f-TPPM scheme. A description of their analysis will be presented in a later Section.

2.1.3 Characterisation of the decoupling sequences

One of the characterisation of decoupling sequences was made on the basis of power spectrum which conveys the distribution of available power into various available frequency components. Taking $f(\tau)$ as the function describing the modulation, its discrete Fourier-transformation is given by [62]:

$$F(\nu) = N^{-1} \sum_{\tau=0}^{N-1} f(\tau) e^{-i2\pi(\nu/N)\tau} \tag{2.4}$$

The square of the Fourier coefficients, $|F(\nu)|^2$, of a modulation scheme is plotted against frequency to represent the corresponding power spectrum. It can be of direct consequence if the system behaves linearly with frequency, which is often not true in NMR. In the intuitive and semi-quatitative arguments of Fung et al. [48], the multi-frequency power spectrum for SPINAL series was suggested to be the cause of its improved performance over TPPM. For SW_f-TPPM and its analogues, power spectrum represents the modulation frequencies generated by the variation of pulse length. Power spectrum of SW_f-TPPM was compared with TPPM and SPINAL-64, which is shown in

Figure 2.2 with time profiles of phase and pulse durations shown in the inset.

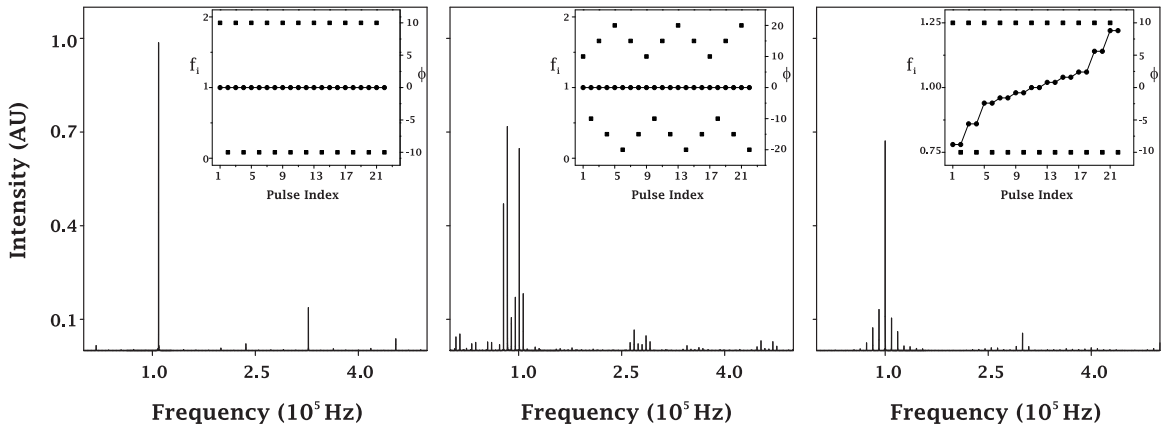

Figure 2.2: Power spectrum of (a) TPPM, (b) SPINAL-64, and (c) SW$_f$-TPPM sequence with $\nu_1 = 100$ kHz, pulse duration corresponding to flip angle of 165°, and phase difference $2\phi = 20°$. For SPINAL-64, the prescribed values of phases were taken with starting phase of 10°. The sampling time was 1 μs. The insets of each plot shows time domain (•) and phase profile (■) of a set of eleven pairs of pulses for each of the sequences.

Like SPINAL-64, SW$_f$-TPPM also contains additional frequency components in its power spectrum but with a more normal distribution. The optimal distribution for efficient decoupling is far from obvious and there one is inclined to prefer uniform or normal distribution.

2.2 Theoretical understanding of SW$_f$-TPPM

The dominance of coherence in NMR was explained in Section 1.3, where the simplification of spectroscopy by this phenomenon and the feasibility and implementation of multiple-pulse NMR was discussed. The time evolution of non-interacting spins in multi-pulse experiments is extremely simple where the evolution of a single spin can be calculated by taking pulses as rotation operators. In the case of isotropic solutions, the averaging of large anisotropic interaction by motional averaging leads to survival of isotropic interaction of significantly smaller magnitude and single-spin calculations hold good. The averaging of J-coupling was understood on the basis of single-spin calcula-

tions and the analysis also suggested ways to improve the decoupling schemes [13].

The analyses of multiple-pulse schemes on rotating rigid solids is involved. The assumption of non-interacting spin is broken in dipolar coupled system as homonuclear dipolar coupling between pairs of spins does not commute and this complicates the analysis of both heteronuclear and homonuclear dipolar coupled systems. The analysis of quadrupolar systems is made complicated as the internal interaction is often orders of magnitude larger than the strength of the RF field. The presence of two sources of time dependence in multiple-pulse experiments of spinning solids makes their analysis complicated.

A simple way to deal with time dependence in solids is by the average Hamiltonian theory, where the average of modulated anisotropic interactions is taken over the cycle time imposed by the modulation source [63]. Thus, averaging of the anisotropic interaction of certain strength demands larger amplitude of modulation. This scheme is insufficient for systems having two periodicities of incommensurate time scales. Thus, it can not handle the general scenario of RF perturbation on spinning samples.

The problem of two periodicities is general in the NMR of solids where RF schemes and MAS are often applied simultaneously. The scenario of commensurate time scales is seldom met and both time dependences have to be dealt with explicitly. The application of phase-modulated heteronuclear dipolar decoupling (RF) schemes on spinning samples is often done on unrelated time scales and integral ratios of these periodicities are known to interfere. Thus, a more elaborate theoretical treatment is needed to understand phase-modulated heteronuclear dipolar decoupling schemes.

A fitting technique to examine time dependence of systems with many periodicities, Floquet theory in solid-state NMR, was pioneered by Vega [64, 65] and Meier [66, 67]. Vega and coworkers applied this tool to understand and improve homonuclear dipolar decoupling schemes [65]. Ernst and coworkers used it to explain some features of heteronuclear dipolar decoupling [54, 56] and developed a simplified version of this ap-

proach in this process [68]. Floquet theory involves transformation of time dependent systems into frequency domain where periodicities appear in respective frequencies and their multiples. The spin system is described in the form of an infinite matrix where eigenstates of various Hamiltonians appear in the diagonal whereas the off-diagonal elements represent the terms of Hamiltonian connecting these eigenstates. The time dependence arising from modulations of incommensurate scales is described by modes, where a mode represents the basic frequency of a modulation and its multiples. Thus, bimodal treatment is needed to describe the spin system under combined influence of MAS and RF. The effect of periodic schemes on the spin interactions is calculated exactly by diagonalisation of the Floquet matrix or approximate solutions are achieved by suitable perturbation treatment.

An extensive theoretical analysis of heteronuclear dipolar decoupling under MAS was undertaken by Leskes et al. [55]. Bimodal Floquet theory was applied to the spin system and the study explained the efficiency of phase modulation for heteronuclear dipolar decoupling. The decoupling conditions explored earlier by Ernst et al. [54, 56] and some results of Paëpe et al. [46] were also reproduced. This study unified the understanding of heteronuclear dipolar decoupling to deliver an intuitive picture and concrete conclusions. Additionally, the adiabatic frequency sweep in SW_f-TPPM was found to be the source of robustness. It also explained the results of many experimental attempts. The complete treatment is given in the original report [55]. The results are reproduced in this Section with bare essentials of the treatment.

2.2.1 Bimodal Floquet theory of heteronuclear dipolar decoupling under MAS

A spin system is taken with various interactions, namely chemical shift, heteronuclear dipolar couplings, and homonuclear dipolar couplings. In the notation of Leskes et al. the equation describing the spin system with phase-modulated decoupling in the frame

of rotor is given by

$$H(t) = \sum_a \Delta\omega_a I^1_{0,a} + \sum_{n,a} \sigma_a g_{n,a} I^1_{0,a} e^{in\omega_r t} + \sum_{n,a} \omega_a G_{n,a} I^1_{0,a} S^1_0 e^{in\omega_r t}$$

$$+ \omega_1(\epsilon_{+1}(t) I^1_1 + \epsilon_{-1}(t) I^1_{-1}) + \sum_{n,a<b} \omega_{ab} G_{n,ab} I^2_{0,ab} e^{in\omega_r t} \tag{2.5}$$

where the first and second term represent respectively the isotropic chemical shift and associated anisotropy of the abundant spins, the labels I and S are used for abundant and rare spins respectively. The third and fifth term represent respectively the heteronuclear and homonuclear dipolar coupling among spin pairs. g and G represent the geometric factors of corresponding interactions, arising from their orientation dependence. Phase-modulated irradiation scheme applied on abundant spins is represented in the fourth term where ω_1 represents the amplitude of RF field, and the ϵ-coefficients in the this term come from the phase modulation. The basic TPPM block can be deconvoluted into two fields: a small phase-modulated component and the large time-independent (in the interaction frame of the RF) component, a diagrammatic representation being shown in Figure 2.6. The large component is similar to CW scheme and is taken along y-axis in the treatment.

In the laboratory frame, the Hamiltonian is decomposed into two parts, arising from the eigenstates (α and β) of the rare spin (S_z). The difference in these Hamiltonians determines the line width of rare spins. The purpose of the RF irradiation is to make the two Hamiltonians equivalent.

The system is transformed into the interaction frame of the RF, the frame rotating with the cycle time of TPPM and this cycle time is equivalent to RF field for the pulse length of 180°. This transformation removes the large static component of TPPM scheme. In this frame, the time-dependent component arising from phase modulation remains and its analysis should explain the efficiency of phase modulation. The transformation of the spin system in this interaction frame led to Hamiltonians of the form,

$$H^{\pm}(t) = \sum_{m,n,k,a} \Delta\Omega^{\pm}_{n,a} d^1_{m,k} I^1_{m,a} e^{in\omega_r t} e^{ik\omega_c t} + \sum_{m,k} \omega_1 \epsilon_{m,k} I^1_m e^{ik\omega_c t}$$

$$+ \sum_{m,n,k,a<b} \omega_{ab} G_{n,ab} d^2_{m,k} I^2_{m,ab} e^{in\omega_r t} e^{ik\omega_c t} \tag{2.6}$$

where $\Delta\Omega^{\pm}_{n,a}$ represents the following coefficients:

$$\Delta\Omega^{\pm}_{n,a} = \Delta\omega_a \delta_{n,0} + \sigma_a g_{n,a} \pm \frac{1}{2} \omega_a G_{n,a} \tag{2.7}$$

The term of $\Delta\Omega^{\pm}_{n,a}$ creates differences in the Hamiltonians. The decoupling pulse scheme must create appropriate $\epsilon_{m,k}$ coefficients which can remove the influence of this term. The equations of the spin system are transformed in the Floquet space to determine the evolution and to derive the decoupling conditions. The influence of II couplings was ignored in deriving the decoupling condition and its effect on the decoupling condition will be investigated at a later stage.

The Hamiltonian containing the line width contributions under CW decoupling in Floquet representation is given by

$$\tilde{H}^{(CS-IS)(\pm)}_{eff} = -\frac{1}{2} \sum_{a,n\neq 0} \Delta\Omega^{\pm}_{n,a} \Delta\Omega^{\pm}_{-n,a} \frac{q\omega_c}{n^2\omega_r^2 - q^2\omega_c^2} I_y \tag{2.8}$$

which arises from correlation of CSA and heteronuclear dipolar coupling with themselves and with each other. q is incorporated here to give a unified treatment for TPPM and its variants and is defined as the ratio between RF field intensity along y-axis (ω_{int}) and the cycle time of the sequence (ω_{int}), i. e. $q = \frac{\omega_{int}}{\omega_c}$. ω_{int} is very close to ω_1, the actual RF field strength. This equation clearly indicates the presence of spin components along the time-independent component of the RF field which can not be averaged under CW scheme.

The effective Hamiltonian pointing towards I_y terms can only be cancelled by RF

terms pointing towards x and z. The exact magnitudes of x and z coefficients of the decoupling scheme are governed by the values of RF phase and pulse durations of the decoupling sequence. Thus, the first decoupling criterion is the elimination of I_y terms in Equation 2.8 by optimisation of the RF parameters. This decoupling condition can be seen in the simulated contour plots for TPPM and SW_f-TPPM displayed in Figure 2.3. The vertical band of efficient decoupling in both these plots corresponds to the first decoupling condition. The intensity of a ^{13}C spin dipolar coupled to five ^{1}H spins is numerically calculated with SPINEVOLUTION package [69]. The spatial coordinates and the NMR parameters of the spin system were also provided with the simulation package. These contour plots represent the decoupling efficiency of TPPM (left) and SW_f-TPPM (right) as functions of RF field strength (ν_1) and phase difference (2ϕ), along the x and y axes respectively. The lighter areas in these contours represent efficient decoupling, and SW_f-TPPM scheme delivers efficient performance uniformly over a larger range of parameters. As in the theoretical analysis, homonuclear dipolar couplings between ^{1}H spins are turned off in the simulation. The effects of incorporation of homonuclear coupling in explained later in this Section and some simulations of these effects are presented in Chapter 3. It is sufficient to know that incorporation of homonuclear interaction does not shift the position of resonances observed in this contour and it merely broadens the areas of efficient decoupling.

The decoupling condition in Equation 2.8 does predict the achievable high resolution under TPPM, but does not address the dependence on the RF inhomogeneity. The effective Hamiltonian along y varies as a function of crystallites and is also indirectly affected by the strength of CSA and heteronuclear dipolar coupling. This decoupling condition is not universal and is a local effect. Localised nature of decoupling condition of Equation 2.8 suggests experimental optimisation of decoupling efficiency for each case. A spread in the decoupling condition, due to variations in magnitudes of interactions and their orientations can exist, is a contributer to the line width of solids. The analysis of

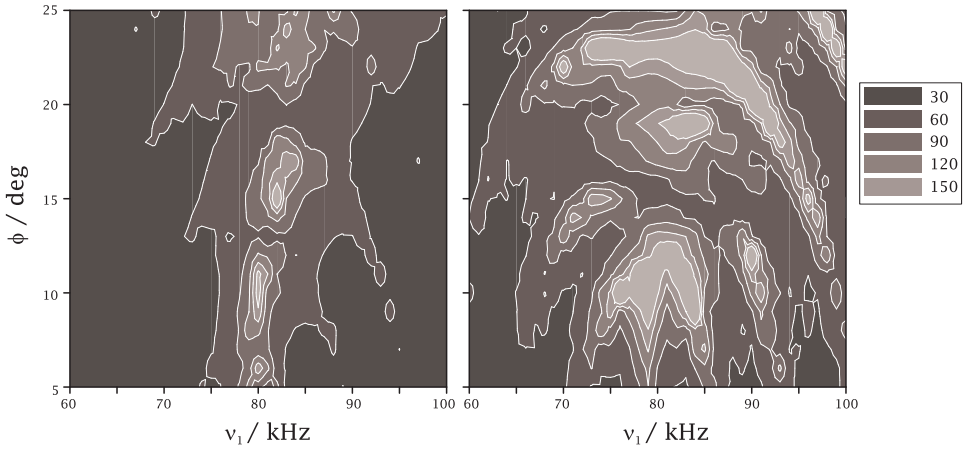

Figure 2.3: Simulated contour plots of intensity of ^{13}C resonance of a CH_5 spin system taken from an isobutyl skeleton. The contour plots on the left and right are obtained by applying TPPM and SW_f-TPPM schemes respectively on ^1H spins, where RF field and phase of these schemes are varied along the x and the y axis respectively. The RF field is varied from 60.0 to 100.0 kHz with a resolution of 1.0 kHz while the variation of phase difference is from 5° to 25° with step size of 1°.

off-resonance also suggested shifting of decoupling condition which can result in distribution of chemical shift of abundant spins to broaden the rare spin spectrum. Thus, an efficient design of the method is needed which can cover the variation and the spread of the decoupling condition, predicted by Equation 2.8.

An effective way to average the influence of the effective Hamiltonian in Equation 2.8 on α and β subspace of spins is to make the $\epsilon_{x/z}$ terms time dependent and sweep their values adiabatically through the adiabatic condition. It can be achieved by changing the RF field strength (ν_1), phase difference (2ϕ), or cycle time (2τ) of the basic TPPM block. SPINAL series was designed by modulating the phase difference of TPPM blocks while SW_f-TPPM was designed by adiabatically sweeping the modulation frequency of the same basic unit. Compared to TPPM, the performance of both these methods is less dependent on experimental parameters while the adiabatic approach of SW_f-TPPM can explain its superior robustness.

The frequency of phase modulation schemes as well as that of MAS influences the first decoupling condition, where the earlier assists the heteronuclear dipolar decoupling, the later leads to broad lines in the spectrum of rare spins. These effects can be seen in the

contour plots of Figure 2.3 as the approximately circular bands of efficient and poor decoupling performance for these schemes.

Another condition for line narrowing is to design schemes with such RF parameters that generate $k\omega_c$ bands which cross the first decoupling condition. Crossing of these two bands generates an area of extreme decoupling which is insensitive to ω_1 variation. The additional requirements for this condition is that the $k\omega_c$ bands are formed by large enough off-diagonal elements which can override the broadening influence of $n\omega_r$ bands. This condition becomes important for SW_f-TPPM as cycle time is reduced in the process of sweep.

The influence of homonuclear dipolar couplings between ^{1}H spins in heteronuclear decoupling is evaluated by measuring its influence on the phase modulated schemes. Since homonuclear dipolar coupling is unaffected by the $\pm$ subscript of Floquet Hamiltonian, it can equalise the corresponding eigenvalues giving rise to line broadening. The interference of MAS and RF can lead to degeneracy conditions defined by,

$$m\epsilon_{0,0} = n\omega_r + k\omega_c \tag{2.9}$$

where m, n, and k represent integral values and $\epsilon_{0,0}$ arises from the perturbation scheme. An area of efficient decoupling is achieved for the HORROR condition where $m = 2$ and $k = 0$. This condition might be interesting to study but implementation is involved.

2.3 Analogues of SW_f-TPPM

Tangential frequency sweep of modulation frequency of TPPM is the major reason for the superior performance of SW_f-TPPM. Following this, various sweep profiles were designed and tested for their performance. The design principles of these schemes are explained here and their experimental comparison is presented in the next Chapter.

The numbers multiplying τ in SW_f-TPPM scheme provide control over the profile of

the sweep and a recipe to generate new sequences. Many sweep profiles were designed with qualitative difference in their power spectrum.

The profiles of the new SW_f-TPPM analogues and their power spectra are given in Figures 2.4 and 2.5 in the left and right columns respectively. The numbers plotted on the ordinate in the left column of Figures 2.4 and 2.5 are the multiplicative factors (denoted by f_i) that determine the profile. The numerical values are given in Table 2.1.

Table 2.1: Pulse durations for various SW_f-TPPM analogues.

#	SW_f-TPPM	SW_f^{inv}-TPPM	$SW_f^{tan_1}$-TPPM	$SW_f^{tan_2}$-TPPM	SW_f^{1/τ_1}-TPPM	SW_f^{1/τ_2}-TPPM	SW_f^{τ}-TPPM	SW_f-$TPPM_6$
1	0.78	0.67	0.65	0.742	0.900	0.800	0.75	0.85333
2	0.86	0.71	0.75	0.789	0.916	0.833	0.80	0.96
3	0.94	0.77	0.85	0.830	0.930	0.870	0.85	0.98667
4	0.96	0.83	0.90	0.868	0.950	0.909	0.90	1.01333
5	0.98	0.91	0.94	0.903	0.970	0.952	0.95	1.04
6	1.00	1.00	0.96	0.936	0.990	1.000	1.00	1.14667
7	1.02	1.11	0.98	0.968	1.010	1.053	1.05	
8	1.04	1.25	1.00	1.000	1.030	1.111	1.10	
9	1.06	1.43	1.02	1.031	1.050	1.190	1.15	
10	1.14	1.67	1.04	1.063	1.100	1.250	1.20	
11	1.22	2.00	1.06	1.097	1.122	1.333	1.25	
12			1.10	1.131				
13			1.15	1.170				
14			1.25	1.211				
15			1.35	1.258				

These SW_f-TPPM variants are designed by varying the pulse length of TPPM pairs in various ways. A summary of obtaining f_i of SW_f-TPPM variants will be described where i denotes the occurrence of the TPPM block.

- The inverse function, $f_i = 1/x_i$ where x_i is given by $1.5 - 0.1 \times (i-1)$ is adopted to design SW_f^{inv}-TPPM.
- $SW_f^{tan_1}$-TPPM and $SW_f^{tan_2}$-TPPM were designed by generating tangential profile around 1. 15 equidistant points were chosen by evaluating $1 + \tan\theta$ with θ varied in the range of $\approx \mp 20^\circ$ in the case of the former and between $\approx \mp 14^\circ$ in the latter. Six equidistant points were sampled in the range $\approx \mp 8^\circ$ to design SW_f-$TPPM_6$.

- A linear sweep was chosen to design SW_f^{τ}-TPPM where pulse durations were swept from 0.75 to 1.25 times τ with increment of 0.05. The corresponding equation of f_i is given by $f_i = 0.75 + 0.05 \times (i - 1)$.

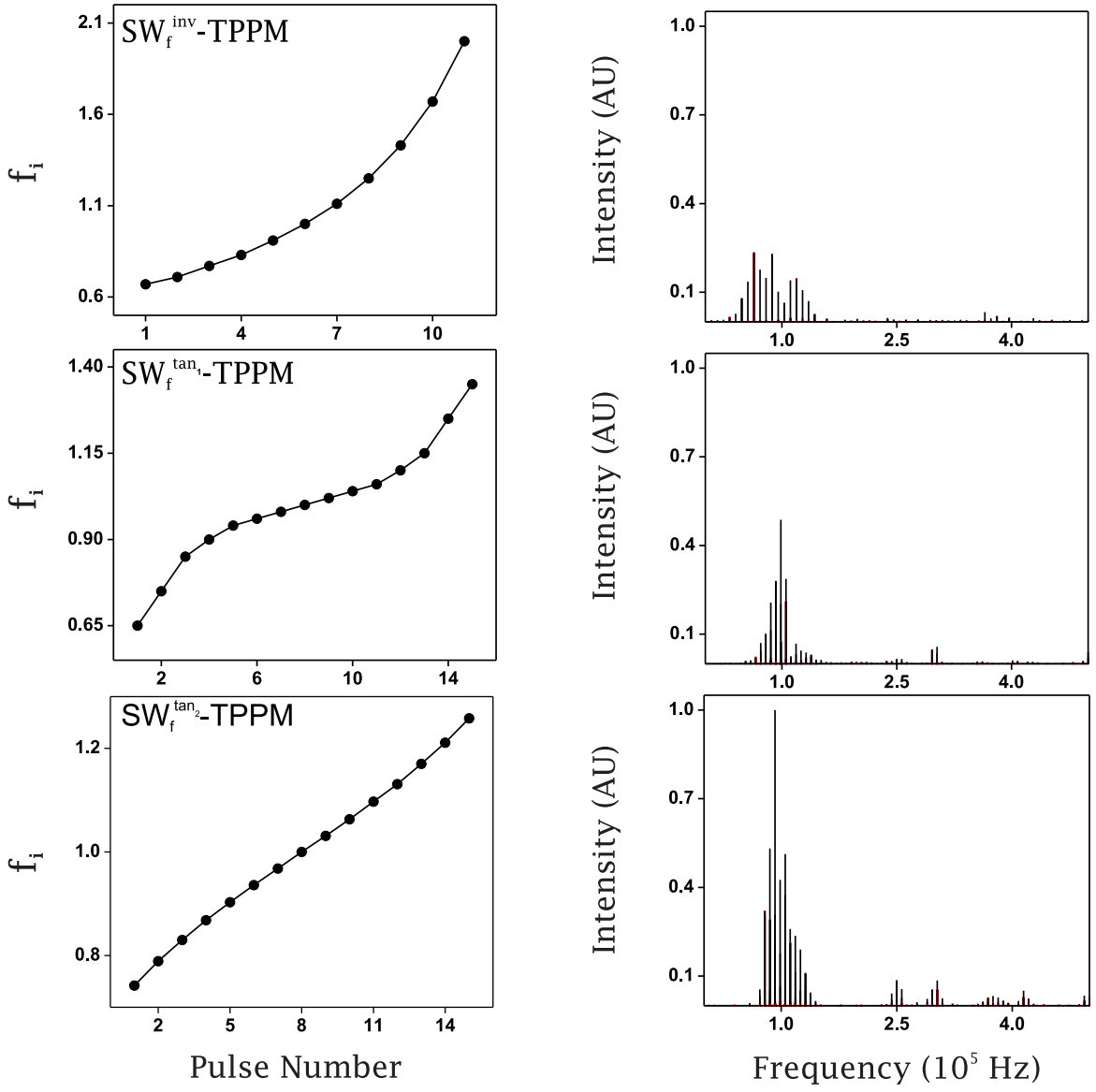

Figure 2.4: Left and right columns show respectively the time and frequency profiles of SW_f^{inv}-TPPM, $SW_f^{tan_1}$-TPPM, and $SW_f^{tan_2}$-TPPM. The power spectrum is calculated with a flip angle of 180° at an RF field of 100 kHz.

- SW_f^{1/τ_1}-TPPM and SW_f^{1/τ_2}-TPPM are distinct forms of inverse function and they are based on the SW$(1/\tau)$-FAM scheme used for the enhancement of the central-

transition signal of half-integer spin quadrupolar nuclei [70]. Increasing the frequency components in a decoupling sequence with a fixed number of pulse pairs and hence a fixed cycle time requires the sweep width to be increased. This approach was originally conceived in the context of FAM and the suitable set of equations were reported by Bräuniger et al. [70]. These equations were adapted to design SW_f^{1/τ_1}-TPPM and SW_f^{1/τ_2}-TPPM with sweep widths of 22 and 50 kHz around the central RF field strength of 100 kHz.

Few shorter SW_f-TPPM analogues were designed in order to suit higher MAS frequencies. The suitability of smaller profiles for higher MAS frequencies will be presented in the Chapter 3. These sweep profiles are approximately tangential and are presented in Table 2.2.

Table 2.2: Pulse durations for shorter SW_f-TPPM schemes.

#	SW_f-TPPM$_{6s}$	SW_f-TPPM$_{6m}$	SW_f-TPPM$_{6l}$	SW_f-TPPM$_{5s}$	SW_f-TPPM$_{5m}$	SW_f-TPPM$_{5l}$	SW_f-TPPM$_{4s}$	SW_f-TPPM$_{4l}$
1	0.90	0.80	0.70	0.95	0.90	0.85	0.93	0.90
2	0.96	0.92	0.91	0.99	0.98	0.97	0.99	0.98
3	0.99	0.98	0.85	1.00	1.00	1.00	1.01	1.01
4	1.01	1.02	0.90	1.01	1.02	1.03	1.07	1.1
5	1.04	1.09	0.94	1.05	1.10	1.15		
6	1.10	1.20	0.96					

In these analogues of SW_f-TPPM scheme, the numbers in the subscript represent the number of TPPM pairs and determines the cycle time of these schemes. The letters at the subscript represents the relative sweep width of these schemes where s, m, and l stands for large, medium, and small respectively.

2.4 Enhanced adiabatic TPPM: Frequency- and phase-swept TPPM

Quantitative analysis of Leskes et al. indicated that the adiabatic frequency sweep realised by tangential variation of pulse length is the main source of robustness in SW_f-TPPM decoupling scheme. Tangent function was a straighforward approach for adiabatic

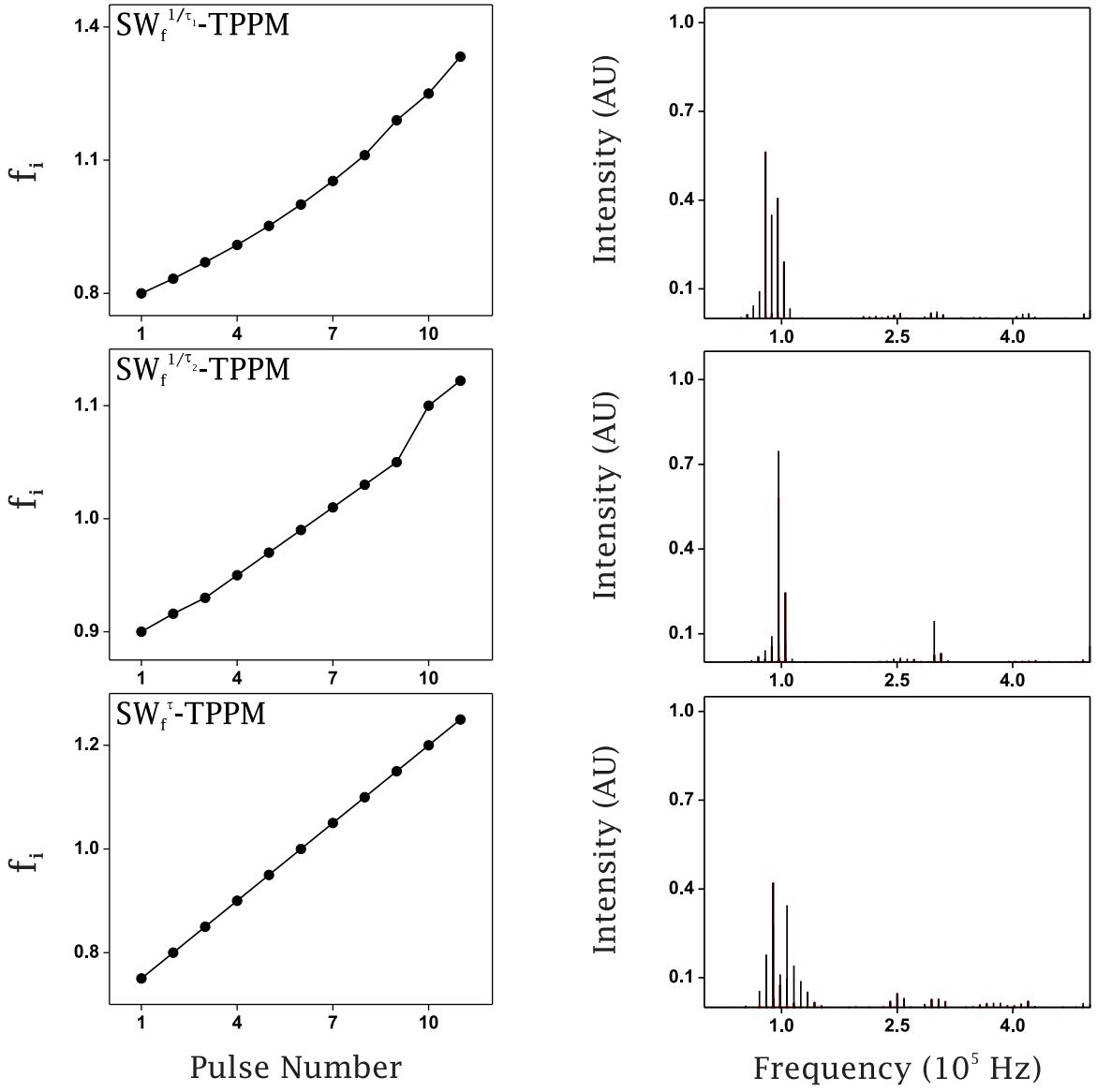

Figure 2.5: Left and right columns show respectively the time and frequency profiles of SW_f^{1/τ_1}-TPPM, SW_f^{1/τ_2}-TPPM, and SW_f^{τ}-TPPM. The power spectrum is calculated with a flip angle of 180° at an RF field of 100 kHz.

sweep and it was used to design SW$_f$-TPPM. According to well known principle of adiabaticity [71] in NMR [4], during the adiabatic sweep, the spins follow the course of RF field. This aspect of adiabatic sweep motivated its use in inversion and J-decoupling experiments [72,73]. Various adiabatic functions were explored numerically and enhanced performance in these applications was demonstrated [72, 73].

One of the improved adiabatic function is $\frac{\tanh}{\tan}$, where amplitude and frequency was varied in the form of hyperbolic tangent and tangent respectively [73]. Frequency was varied tangentially in SW$_f$-TPPM by varying pulse length and amplitude can be varied by varying phase difference hyperbolic-tangentially. The design principle is explained in Figure 2.6. The top row shows the deconvolution of two pulses with small phase modulation into a main time-independent field and a small field with time-dependence given by the frequency of phase modulation. The amplitude of phase modulation is given by the value of phase itself. This picture indeed represents the TPPM in the RF frame, and thus, phase needs to be swept in the form of hyperbolic tangent.

An 11 pulse method was designed on this principle and called SWept-(frequency & phase) TPPM (SW$_{fp}$-TPPM) [41]. According to previous notation, it can be denoted as [$1.22\tau_2$ $1.22\tau_{-2}$] [$1.14\tau_3$ $1.14\tau_{-3}$] [$1.06\tau_4$ $1.06\tau_{-4}$] [$1.04\tau_5$ $1.04\tau_{-5}$] [$1.02\tau_7$ $1.02\tau_{-7}$] [τ_{10} τ_{-10}] [$0.98\tau_{13}$ $0.98\tau_{-13}$] [$0.96\tau_{15}$ $0.96\tau_{-15}$] [$0.94\tau_{16}$ $0.94\tau_{-16}$] [$0.86\tau_{17}$ $0.86\tau_{-17}$] [$0.78\tau_{18}$ $0.78\tau_{-18}$]. SW$_{fp}$-TPPM demonstrated improved off-resonance over TPPM, SPINAL-64 and SW$_f$-TPPM at various MAS frequencies and RF field studied. Smaller profiles were designed in order to suit high MAS frequencies. Various variants of SW$_{fp}$-TPPM are described in Table 2.3 and comparison of their performance to existent methods is presented in the next Chapter.

2.5 Conclusions

This thesis introduces two approaches for designing heteronuclear dipolar decoupling sequences for application is solid-state NMR based upon adiabatic pulses in NMR. The

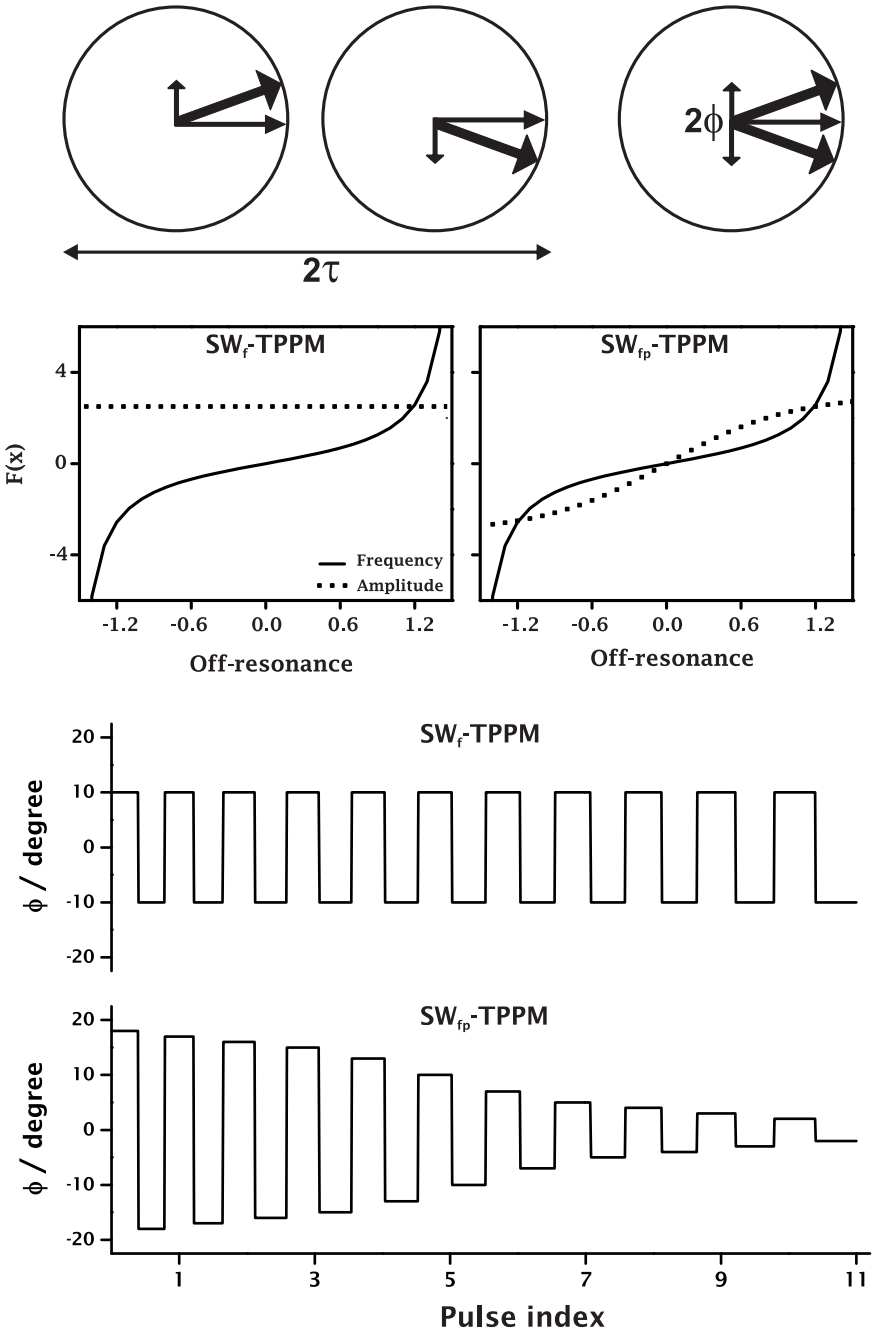

Figure 2.6: Left and middle circles on the top row show deconvolution of RF pulses of phase ϕ and $-\phi$ into two mutually perpendicular components. The circle on the right shows the resultant for a TPPM block, where the large static component represents CW decoupling and the smaller oscillating component perpendicular to it describes the phase modulation. The large static RF field is removed in the interaction frame of RF and the small phase modulation remains which leads to efficient decoupling performance for TPPM and analogues. In this interaction frame, the frequency and amplitude of phase modulation is given by the cycle time (2τ) and phase difference (2ϕ) of the TPPM block. Two graphs in the next row are drawn, showing the principle of adiabatic sweep in SW$_f$-TPPM and SW$_{fp}$-TPPM schemes and marked accordingly. The left graph describes the tangential frequency sweep through the resonance condition in SW$_f$-TPPM where the amplitude of the modulation is kept constant. The graph on the right describes a known way to realise enhanced adiabatic sweep (used to design SW$_{fp}$-TPPM), where amplitude and frequency are varied in the form of tanh and tan respectively. The profile of these modulation schemes are shown in the bottom part of diagram where variation in the duration of pulses can be seen along the X-axis while the modulation of phase difference in shown along the Y-axis.

first approach involves adiabatically sweeping the pulse length of TPPM pairs. Thus, phase-modulation frequency is varied tangentially, and the method is named SWept-frequency TPPM, SW_f-TPPM. This scheme was found to be an improved method on various rigid systems, the experimental demonstrations forming the rest of this thesis.

In order to improve the adiabatic sweep, the frequency and the phase of TPPM block are swept in the form of tangent and hyperbolic tangent functions respectively. The decoupling scheme designed along this principle is named SWept-(frequency & phase) TPPM, SW_{fp}-TPPM. Its experimental performance will be presented in the next Chapter.

Table 2.3: Pulse durations and phase (in subscript) of SW_{fp}-TPPM sequences.

#	SW_{fp}-$TPPM_9$	SW_{fp}-$TPPM_7$	SW_{fp}-$TPPM_5$	SW_{fp}-$TPPM_{5a}$	SW_{fp}-$TPPM_{5b}$
1	1.24_{3°	1.28_{4°	1.20_{5°	1.20_{4°	1.20_{9°
	1.24_{-3°	1.28_{-4°	1.20_{-5°	1.20_{-4°	1.20_{-9°
2	1.12_{4°	1.20_{5°	1.02_{7°	1.02_{6°	1.02_{11°
	1.12_{-4°	1.20_{-5°	1.02_{-7°	1.02_{-6°	1.02_{-11°
3	1.04_{5°	1.02_{7°	1.00_{10°	1.00_{10°	1.00_{15°
	1.04_{-5°	1.02_{-7°	1.00_{-10°	1.00_{-10°	1.00_{-15°
4	1.02_{7°	1.00_{10°	0.98_{13°	0.98_{-14°	0.98_{-19°
	1.02_{-7°	1.00_{-10°	0.98_{-13°	0.98_{-14°	0.98_{-19°
5	1.00_{10°	0.98_{13°	0.8_{15°	0.8_{16°	0.8_{21°
	1.00_{-10°	0.98_{-13°	0.8_{-15°	0.8_{-16°	0.8_{-21°
6	0.98_{13°	0.8_{15°			
	0.98_{-13°	0.8_{-15°			
7	0.96_{15°	0.72_{16°			
	0.96_{-15°	0.72_{16°			
8	0.88_{16°				
	0.88_{-16°				
9	0.76_{17°				
	0.76_{-13°				

In these analogues of SW_{fp}-TPPM scheme, the numbers in the subscript represent the number of TPPM pairs and determines the cycle time of these schemes. For SW_{fp}-$TPPM_5$ scheme, two variants were designed with different range of phase. The range of phase values for SW_{fp}-$TPPM_{5a}$ is slightly larger than SW_{fp}-$TPPM_5$ while the entire range of phase was increased by 5° to design SW_{fp}-$TPPM_{5b}$.

Chapter 3

Heteronuclear dipolar decoupling: Spin $\frac{1}{2}$ nuclei in rigid solids

Dipolar coupling to the abundant nuclei, heteronuclear dipolar coupling, is the strongest interaction governing the resolution of the NMR spectrum of the spin $\frac{1}{2}$ rare nuclei in rigid solids. High resolution in the spectrum of rare spins is obtained with the combined use of MAS and appropriate radiofrequency irradiation on the abundant spins. ^{13}C and ^{1}H is a prominent example of rare and abundant spins and this example alone, illustrates the importance of heteronuclear dipolar decoupling. Other commonly encountered rare spin $\frac{1}{2}$ nuclei are ^{15}N, ^{29}Si, and ^{31}P while another abundant nucleus of significance is ^{19}F. Thus, heteronuclear dipolar decoupling is applicable to a wide range of systems for resolution and sensitivity enhancement.

A continuous burst of RF irradiation, CW, was the first decoupling sequence attempted to enhance the resolution of rare spin nucleus and routinely used till 1995. Two-Pulse Phase Modulation (TPPM) was demonstrated in 1995 to deliver improved decoupling efficiency over CW. TPPM was the breakthrough scheme for heteronuclear dipolar decoupling and many attempts to design schemes with improved performance followed. A survey of these attempts was presented in Chapter 1. A thorough understanding of heteronuclear dipolar decoupling is difficult due to the influence of other

interactions and cross terms among them. A detailed description of these shortcomings was presented in Chapter 1. Various attempts to understand heteronuclear dipolar decoupling were presented in Chapter 1 and a unified mechanism, derived from the bimodal Floquet theory, was presented in Chapter 2. The bimodal Floquet analysis suggested incorporation of adiabatic sweep in TPPM to enhance its performance. A scheme was designed by adiabatically sweeping the modulation frequency of TPPM which was named SW$_f$-TPPM. In order to enhance the adiabatic sweep, frequency and amplitude of the phase modulation were swept to design SW$_{fp}$-TPPM. The design principle of these schemes has been presented in Chapter 2.

This Chapter presents experimental investigation of SW$_f$-TPPM, exploring its improved performance and regions of good decoupling. A general investigation of heteronuclear dipolar decoupling is also presented which covers influence of ^{1}H-^{1}H coupling and MAS frequency on the performance of decoupling sequences. Comparison of various sweep profiles for decoupling efficiency is presented. The profile of SPINAL-64 is also investigated where the prescribed values in the literature [36] are found to be suboptimal. Investigation of heteronuclear dipolar decoupling sequences for J-decoupling in the isotropic liquid phase is also presented. Towards the end, the performance of SW$_{fp}$-TPPM is compared with the existing schemes.

3.1 Materials and methods

Majority of the experiments were done on a Bruker Avance 500 MHz spectrometer equipped with 4 mm triple resonance and 2.5 mm double resonance probes. *U*-^{13}C labelled tyrosine and naturally labelled glycine were used for experiments. The spectra of spinning samples were acquired with ramped cross polarisation method. 4 mm probe was used for experiments involving MAS frequency upto 14 kHz and 2.5 mm probe was used for higher MAS frequencies. Few experiments were done on BBI and 3.2 mm double-resonance probes, and these are mentioned in the corresponding places.

RF field strength on ^{1}H channel was calibrated by nutation experiment on a sample of adamantane.

3.2 Performance evaluation of SW_f-TPPM

The decoupling efficiency of SW_f-TPPM was compared to TPPM and SPINAL-64 in the MAS frequency range of 6-14 kHz at RF field strengths of 70, 90, and 100 kHz on a sample of uniformally ^{13}C labelled tyrosine. A representative spectrum of this compound at MAS frequency of 14 kHz is shown in Figure 3.1, where ^{1}H decoupling was applied with SW_f-TPPM scheme at an RF field strength of 100 kHz. Cross polarisation was used for the labelled sample as it offers the advantage of faster decay of ^{1}H polarisation governs the signal averaging of rare spins. This factor is of larger significance for labeled samples over the regular ^{13}C intensity enhancement of 4 times.

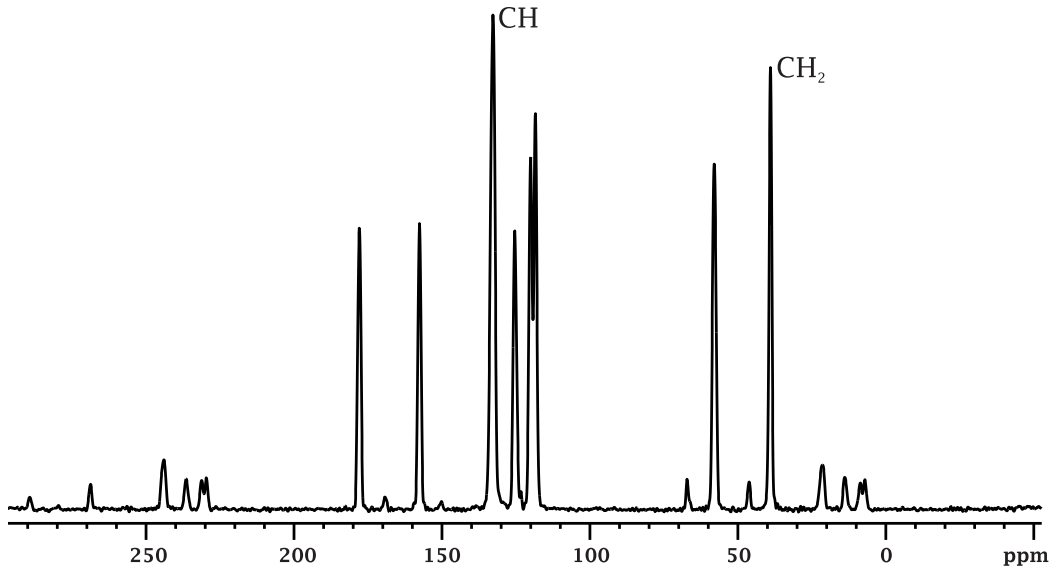

Figure 3.1: Cross-polarised MAS Spectrum of U-^{13}C labelled tyrosine acquired with application of SW_f-TPPM decoupling at 100 kHz of RF field strength and MAS frequency of 14 kHz.

Intensity of CH_2 (at 38 ppm) and CH resonances (at 138 ppm) were taken to compare the efficiency of decoupling sequences, these resonances are marked in Figure 3.1.

Figure 3.2 shows the signal intensity of CH_2 and CH peaks in the left and right columns respectively, as a function of MAS frequency (ν_r) for three different RF field strengths (ν_1) of 100 kHz (top row), 90 kHz (middle row), and 70 kHz (bottom row). SW_f-TPPM performs comparable to or marginally better than the existent decoupling sequences for both the resonances over the range of MAS frequencies and RF field strengths. The performance of XiX is known to be discouraging at low RF field strengths and its decoupling efficiency is only evaluated at the high value of 100 kHz.

The linewidth of both the resonances are over 100 Hz owing to the ^{13}C-^{13}C dipolar couplings. In a sample with natural abundance of ^{13}C, lack of ^{13}C-^{13}C dipolar couplings results in a linewidth of $\approx$ 50 Hz. Increase of peak intensity with MAS frequency suggests resolution enhancement at higher frequencies. This might be arising from the scaling of ^{13}C-^{13}C dipolar couplings. The presence of a dip at 9.8 kHz in CH_2 comparison (left column in Figure 3.2) is due to a rotational-resonance condition, where a spinning sideband of a resonance (unresolved doublet at 120 ppm) falls on to that of CH_2. Choosing a MAS frequency to avoid rotational-resonance condition for a sample with many resonances is not straightforward. A simple strategy to avoid rotational-resonance condition is to spin the sample at a frequency higher than the largest chemical shift difference of the sample.

3.2.1 Robustness of SW_f-TPPM

Robustness of decoupling sequences was compared by systematically varying the paramaters at MAS frequency of 14 kHz and RF field strength of 100 kHz. Intensity of CH_2 resonance was monitored as a function of (plot A) pulse length, (B) phase, and (C) ^{1}H off-resonance in Figure 3.3. The intensity values were normalised to individual optimum values under various decoupling sequences for ^{1}H off-resonance investigation. For other comparisons, a universal optimum value among all decoupling sequences was taken.

The efficiency of TPPM and SPINAL-64 was found to be sensitive to pulse length and

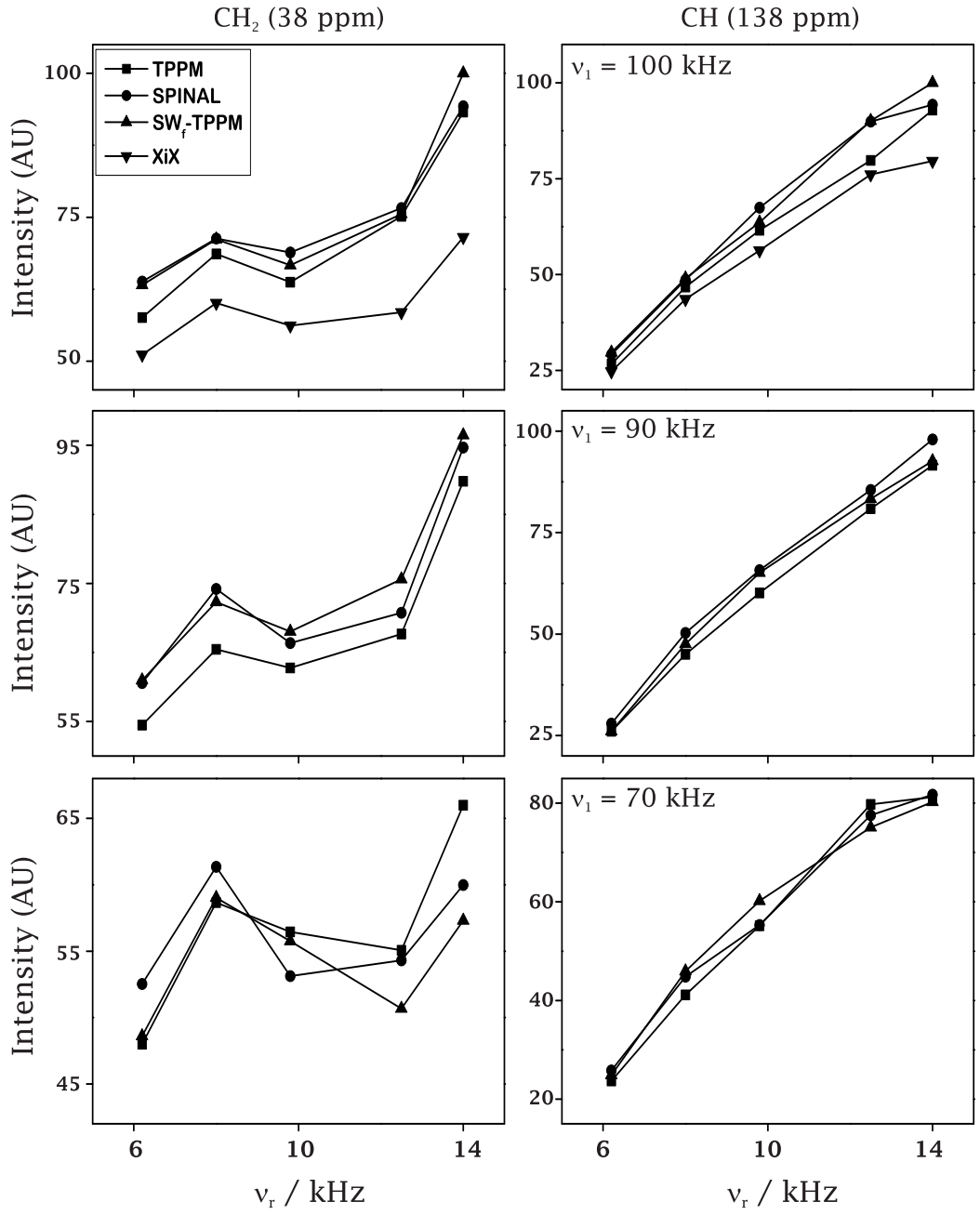

Figure 3.2: Spectral intensity comparison of TPPM (■), SPINAL-64 (•), XiX (▼), and SW_f-TPPM (▲) on the CH_2 (at 38 ppm: left column) and CH (at 138 ppm: right column) peaks as a function of MAS frequency, $\nu_r = 6.2$, 8.0, 9.8, 12.5, and 14 kHz. Top, middle, and bottom rows show the comparison at RF field strength of 100, 90, and 70 kHz respectively.

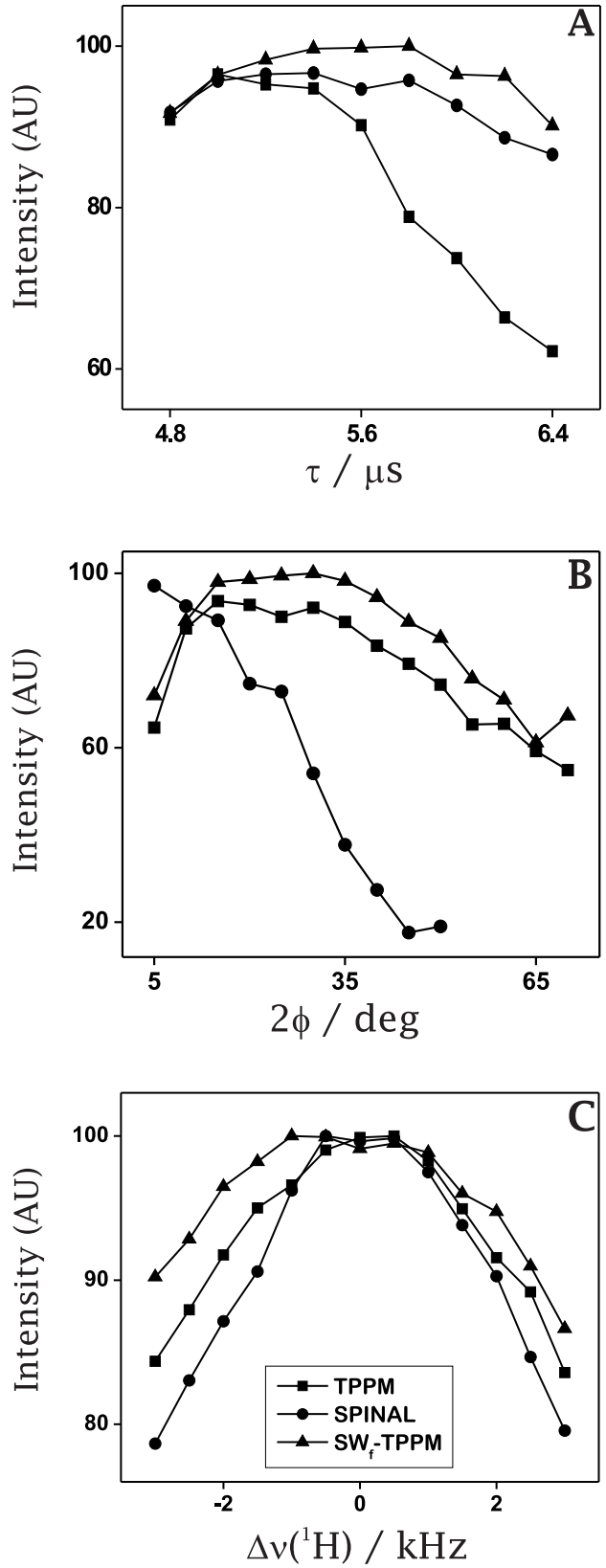

Figure 3.3: Intensity of the CH_2 peak monitored as a function of (A) pulse duration (τ), (B) phase difference (2ϕ), and (C) ^{1}H off-resonance ($\Delta\nu(^1\text{H})$) for TPPM (■), SPINAL-64 (•), and SW$_f$-TPPM (▲). In (A) and (B), all intensities are normalised with respect to those of SW$_f$-TPPM. In (C), intensities with a scheme are normalised with its optimum value.

phase respectively but that of SW_f-TPPM was insensitive to either of these. The efficiency of SW_f-TPPM was also found to be the least affected by ^{1}H off-resonance compared to TPPM and SPINAL-64. Thus, efficient performance of SW_f-TPPM can be realised over a wide range of pulse length, phase, and ^{1}H off-resonance, making it a ready to use method.

Robustness of a method is important as it reduces the time to set it up experimentally for optimum performance. It also takes care of instrumental fluctuations. Instrumental fluctuations are of various origin and are of uncontrolled nature and can only be tackled by the suitable design of methods.

3.2.2 Performance evaluation of SW_f-TPPM on unlabelled sample

Efficiency and robustness of SW_f-TPPM was compared to that of TPPM and SPINAL-64 on unlabelled glycine, shown in Figure 3.4. The intensity of the C_α resonance is plotted as a function of MAS frequency at RF field strength of 100, 90, and 70 kHz in the (1A), (1B), and (1C) plots of Figure 3.4. Robustness of the decoupling methods are compared in the right column where intensity of the C_α resonance is plotted as a function of pulse length, ^{1}H off-resonance, and phase respectively in (2A), (2B), and (2C) plots of Figure 3.4. The peak intensity for the three decoupling sequences is clearly differentiable in the left column, which were similar for the labelled sample. The intensity of C_α resonance decreases with MAS frequency, which is due to inefficient cross-polarisation. Modulated TPPM methods, SW_f-TPPM and SPINAL-64 perform superior to TPPM at low MAS frequency of 6.2 kHz for RF field strength of 100 kHz and their performance drops with increase in MAS frequency. Towards lower RF field strengths, performance gains of modulated TPPM methods at MAS frequency of 6.2 kHz reduce and at RF field strength of 70 kHz, they perform comparable to TPPM. SW_f-TPPM is less affected by this trend compared to SPINAL-64. Thus, performance of modulated TPPM methods deteriorates with decrease in RF field strength where SPINAL-64 is more affected by this trend.

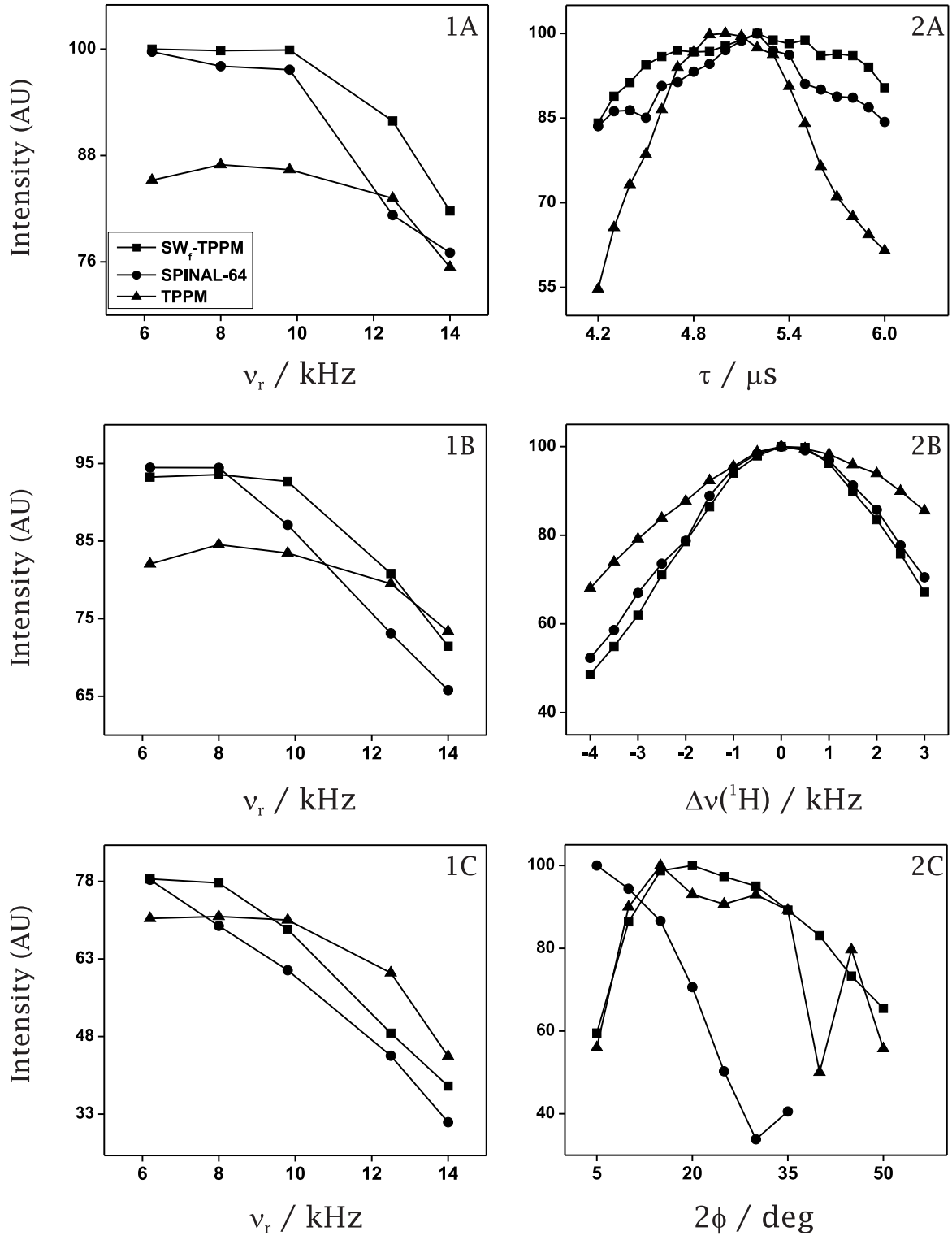

Figure 3.4: Decoupling efficiency comparison of TPPM (▲), SPINAL-64 (●), and SW$_f$-TPPM (■) on glycine with natural abundance of ^{13}C. The left column shows the peak intensity of CH_2 resonance of glycine as a function of MAS frequency (ν_r) at RF field strengths (ν_1) of 100 kHz (1A), 90 kHz (1B), and 70 kHz (1C). The right column compares the the intensity at RF field strength of 100 kHz and MAS frequency of 14 kHz as a function of the (2A) pulse length (τ), (2B) ^1H off-resonance ($\Delta\nu(^1H)$) and (2C) phase difference (2ϕ), from top to bottom. All intensities are normalised with respect to those of SW$_f$-TPPM.

The sensitivity of performance of decoupling sequences to the experimental parameters shown on the right column of Figure 3.4, conforms with the observation on labelled tyrosine sample. One noticeable difference is the higher sensitivity of SW_f-TPPM to the ^{1}H off-resonance over TPPM and SPINAL-64. This sample dependent phenomena may arise from the smaller ^{1}H bath present in glycine compared to the earlier studied tyrosine. The explanation could be the smaller differences in resonance frequency of ^{1}H nuclei in the tyrosine molecule compared to glycine. As the process of spin diffusion spreads the influence of RF irradiation by means of $I^{\pm}I^{\mp} \pm I^{\mp}I^{\pm}$ kind of terms from the Hamiltonian of homonuclear dipolar coupling. The ^{1}H resonances with smaller chemical shift differences between them will lead to efficient propagation of RF perturbation. This scenario suggests for better off-resonance behaviour of all decoupling sequences on (uniformly labelled) tyrosine. The relative drop in intensity with the variation of ^{1}H off-resonance for glycine was indeed higher than that for tyrosine. The role of homonuclear dipolar couplings in heteronuclear dipolar decoupling will be presented in Section 3.3.

The ^{1}H off-resonance behaviour of TPPM, SPINAL-64, and SW_f-TPPM has been explored with MAS frequency, as both RF decoupling and MAS are time dependent averaging processes and likely to interfere. Three cases of relative values of cycle time, τ_c, of modulated TPPM sequences and rotor period, τ_r, were taken by suitably adjusting RF field strength and MAS frequency. A smaller analog of SW_f-TPPM, SW_f-$TPPM_6$ consisting of 6 TPPM pairs, was also studied. The results are shown in Figure 3.5 wherein the MAS frequencies and RF field strengths are mentioned for each case.

The relative insensitivity in the ^{1}H off-resonance behaviour of modulated TPPM sequences is observed when the cycle time of the sequences is shorter than the rotor period. Plot (A) and (B) of Figure 3.5 show the performance of TPPM, SPINAL-64, SW_f-TPPM, and SW_f-$TPPM_6$ at MAS frequency of 14 kHz and RF field strength of 100 kHz and 80 kHz respectively. Plot (C) shows the comparison at MAS frequency of 8.8 kHz and RF field strength of 100 kHz. The cycle time for TPPM, SPINAL-64, SW_f-TPPM, and SW_f-

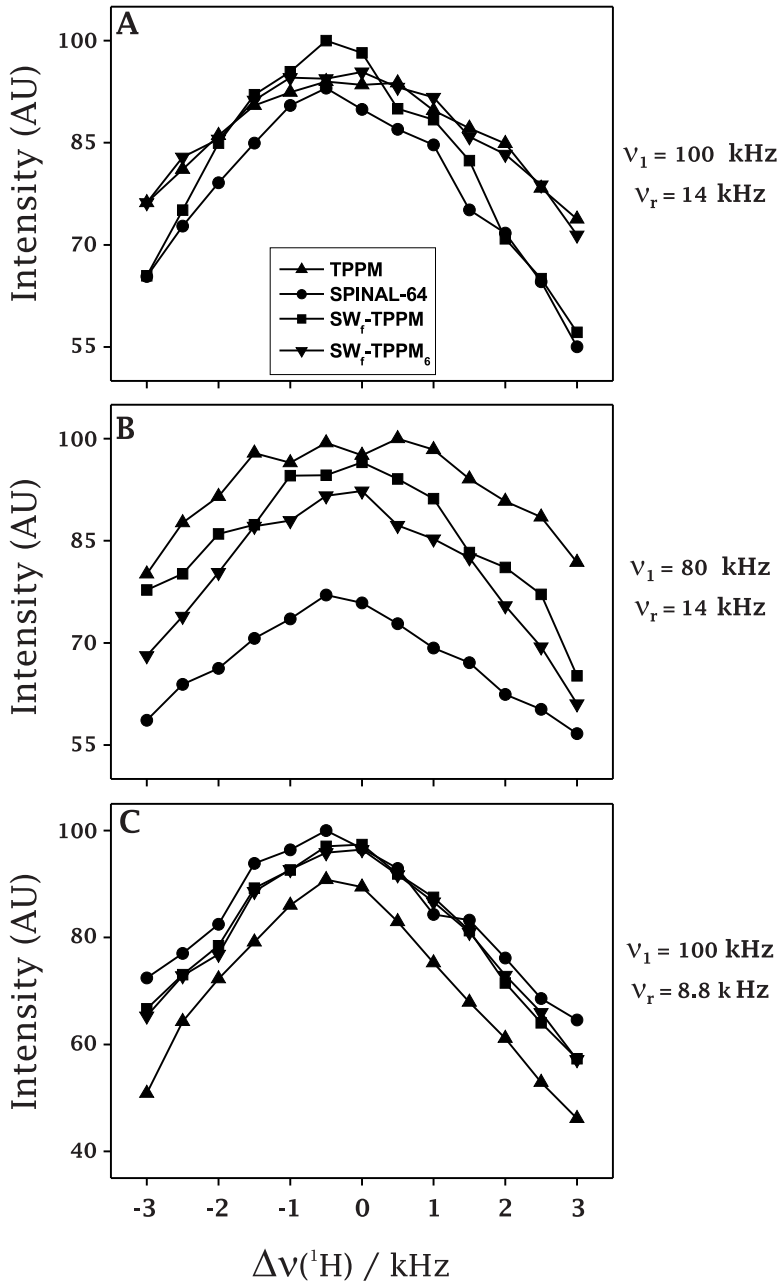

Figure 3.5: Decoupling efficiency comparison of TPPM (▲), SPINAL-64 (●), SW$_f$-TPPM (■), and SW$_f$-TPPM$_6$ (▼) on glycine with natural abundance of ^{13}C. Plots (A) and (B) show the ^{1}H off-resonance ($\Delta\nu(^1H)$) dependence of the intensity of CH_2 resonance as a function at MAS frequency (ν_r) of 14 kHz at RF field strengths (ν_1) of 100 and 80 kHz. Plot (C) corresponds to a MAS frequency of 8.8 kHz and RF field strength of 100 kHz. All intensities are normalised with respect to the most intense values in each comparison.

$TPPM_6$ at RF field strength of 100 kHz are 10, 80, 110, and 60 μs respectively. A MAS frequency of 14 kHz corresponds to a rotor period of 71.4 μs, and for application of decoupling sequences at this MAS frequency with RF field strength of 100 kHz, only TPPM and SW_f-$TPPM_6$ have $\tau_c < \tau_r$. The (A) plot indicates that these two modulation schemes are the least affected by ^{1}H off-resonance variation. For an RF field strength of 80 kHz, the cycle time of SW_f-$TPPM_6$, 75 μs, becomes longer than the rotor period of 71.4 μs and performance of the modulation scheme becomes very sensitive to ^{1}H off-resonance in the (B) plot, while TPPM with cycle time of only 12.5 μs is relatively insensitive to misset of carrier frequency. At lower MAS frequencies of 8.8 kHz with rotor period of 113.6 μs, as the case in plot (C), the cycle time of all the modulation schemes are shorter than τ_r, and all the modulated TPPM sequences are less sensitive to ^{1}H off-resonance than TPPM.

This comparison clearly suggests shorter analogues of SW_f-TPPM to be more effective at higher MAS frequencies.

3.2.3 Robustness evaluation of SW_f-TPPM

Experimental comparison of decoupling efficiency away from the ideal values of phase and flip angle was carried out for TPPM, SPINAL-64, and SW_f-TPPM. The intensity of the C_α peak of glycine as a function of phase difference (2ϕ) and ^{1}H RF field strength (ν_1, which correspond to the flip angle for fixed value of pulse length of 6.25 μs) for the three decoupling sequences (mentioned in the figure) are shown in Figure 3.6. The comparison at MAS frequency of 5.7 kHz and 11.0 kHz is shown in left and right columns respectively and decoupling sequences of TPPM, SPINAL-64, and SW_f-TPPM are compared in top, middle, and bottom row. The initial phase, ϕ, is varied for SPINAL-64 keeping the increment constant. Lighter colours represent more efficient regions of decoupling.

The modulated TPPM sequences possess broader regions of decoupling efficiency at

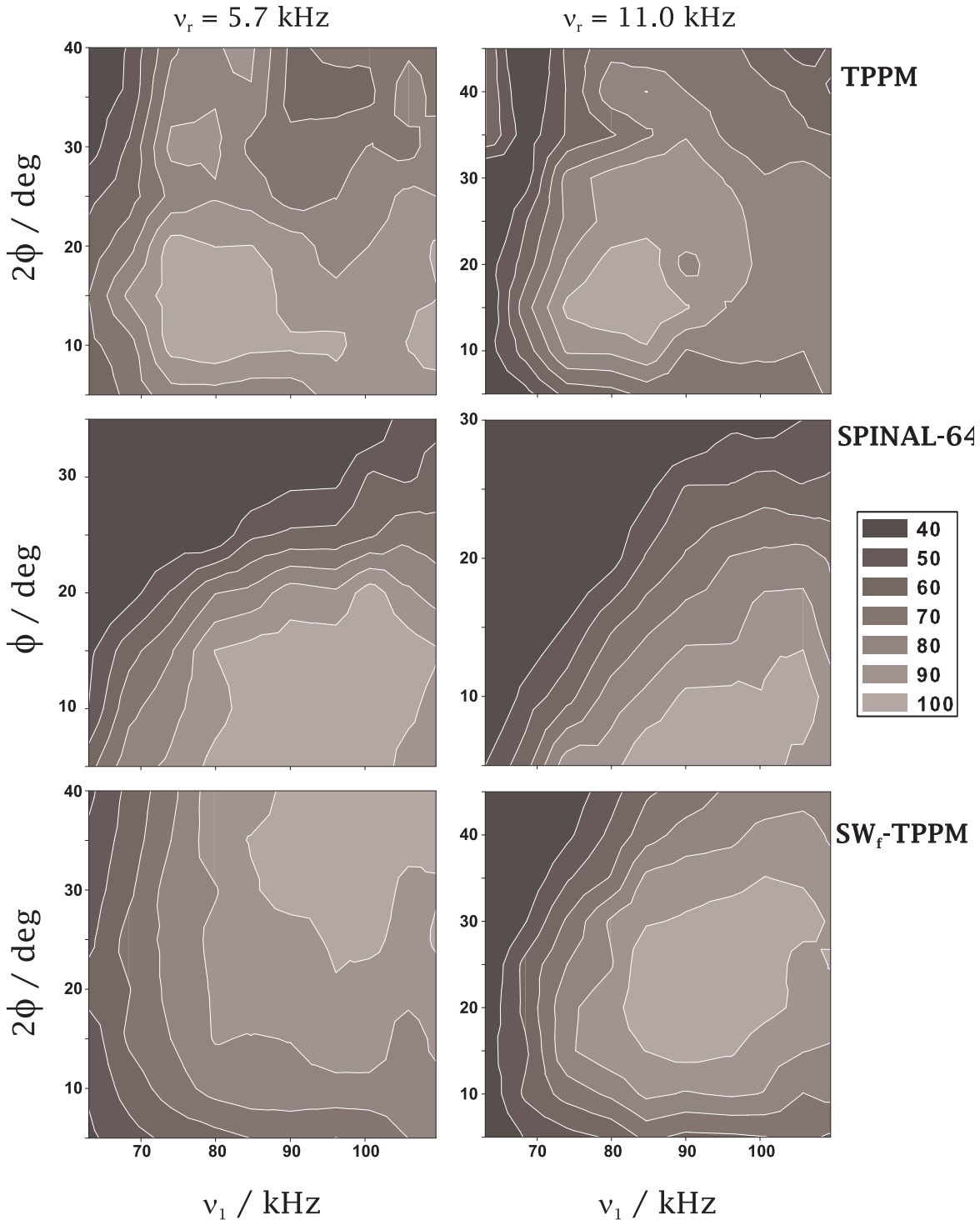

Figure 3.6: The intensity variation of the CH_2 resonance of glycine under TPPM, SPINAL-64, and SW_f-TPPM decoupling measured as a function of RF field strength (ν_1, along X-axis) and phase difference (2ϕ, along Y-axis). For SPINAL-64, phase (ϕ) is plotted along Y-axis. The left column is for a MAS frequency of 5.7 kHz and the right column is for 11.0 kHz. The values of phase difference (2ϕ) increases in steps of 5° with an initial value of 5°. The maximum values are 40° and 45° for SW_f-TPPM and TPPM at MAS frequency of 5.7 and 11.0 kHz, respectively whilst for SPINAL-64 these are 35° and 30° respectively. A duration of 6.25 μs was taken for pulses in TPPM and SPINAL-64 and the central pair of pulses in SW_f-TPPM. The RF field strengths taken were 63.0, 68.4, 74.0, 79.9, 84.7, 90.0, 96.1, 100.6, 105.8, and 109.5 kHz

lower MAS frequency of 5.7 kHz. The efficient performance of SW_f-TPPM at lower MAS frequency is achieved at higher values of both parameters, namely phase and RF field strength, which is also apparent in Figure 3.7.

The area of efficient decoupling is quenched for all decoupling sequences at MAS frequency of 11.0 kHz, with significant reduction in the optimum values of ϕ for SPINAL-64 and SW_f-TPPM. The quenching of robustness can be explained on the basis of scaling of homonuclear dipolar couplings with increasing MAS frequencies. The performance of SPINAL-64 at MAS frequency of 11.0 kHz becomes comparable to TPPM while SW_f-TPPM remains a method of choice even at higher MAS frequencies as it has a broader and homogeneous area of efficient decoupling. The influence of II couplings on IS decoupling will be explored in the next Section.

The robustness of SW_f-TPPM was systematically investigated as a function of MAS frequency and the results are shown in Figure 3.7. The aim was to investigate the influence of MAS frequency on the robustness together with finding the optimum values of pulse length and phase at various MAS frequencies. Figures 3.7A and 3.7B show the efficiency comparison of SW_f-TPPM as a function of phase difference (2ϕ) and pulse length (τ) respectively. The decrease of robustness and optimum values of 2ϕ and τ of the method with MAS frequency can be noticed.

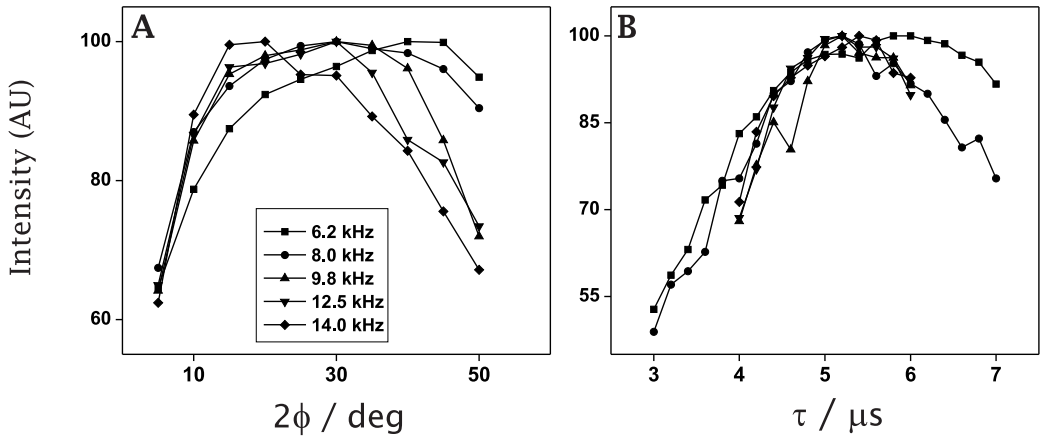

Figure 3.7: The optimum values of (A) phase and (B) pulse length determined for SW_f-TPPM at MAS frequencies mentioned in the plots. The RF field strength was kept at 100 kHz.

3.3 The role of homonuclear couplings among abundant nuclei: Simulations

Deterioration of efficiency of CW scheme with increasing MAS frequency is the significant disadvantage of it. In a study by Ernst et al. [54], rate of spin diffusion among ^{1}H spins was found to decrease with increase in MAS frequency and it was used to explain the inefficient performance of CW at higher MAS frequencies. The process of spin diffusion is mediated by the non-secular terms of homonuclear dipolar couplings and this process leads to averaging of heteronuclear dipolar couplings. The residual linewidth under CW decoupling scheme is larger than that of TPPM, and it even leads to splitting of a resonance in the absence of II couplings [54]. The prominent line narrowing influence of II couplings at low MAS frequencies helps CW scheme to perform efficiently. The reduced rate of this process at high MAS frequencies reduces the contribution of this factor in the residual linewidth under TPPM and other decoupling schemes. Thus, efficient design of decoupling schemes becomes critical at high MAS frequencies, $\nu_r >$ 30 kHz.

Sustained or improved efficiency of decoupling with MAS frequency is the desired characteristics for the heteronuclear decoupling schemes. The choice of heteronuclear decoupling schemes is also decided by the range of MAS frequency. TPPM and SPINAL-64 are effective in lower and intermediate MAS frequencies upto 25 kHz, while XiX was demonstrated to surpass either of them at higher MAS frequencies. The SW$_f$-TPPM scheme was shown to be equally efficient to TPPM and SPINAL-64 in lower MAS frequencies together with the advantage of robustness with respect to experimental parameters. The influence of MAS frequency and II coupling on the efficiency and robustness of SW$_f$-TPPM and TPPM are now investigated by numerical simulations.

The role of ^{1}H-^{1}H coupled bath on ^{13}C-^{1}H decoupling was evaluated by measuring the intensity of ^{13}C resonance dipolar coupled to n ^{1}H nuclei. The simulations were per-

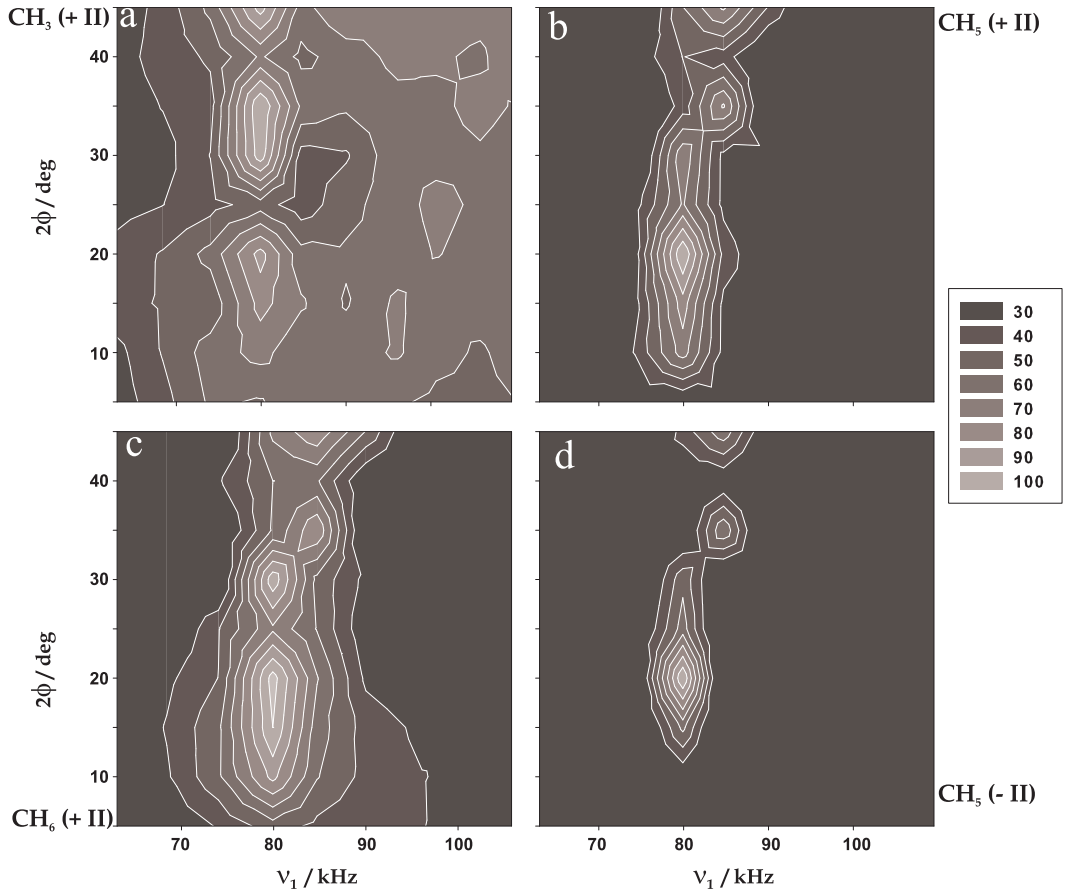

Figure 3.8: The peak intensity of TPPM decoupled ^{13}C resonance of isobutyl skeleton simulated with various spin systems, namely, CH_3, CH_5, CH_6 (with II couplings), and CH_5 (without II couplings). The simulations were done at a MAS frequency of 5.818 kHz and pulse length of $\tau = 6.25\ \mu s$ by varying phase difference (2ϕ, along Y-axis) and RF field strength (ν_1, along X-axis). Phase difference (2ϕ) was varied from 5° to 45° in steps of 5°. The RF field strengths taken are those implemented in experiments, shown in Figure 3.6.

formed with SPINEVOLUTION package which is able to handle large spin systems [69]. An isobutyl skeleton with NMR parameters and spatial co-ordinates was distributed with this package which was used to generate desired spin systems. The addition of ^{1}H was also done according to the numbering scheme of resonances in the original report [69].

The simulations shown in Figures 3.8 and 3.9 were performed in order to verify the experimental observations in Figure 3.6. The relative robustness of TPPM and SW$_f$-TPPM were compared at MAS frequency of 5.818 kHz on spin systems of CH_3, CH_5, and CH_6 with II couplings and CH_5 without II couplings. The intensity of ^{13}C resonance is normalised and these plots represent relative variation of intensity and are a clear indicator of robustness. The area of efficient decoupling, shown by contours in light colours, increases with the size of spin systems as evident in spin systems of CH_3, CH_5, and CH_6 with II couplings.

The expansion of area of efficient decoupling is more prominent for SW$_f$-TPPM than for TPPM. Another significant observation is the severe shrinking of area of efficient decoupling upon removal of II couplings, as shown in the spin system of CH_5 without II couplings, which indicates the controlling influence of the interaction on robustness. SW$_f$-TPPM is more affected by the II couplings as the method is robust due to inherent adiabaticity which can be improved by an additional support mechanism. Realistic spin systems consist of a strong ^{1}H bath which leads to robust performance for both TPPM and SW$_f$-TPPM and among these the later method is expected to achieve larger gains due to adiabatic sweep through the resonance conditions [55].

The influence of II couplings on the efficiency of TPPM and SW$_f$-TPPM schemes was also explored numerically at MAS frequencies of 5.8 kHz, 11.6 kHz, and 17.4 kHz which are respectively shown in Figures 3.10, 3.11, and 3.12. Optimum values of RF field strength and phase were found for both decoupling schemes at each spinning speed, the choice of which is crucial for smaller spin systems. Nominal values of these experimental parameters give rise to inefficient decoupling, as shown in contour plots of Figure 3.8

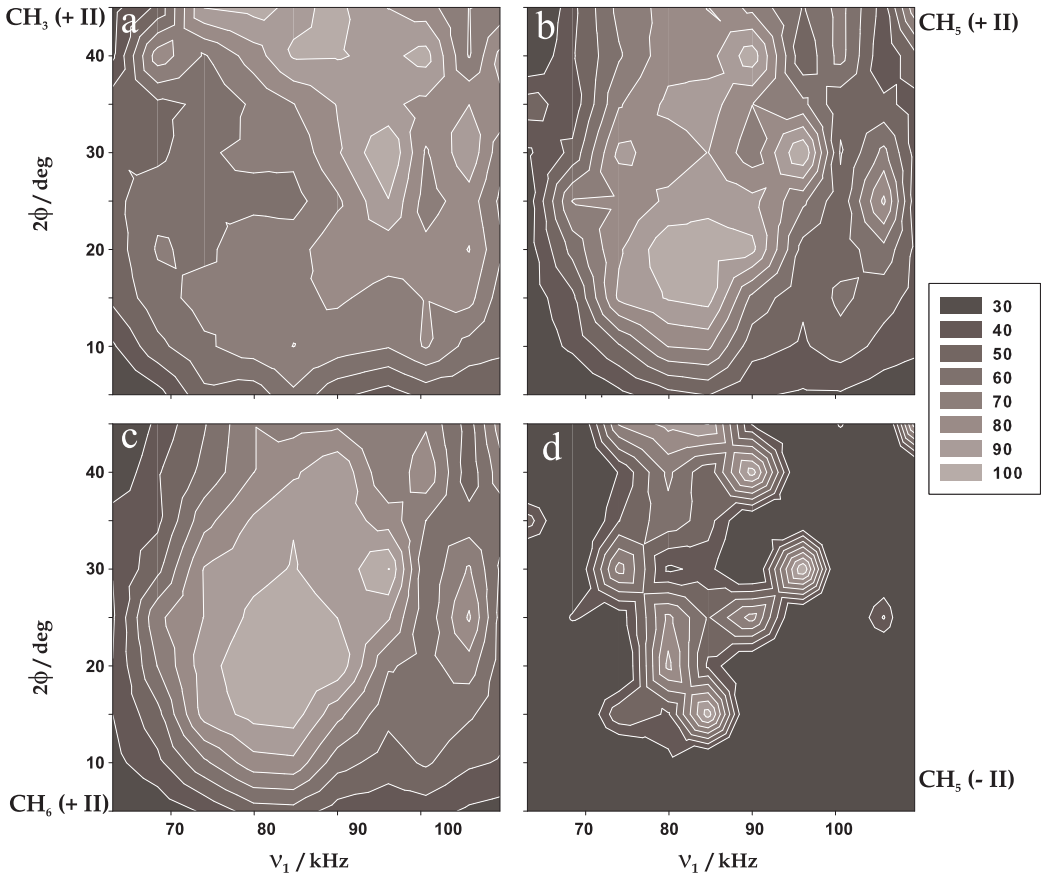

Figure 3.9: The peak intensity of SW_f-TPPM decoupled ^{13}C resonance of isobutyl skeleton simulated with various spin systems, namely, CH_3, CH_5, CH_6 (with II couplings), and CH_5 (without II couplings). The rest of the parameters are as in Figure 3.8.

and Figure 3.9, leading to strange peak shapes. However, higher spin systems are less affected by this trend due to robustness created by the II couplings.

Intensity of ^{13}C resonance decreases with the introduction of II couplings upto three ^{1}H resonances under both decoupling schemes at lower MAS frequency of 5.8 kHz. For larger number of ^{1}H resonances, efficiency of SW$_f$-TPPM scheme improves while that of TPPM stays at the same level. This clearly highlights the intuition of cooperative effect of II coupling on the performance of SW$_f$-TPPM.

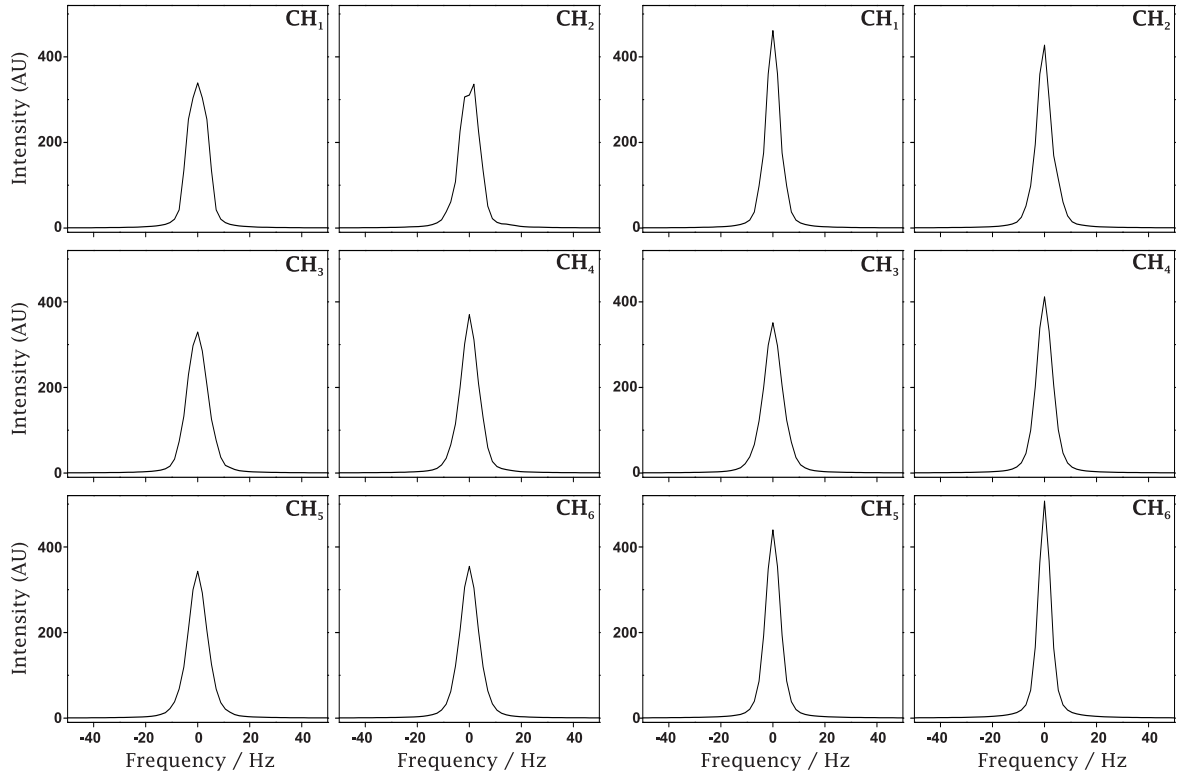

Figure 3.10: The simulated spectra of isobutyl skeleton with various spin systems at a MAS frequency of 5.8 kHz taking a pulse length of 6.25 μs. The spectra of CH$_1$ to CH$_6$ are simulated with TPPM (first and second columns at optimum RF field strength of 79 kHz and phase difference of 20°) and SW$_f$-TPPM (third and fourth columns at optimum RF field strength of 81 kHz and phase difference of 20°).

The performance of both decoupling schemes at higher MAS frequency of 11.6 kHz are similar to that at lower MAS frequency. The scaled II couplings at this MAS frequencies led SW$_f$-TPPM performance to stay at a constant level with increase in the size of

spin system. Another noticeable observation is the broad baseline for higher spin systems (5 or more ^{1}H nuclei) which is more pronounced for TPPM. The broad baseline under TPPM decoupling was experimentally observed by Ernst et al. [52] and their scheme XiX was shown to improve performance in this aspect leading to remarkable intensity enhancement.

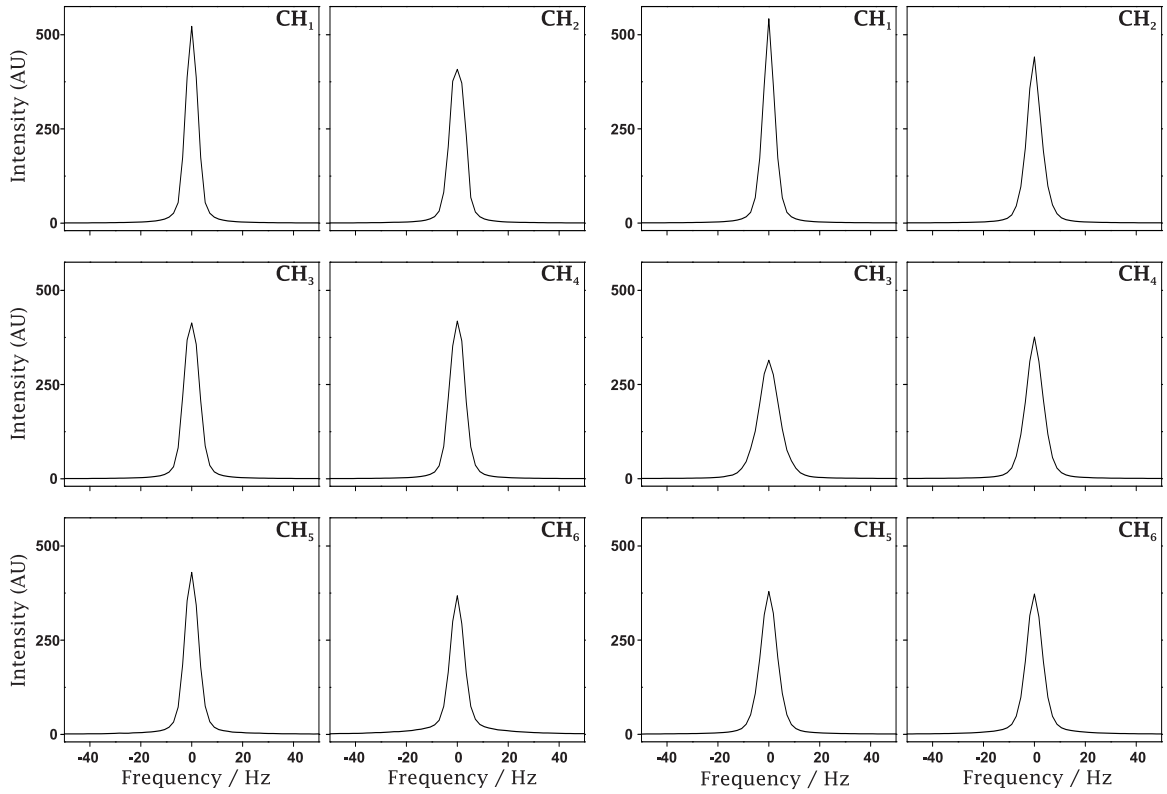

Figure 3.11: The simulated spectra of isobutyl skeleton with various spin systems at a MAS frequency of 11.6 kHz taking a pulse length of 6.25 μs. The spectra of CH_1 to CH_6 are simulated with TPPM (first and second columns at optimum RF field strength of 79 kHz and phase difference of 20°) and SW_f-TPPM (third and fourth columns at optimum RF field strength of 83 kHz and phase difference of 20°).

The same set of simulations for an even higher MAS frequency of 17.4 kHz is shown in Figure 3.12 where further enhanced baseline can be noticed for higher spin systems. SW_f-TPPM is clearly inefficient at this MAS frequency and this trend is expected to continue at higher MAS frequencies. The inefficiency of SW_f-TPPM at higher MAS frequency could be due to off-resonance effect of decoupling as shown in Figure 3.5. Efficient

sweep profiles at higher MAS frequencies can be designed with suitable modifications.

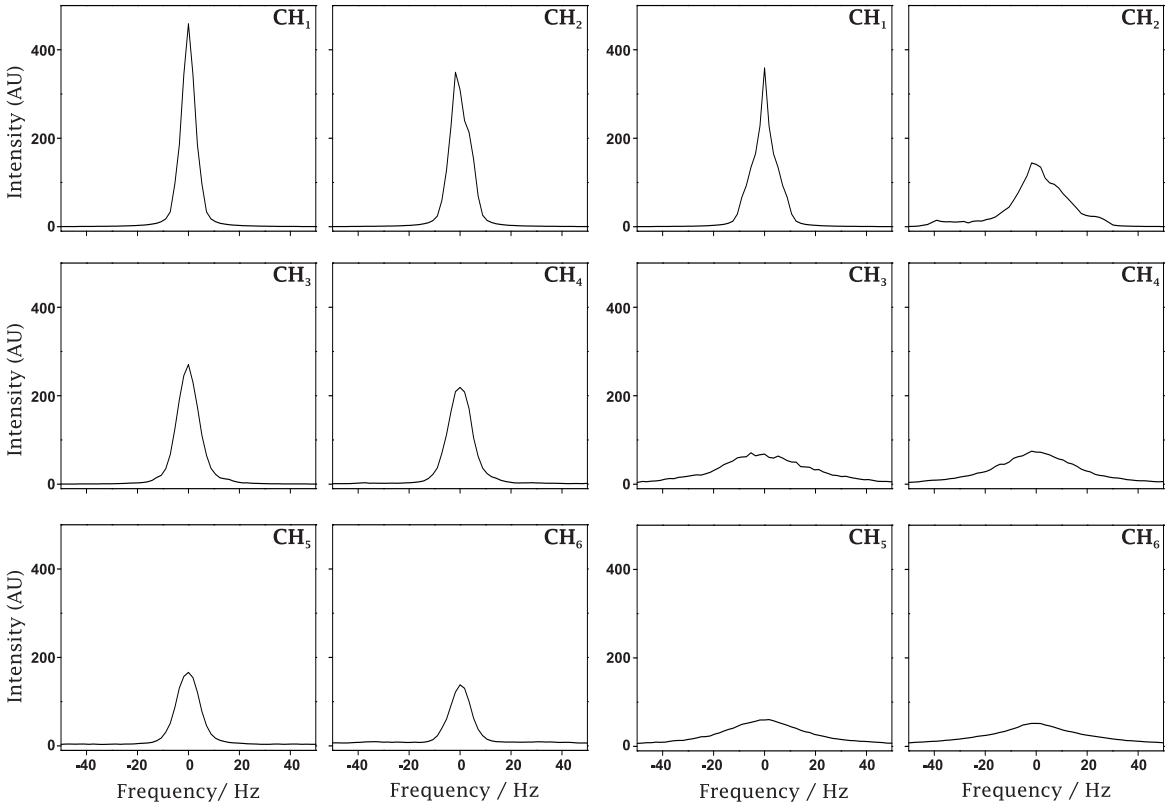

Figure 3.12: The simulated spectra of isobutyl skeleton with various spin systems at a MAS frequency of 17.4 kHz taking a pulse length of 6.25 μs. The spectra of CH_1 to CH_6 are simulated with TPPM (first and second columns at optimum RF field strength of 85 kHz and phase difference of 48°) and SW_f-TPPM (third and fourth columns at optimum RF field strength of 97 kHz and phase difference of 50°).

3.4 Performance of SW_f-TPPM analogs

Adiabatic sweep of modulation frequency of TPPM through the decoupling condition was found to be the cause of robust performance of SW_f-TPPM where the adiabatic sweep was mimicked by the tangential variation of pulse length. Other profiles were attempted to estimate the influence of adiabaticity on the performance of decoupling schemes. Sweep profiles of various forms were explored to design corresponding schemes, which were explained in Section 2.3. The experimental investigation of efficiency and robust-

ness of various sweep profiles i.e. SW_f-TPPM, SW_f^{inv}-TPPM, $SW_f^{tan_1}$-TPPM, $SW_f^{tan_2}$-TPPM, SW_f^{1/τ_1}-TPPM, SW_f^{1/τ_2}-TPPM, and SW_f^{τ}-TPPM are presented in left and right columns respectively of Figure 3.13. The intensity of C_α resonance obtained with these schemes are plotted as a function of MAS frequency are shown in (1A), (1B), and (1C) plots for RF field strengths of 70, 90, and 100 kHz respectively. The sensitivity of performance of decoupling sequences towards various experimental parameters, i.e. pulse length, ^{1}H off-resonance, and phase are compared in the (2A), (2B), and (2C) plots respectively.

The sweep width and its symmetry along with the cycle time of the sequences will be used to explain the observations. Sweep width of a sequence describes the spectrum of modulation frequency associated with the particular scheme and intuitively, the sweep is ineffective if the width is smaller than the dispersion of decoupling condition as explained in Section 2.2. Owing to the design of swept TPPM sequences, their sweep width is a fraction of applied RF field strength. Power spectrum of a scheme is representative of the sweep width and it will be correlated with their performance. The symmetry of a sequence refers to the distribution of amplitude of frequency components in the power spectrum, displayed in Section 2.3. SW_f^{inv}-TPPM has the largest width and asymmetry in sweep among all methods. Another method lacking symmetry is SW_f^{τ}-TPPM which has significantly smaller sweep width and asymmetry. $SW_f^{tan_1}$-TPPM and $SW_f^{tan_2}$-TPPM consist of 15 TPPM pairs while others contain 11 such pairs. SW_f^{1/τ_1}-TPPM and SW_f^{1/τ_2}-TPPM are symmetric methods but its linear sweep profile is far from being adiabatic.

Among all sweep profiles, methods with tangential profiles i.e. SW_f-TPPM, $SW_f^{tan_1}$-TPPM, and $SW_f^{tan_2}$-TPPM, remain efficient over the range of MAS frequency and RF field strength, however performance of $SW_f^{tan_1}$-TPPM lags at higher RF field strength owing to its large sweep width. The robustness of these methods is also appreciable in the normalised plot on the right, whereas the pure tangential profiles, $SW_f^{tan_1}$-TPPM and $SW_f^{tan_2}$-TPPM outperform the approximated profile of SW_f-TPPM with best performance delivered by the $SW_f^{tan_1}$-TPPM method owing to its largest sweep width. The large sweep

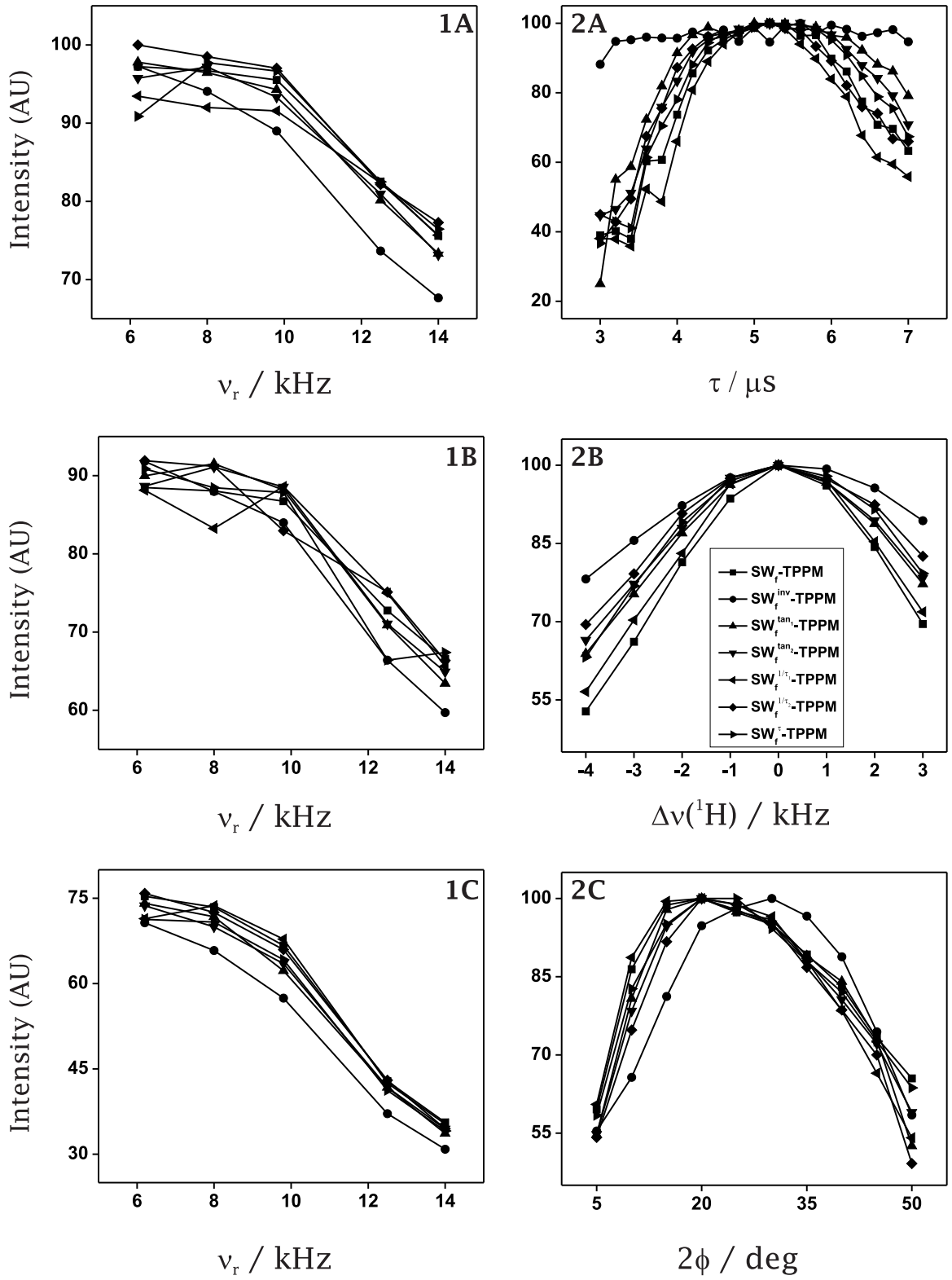

Figure 3.13: The left column shows peak intensity of CH_2 resonance of glycine plotted at various MAS frequencies at RF field strengths of 100 kHz (1A), 90 kHz (1B), and 70 kHz (1C). The right row shows the comparison of decoupling efficiency of these schemse as a function of (2A) pulse length (τ), (2B) ^{1}H off-resonance ($\Delta\nu(^1H)$), and (2C) phase difference (2ϕ). The robustness comparison were done at an RF field strength of 100 kHz and MAS frequency of 14 kHz.

width of SW_f^{inv}-TPPM makes it least affected by the variation but the lack of symmetry clearly affects its efficiency. The efficiency of linear sweep profile with smaller asymmetry and sweep width, SW_f^{τ}-TPPM, is inferior to adiabatic methods, SW_f-TPPM and SW_f^{tan}-TPPM sequences.

To conclude, adiabatic sweep profiles lead to better decoupling methods. The insensitivity to the experimental parameters stems from the sweep width of the sequences. Methods with enhanced adiabaticity are expected to perform better, the demonstration of this approach will be explored towards the end of this Chapter.

3.5 Modified swept-TPPM methods for higher MAS frequencies

The regular SW_f-TPPM sequence was found to be ineffective at higher MAS frequencies owing to its longer cycle time. This observation was also verified in numerical simulations. The cycle time of SW_f-TPPM needs to be reduced in order to suit higher MAS frequencies. The cycle time of SW_f-TPPM is a product of number of TPPM pairs (11) and the duration of $\approx 180^\circ$ pulse. Thus, effective sweep profiles at higher MAS frequencies can be designed by either applying higher RF field strength to reduce the duration of 180° pulse or by reducing the number of pulses to realise the sweep. Higher RF field strength leads to heating of the sample and this approach is not suitable for all samples, and the appropriate approach could be the reduction in the number of TPPM pairs to achieve the adiabatic sweep. Few analogues of SW_f-TPPM are designed with small number (4 to 6) of TPPM pairs, which are described in Section 2.3. The efficiency of these shorter schemes is tested against TPPM and XiX.

The efficiency of shorter SW_f-TPPM sequences is compared with TPPM by observing the C_α resonance of natural labelled glycine at 20.6 kHz of MAS frequency with ^1H decoupling applied at an RF field strength of 110 kHz, which is shown in Figure 3.14.

The spectrum marked with (1) is acquired with TPPM scheme while other spectra towards right are acquired with SW_f-$TPPM_{6s}$ (2), SW_f-$TPPM_{6m}$ (3), SW_f-$TPPM_{6l}$ (4), SW_f-$TPPM_{5s}$ (5), SW_f-$TPPM_{5m}$ (6), and SW_f-$TPPM_{5l}$ (7) respectively. The efficiency of swept TPPM sequences improves with increase in sweep width for both SW_f-$TPPM_6$ and SW_f-$TPPM_5$ family of sequences. This effect is dramatic for the later SW_f-$TPPM_5$ class which could be due to the smaller sweep width or the smaller number of TPPM pairs achieving the sweep.

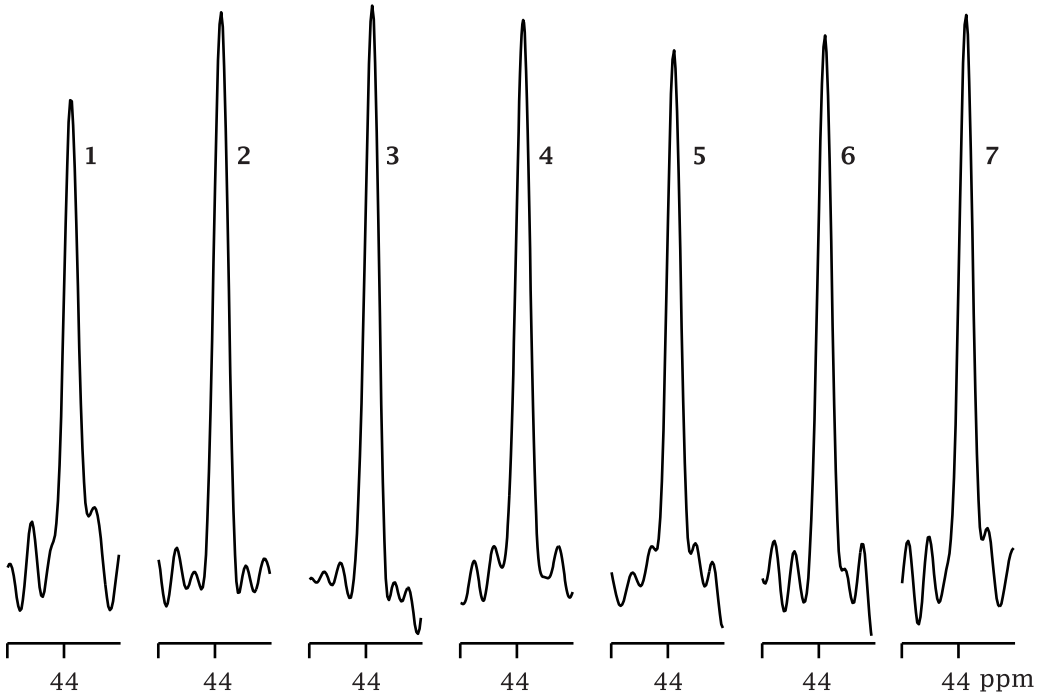

Figure 3.14: C_α resonance of glycine spinning at MAS frequency of 20.6 kHz acquired with various ^1H decoupling schemes applied at an RF field strength of 110 kHz. The spectrum marked with 1 is acquired with TPPM scheme while others are obtained with shorter SW_f-TPPM variants. Spectra marked with 2-4 are acquired with SW_f-$TPPM_6$ schemes i.e. SW_f-$TPPM_{6s}$ (2), SW_f-$TPPM_{6m}$ (3), and SW_f-$TPPM_{6l}$ (4) schemes, while those marked with 5-7 are acquired with SW_f-$TPPM_5$ schemes i.e. SW_f-$TPPM_{5s}$ (5), SW_f-$TPPM_{5m}$ (6), and SW_f-$TPPM_{5l}$ (7) respectively.

SW_f-$TPPM_4$ series of sequences are found to be more efficient than the longer analogues at even higher MAS frequencies, results are presented towards the end of this Section. The decoupling efficiency of TPPM, SW_f-$TPPM_{4l}$, and XiX at MAS frequency

of 30.2 kHz are compared at an RF field strength of 122 kHz, the peak shapes of C_α resonance (of glycine) obtained with these schemes are shown in Figure 3.15 from left in the same order. With XiX decoupling scheme, an intensity enhancement 20% over TPPM is achieved and SW_f-$TPPM_{4l}$ performs comparable. This intensity enhancement is lesser than that mentioned in the original report, 29% [52].

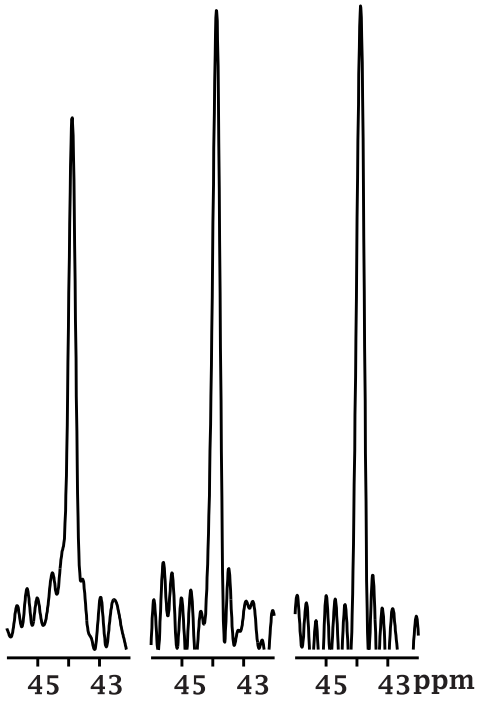

Figure 3.15: Intensity of C_α resonance of glycine spinning at MAS frequency of 30.2 kHz acquired with ^{1}H decoupling applied at an RF field strength of 122 kHz. The spectrum on the left, middle, and right is obtained with TPPM, SW_f-$TPPM_{4l}$, and XiX schemes respectively.

The influence of ^{1}H off-resonance on the performance of these decoupling sequences is compared in Figure 3.16 at the same values of MAS frequency and RF field strength. The (A), (B), and (C) rows in this plot show the ^{1}H off-resonance dependence of XiX, TPPM, and SW_f-$TPPM_{4l}$ respectively where carrier frequency is varied in a range of 7.0 kHz for each case with a step size of 0.5 kHz. It can be noticed that the performance of TPPM and XiX are severely affected by the ^{1}H off-resonance while the SW_f-$TPPM_{4l}$ scheme is more tolerant to this effect. For a bigger molecule, containing large number

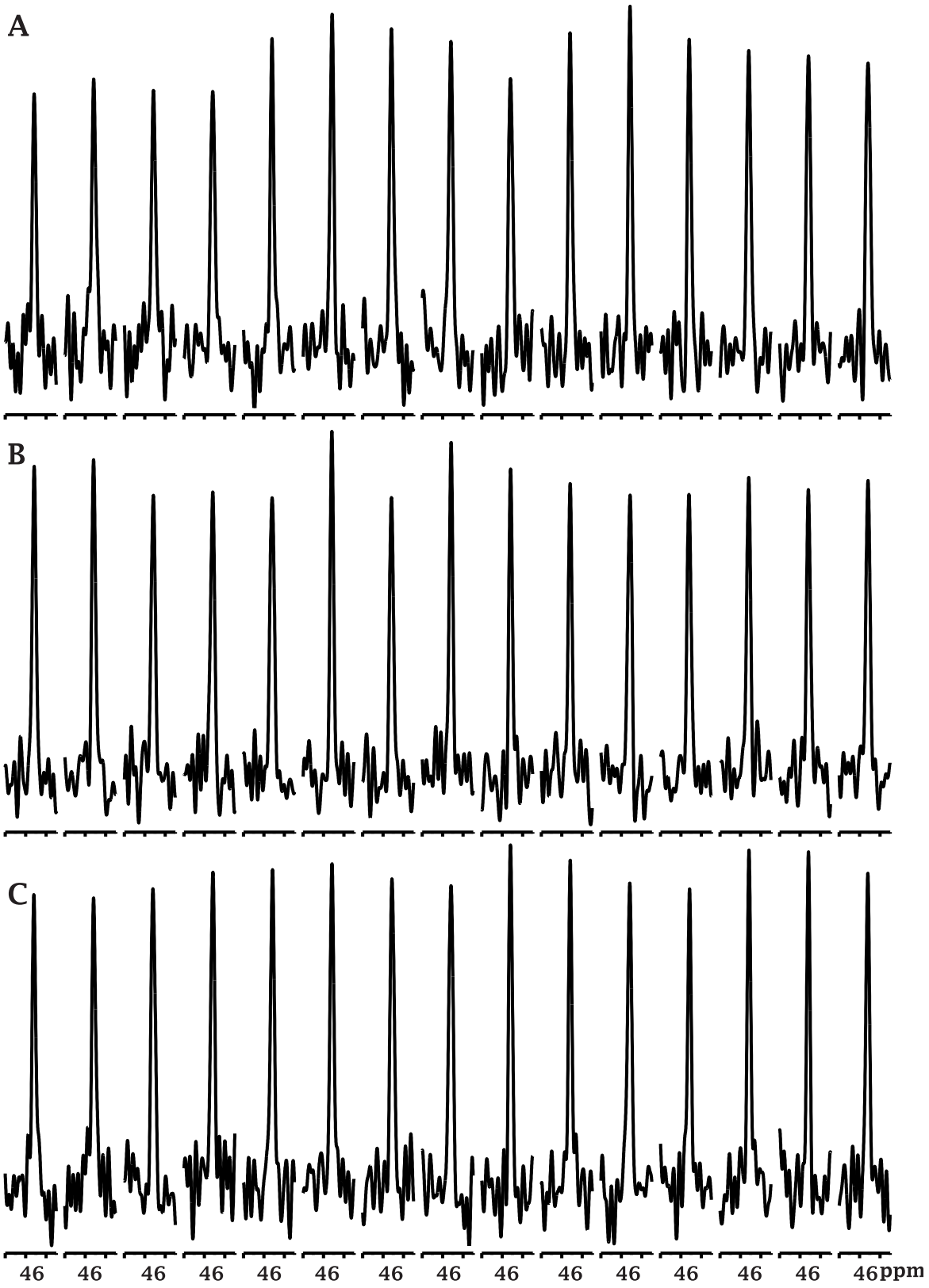

Figure 3.16: Comparison of ^{1}H off-resonance behaviour of XiX (A), TPPM (B), and SW$_f$-TPPM$_{4l}$ (C) schemes. The carrier frequency was varied in the steps of 500 Hz (increasing from left to right), spanning a range of 7 kHz in each case. The decoupling schemes were applied at an RF field strength of 122 kHz on the glycine sample spinning at a MAS frequency of 30.2 kHz.

of ^{1}H resonances with a distribution of chemical shifts, improved ^{1}H off-resonance will lead to spectral enhancement and thus, SW$_f$-TPPM$_{4l}$ is a method of choice at this MAS frequency.

The dependence of decoupling efficiency on the pulse length was compared for TPPM and SW$_f$-TPPM$_{4l}$, and is presented in (A) and (B) rows respectively, of Figure 3.17. The pulse length was increased from 3.4 μs to 3.8 μs (from left to right) in steps of 0.05 μs for both the schemes. The robustness of swept TPPM sequences towards pulse length, which was prominent at lower MAS frequencies, is absent for SW$_f$-TPPM$_{4l}$ in this comparison. It is a direct effect of reduction of robustness with increasing MAS frequencies. At lower MAS frequency the performance of TPPM depends acutely on pulse length but the sudden dip, seen here, was not observed in Figures 3.4, 3.7, and 3.5. The dip in the intensity variation is also observed for SW$_f$-TPPM$_{4l}$ scheme. This seems to be arising from the interference of cycle time of RF modulation scheme to that of MAS.

The decoupling efficiency of TPPM (marked with 1), SW$_f$-TPPM$_{6l}$ (2), SW$_f$-TPPM$_{5l}$ (3), SW$_f$-TPPM$_{4l}$ (4), and XiX (5) is compared at MAS frequency of 32.0 kHz and RF field strength of 130 kHz. The corresponding peak shape obtained for C$_\alpha$ resonance is displayed in Figure 3.18 in the same order from left. TPPM is the most effective method in these comparisons while the efficiency of swept-TPPM sequences improves with reduction in the number of TPPM blocks. The inferior performance of the XiX scheme is surprising, and it can be due to couple of factors. The first is the sensitivity of decoupling efficiency of TPPM on the RF inhomogeneity and amplifier stability and this factor can be seen in Figure 3.6. This is due to the fact that the efficiency of TPPM scheme is a function of flip angle at a given RF field strength. Thus, decoupling efficiency of TPPM will improve with amplifier stability and better RF homogeneity. Efficient decoupling under XiX scheme, on the other hand is realised at values of pulse length governed by rotor period and its performance is relatively unaffected by the variation of RF field strength,

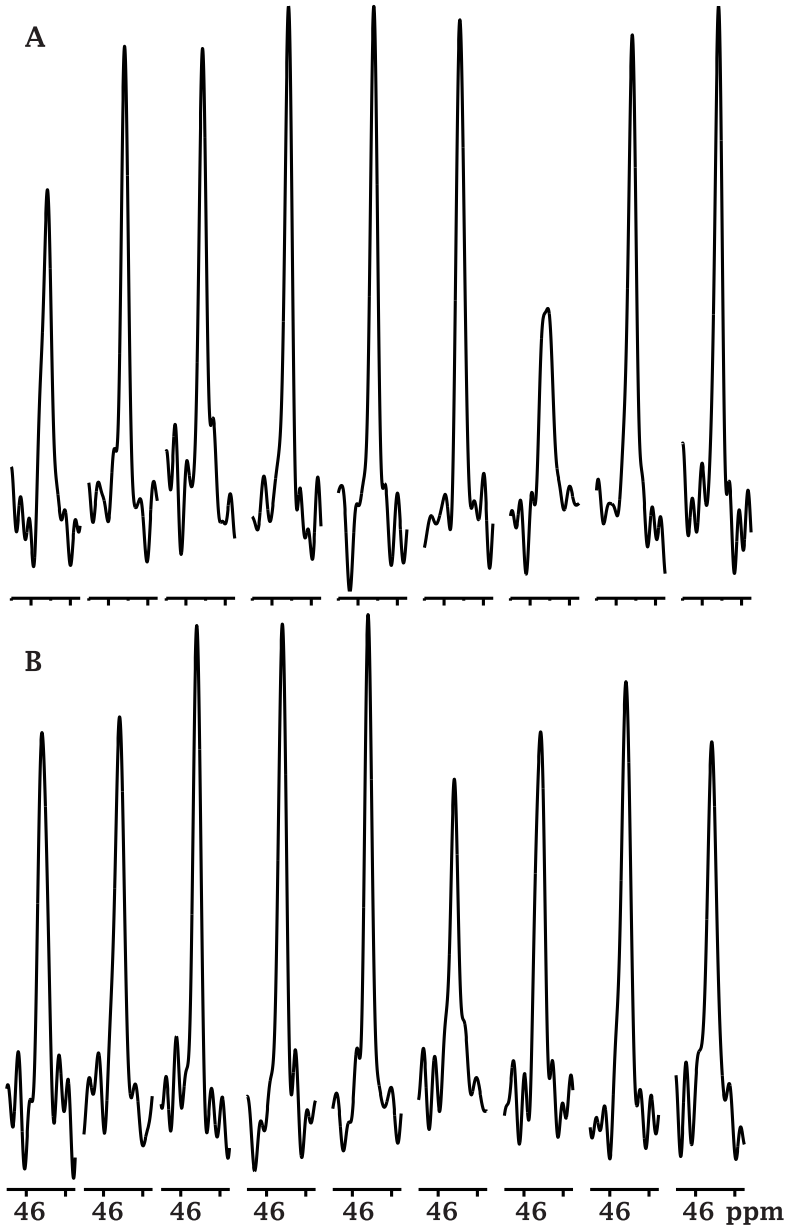

Figure 3.17: A and B rows compare the intensity of C_α resonance of glycine as a function of pulse length for TPPM and SW_f-$TPPM_{4l}$ schemes respectively. The decoupling schemes were applied at an RF field strength of 122 kHz on the glycine sample spinning at a MAS frequency of 30.2 kHz.

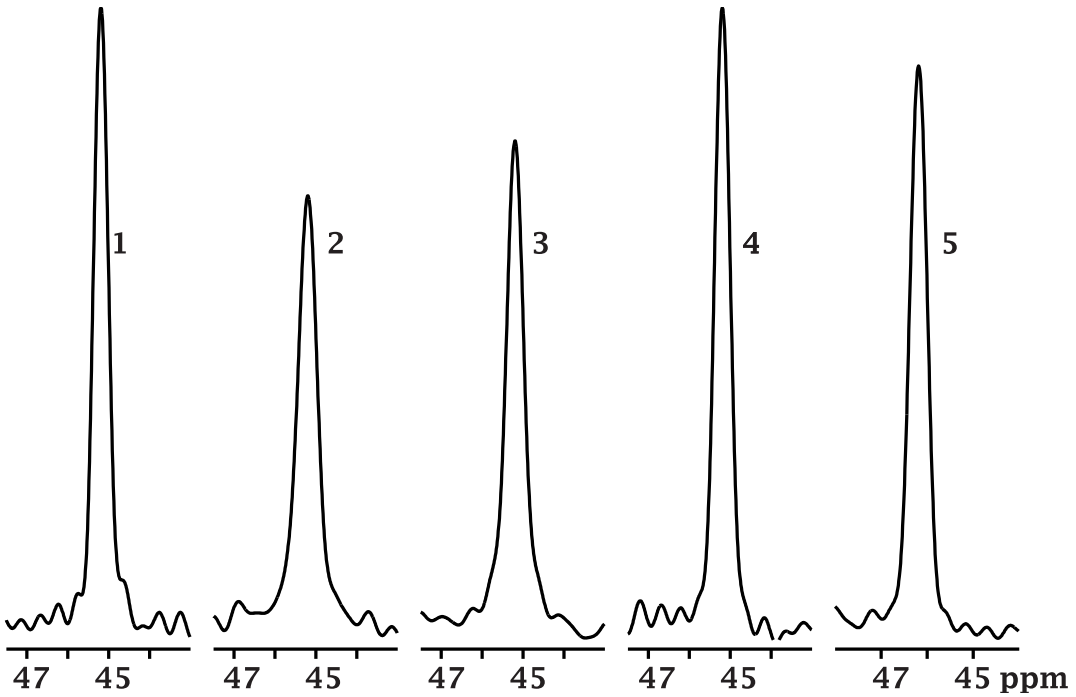

Figure 3.18: The decoupling efficiency on C_α resonance of glycine was compared for TPPM (1), SW_f-$TPPM_{6l}$ (2), SW_f-$TPPM_{5l}$ (3), SW_f-$TPPM_{4l}$ (4), and XiX (5) at MAS frequency of 32.0 kHz and RF field strength of 130 kHz.

a fact demonstrated in the original report [52]. Spectrometer manufacturers keep improving these aspects of their products and experiments reported here were done on a newer hardware. The second aspect in this consideration is the interference of ν_1 and ν_r on the decoupling efficiency of TPPM, as even 10^{th} order interference was reported in simulation [69]. In the original report of XiX, its efficiency is often compared with TPPM at such values of ν_1 and ν_r where higher order interference is indeed possible [52].

To conclude, shorter SW_f-TPPM analogues are effective at higher MAS frequencies as they are comparable if not superior than existing methods. Shorter SW_f-TPPM analogues are far superior in performance than other methods considering the ^{1}H off-resonance bandwidth. In the original report, XiX scheme was reported to be superior than TPPM at high MAS frequencies, $\nu_r > 30$ kHz on the same sample, however the intensity enhancement is lesser than the reported value which can be explained on the basis of evolution of spectrometer hardwares. In some values of MAS frequency and RF field strength, XiX

was outperformed by TPPM. This could be due to certain combination of the cycle time of the two averaging processes, this factor needs further investigation. Influence of some other factors can not be ruled out.

3.6 J-decoupling by phase modulation

In their semi-quantitative study of heteronuclear dipolar decoupling, Fung et al. [48] suggested inhomogeneity in the RF field strength across the sample as well as the distribution of ^{1}H chemical shift in the sample as a source of line width of rare spin spectrum of solids when abundant spins are decoupled with TPPM. They investigated J-decoupling in isotropic phase with TPPM and found optimum pulse length to have a constant flip angle. Thus, pulse length at ^{1}H off-resonance is governed by the effective field and a hyperbolic variation of pulse length with ^{1}H off-resonance was found optimal for decoupling. As a remedy to the situation and to enhance the decoupling performance, they designed and demonstrated the use of multifrequency excitation approach for heteronuclear dipolar decoupling. This also justified their argument of multifrequency "irradiation spectrum" of SPINAL series of heteronuclear dipolar decoupling sequences [36].

SW$_f$-TPPM also possess a series of frequency components in the power spectrum but with a normal distribution which might be an advantage. Under MAS, this method was also found to be insensitive to pulse length and this might explain the superior performance at lower MAS frequencies. The performance of SW$_f$-TPPM was compared to TPPM for J-decoupling in an aqueous solution of methanol. These experiments were done on a BBI probe. The spectra were acquired with a 90° pulse and decoupling sequences were applied with an RF field strength of 5 kHz, which is measured by the duration of corresponding 360° pulse.

A doublet structure of ^{13}C resonance was found when ^{1}H decoupling was either not applied or inefficient. Hydroxyl ^{1}H was not observed (in doublet) due to prominent exchange with water molecules. This suggested that sequences of shorter time scales are

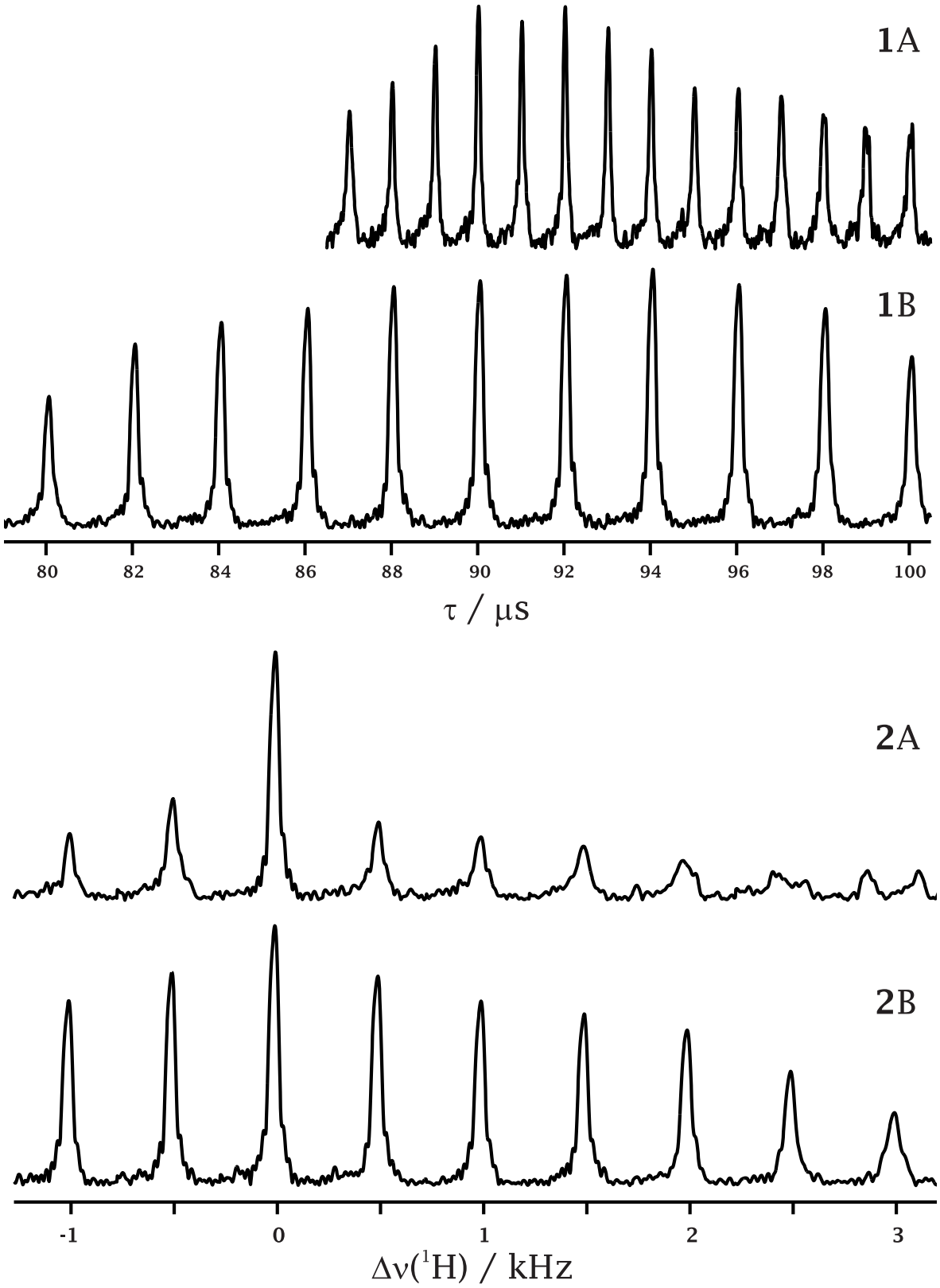

Figure 3.19: Comparison of TPPM and SW_f-TPPM for J-decoupling on methanol. 1A and 1B plots show intensity of ^{13}C resonance as a function of pulse length for TPPM and SW_f-TPPM schemes respectively. Smaller step size for TPPM was taken owing to acute dependence on the pulse length. The carrier frequency on ^{1}H channel was set 500 Hz off-resonant for this study. 2A and 2B plots show the influence ^{1}H off-resonance on the intensity of ^{13}C resonance for the same set of decoupling schemes. The pulse length for TPPM and SW_f-TPPM decoupling schemes were taken as 88 μs.

effective on longer time scales. The sequences for J-decoupling (long time scales) was found ineffective for heteronuclear dipolar decoupling [35]. The optimum pulse length was determined by the maximum intensity of ^{13}C resonance. The optimum pulse length under TPPM decoupling scheme is crucial while that under SW$_f$-TPPM is unaffected over a large range of values. A representative data is shown in 1A (TPPM) and 1B (SW$_f$-TPPM) sub-plots of Figure 3.19.

The optimum pulse length under TPPM decoupling was found to vary as a function of ^{1}H off resonance as reported by Fung et al. [48]. The range of optimum pulse length under SW$_f$-TPPM decoupling underwent negligible shift at large off-resonance. A common optimum pulse length for a large range of ^{1}H off-resonance will result in broadbanded performance for SW$_f$-TPPM. This intuition appears in the ^{1}H off resonance comparison, which is shown in 2A (TPPM) and 2B (SW$_f$-TPPM) sub-plots of Figure 3.19.

These observations suggest narrower line width of ^{13}C resonance with SW$_f$-TPPM than with TPPM in the presence of RF field strength inhomogeneity and/or distribution of chemical shifts. It results from larger ^{1}H off-resonance bandwidth for SW$_f$-TPPM decoupling.

The intensity of ^{13}C resonance decays at sub-optimal values of pulse length as well as ^{1}H off-resonance under both decoupling schemes and the splitting into doublet appears at values significantly away from the optimum. This observation may translate to enhanced intensities with phase modulated decoupling schemes over the conventional J-decoupling schemes. Thus, efficiency and ^{1}H off-resonance of SW$_f$-TPPM and SW$_{fp}$-TPPM (Section 3.8) can be compared with the conventional sequences for J-decoupling in isotropic solutions. Since these sequences are effective for extremely smaller time scales for heteronuclear dipolar decoupling as well as for long time scales for J-decoupling, these methods can also decouple interactions of the intermediate order. These decoupling schemes can also be used for decoupling the residual dipolar interactions in biological systems of large molecular mass.

3.7 Significance of phase in SPINAL performance

SPINAL was designed by modulating the phase of the TPPM blocks. Four TPPM blocks were taken in the original design of SPINAL-8 with the phases $(10^\circ, -10^\circ)$, $(15^\circ, -15^\circ)$, $(20^\circ, -20^\circ)$, and $(15^\circ, -15^\circ)$. If the phases of the TPPM blocks in SPINAL-8 were taken against their order of occurence, the profile approximates to three quarter of a Gaussian. The higher members of the SPINAL series were designed by supercycling, explained in Section 2.1.

Pulse length is the only parameter which is generally optimised in SPINAL, but the design of SPINAL allows variation of the initial phase ϕ and the phase increment step δ. In the original report the combination of initial phase ($\phi = 10^\circ$) and phase increment step ($\delta = 5^\circ$) was defined and fixed but it was found to be sub-optimal in our studies on spinning rigid solid as well as static liquid crystal. While the initial phase (ϕ) of 5° delivered better performance over the prescribed value of 10° for rigid solids under MAS, a higher value of 15° was an improvement for liquid crystals under static conditions. Liquid crystal studies are presented in Chapter 4.

The performance of SPINAL-8 and SPINAL-64 with different ϕ and δ was investigated. The initial phase of 5° was the maximum value studied as it was repeatedly found to be better than the larger values, shown in Figure 3.3 and 3.4.

The efficiency comparison of SPINAL-8 scheme as a function of step size (δ) is shown in Figure 3.20. The comparison is done for initial phase (ϕ) values of 1°, 3°, and 5° at MAS frequencies of 5, 10, 15, and 20 kHz, and the plots are marked with corresponding values. The first striking observation is the lack of universal optimum step size and its value depends upon the initial phase as well as on the MAS frequency. Another distinct feature is the significance of optimum combination with the MAS frequency, as the optimum combination is critical for higher MAS frequency of 20 kHz and is not significant for lower MAS frequency of 5 kHz. The comparisons at MAS frequency of 10 and 15 kHz display the intermediate behaviour between the low MAS frequency (5

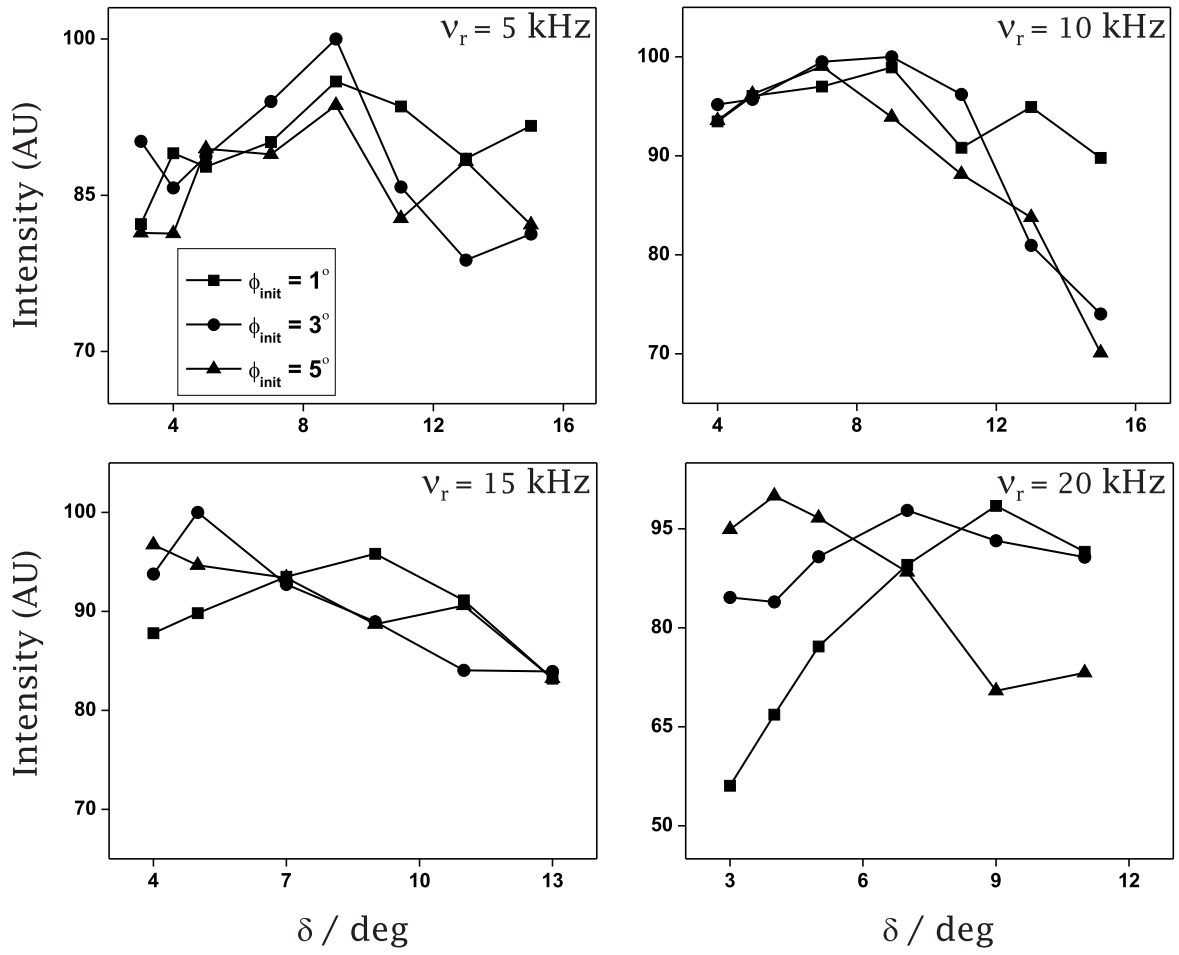

Figure 3.20: The decoupling efficiency of SPINAL-8 block compared as a function of the step size (δ) at various MAS frequencies. The initial value of the phase (ϕ_{init}) was 1°, 3°, and 5° for square (■), circle (•), and triangle (▲) respectively.

kHz) to high MAS frequency (20 kHz). These observations are understandable in the light of robustness created by ^{1}H-^{1}H couplings. As robustness scales with the scaling of ^{1}H-^{1}H under MAS, the optimum combination becomes critical at MAS frequency of 20 kHz. The efficiency delivered by the optimum combination found from the study is comparable to SPINAL-64, suggesting that supercycling is perhaps not critical.

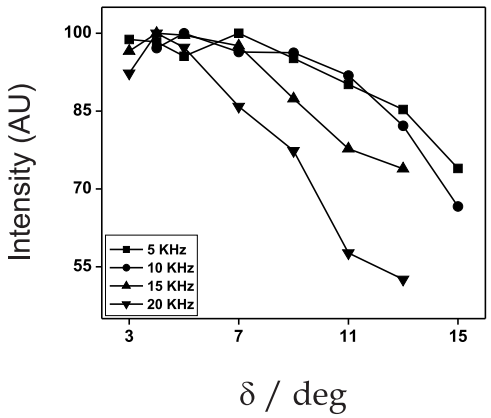

Figure 3.21: The decoupling efficiency of SPINAL-64 sequence compared as a function of the step size (δ) at various MAS frequencies. The initial value of the phase (ϕ_{init}) was 1° and the MAS frequencies are mentioned in the Figure.

The efficiency of SPINAL-64 as a function of step size was investigated at various MAS frequencies, the results are plotted in Figure 3.21. In the original report of SPINAL, initial phase of 10° was prescribed, but a value of 5° was found to be superior in the study presented in Section 3.2. The comparison was done at initial phase of 1° as this starting phase was found to be more efficient than the higher values. Taking the optimum initial phase, step size was varied to maximise the efficiency in this study. In this comparison also, the combination of these parameters are not critical at lower MAS frequencies of 5 and 10 kHz but combinations become increasingly critical at higher MAS frequencies of 15 and 20 kHz. Thus, optimum combination changes with MAS frequency and the selection of combination becomes critical at higher MAS frequencies. The efficiency of the optimum combination is comparable to the prescribed combination at lower MAS frequencies but is far superior at higher MAS frequencies.

The experimental investigations suggest that besides the pulse length (τ), the initial phase (ϕ) and the phase increment step (δ), need to be optimised for efficient performance of SPINAL scheme. Optimum value of both these parameters are governed by the MAS frequency. Reduction in robustness with MAS frequency was also observed for SW_f-TPPM, shown in Figure 3.7.

3.8 Enhanced adiabatic SW_f-TPPM: SW_{fp}-TPPM

SW_f-TPPM was designed by incorporating tangential frequency sweep in the TPPM by corresponding pulse length variation. In theoretical analysis, the tangential frequency sweep in SW_f-TPPM was found to result in adiabatic sweep through decoupling condition of phase modulation [55]. A brief discussion of theoretical analysis was presented in Section 2.2.

A decoupling sequence with enhanced adiabaticity, SW_{fp}-TPPM was designed by modulating the phase in the form of hyperbolic tangent combined with tangential variation of the pulse length. The design alongwith the involved principles were explained in Section 2.4. The values of phase were chosen keeping SPINAL study in hindsight. Few smaller sweep profiles are designed in order to suit higher MAS frequencies. Enhanced insensitivity to experimental parameters are expected from SW_{fp}-TPPM. A set of simulations was run to verify the expectations, scanning a range of RF field strength and ^{1}H off-resonance for ^{1}H decoupling under TPPM, SW_f-TPPM, and SW_{fp}-TPPM decoupling schemes. A CH_4 spin system was taken from isobutyl skeleton, the NMR parameters and spatial coordinates of which was provided in the SPINEVOLUTION package [69]. Figure 3.22 shows the intensity of ^{13}C resonance at MAS frequency of 8.08 kHz acquired with TPPM, SW_f-TPPM, and SW_{fp}-TPPM schemes where the top and bottom rows show the simulations with and without II couplings. The simulations were performed keeping the pulse length of TPPM, or central pulse pair of swept-TPPM sequences at 6.25 μs while RF field strength and off-resonance of ^{1}H channel were varied along the horizon-

tal and vertical axes respectively. The regions of efficient decoupling is shown by lighter colours, and elongation of this region along an axis indicates robust performance with the corresponding parameter.

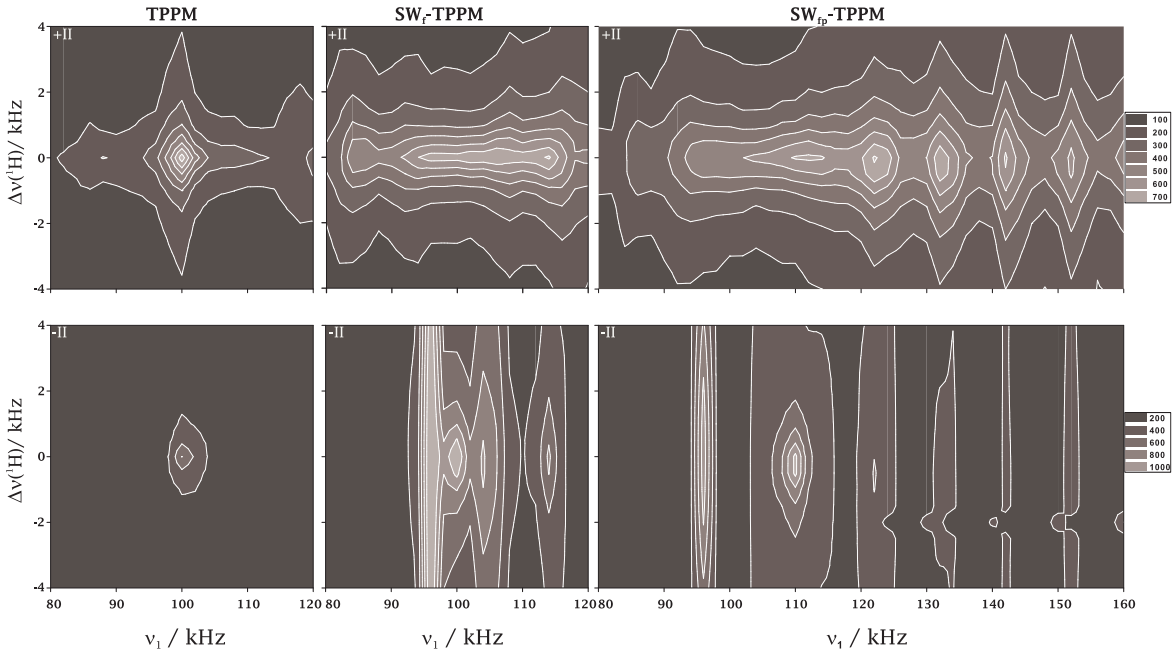

Figure 3.22: Simulated intensity of CH_4 peak of isobutyl skeleton is plotted as a function of RF field strength and ^{1}H off-resonance. The top row shows the simulation with II couplings and bottom row shows without II couplings. MAS frequency of 8.08 kHz was taken in these simulations.

The circular area of efficient decoupling for TPPM highlights the sensitivity of decoupling efficiency on both parameters, which was indeed observed experimentally. This area is broadened by II couplings in the upper row but with a loss in decoupling performance, an observation true for all decoupling sequences investigated. The maximum intensity for lower row of contours is a larger value than that of the upper row and contours are plotted accordingly. The area of efficient decoupling for SW_f-TPPM under the presence of II couplings is elongated along the axis of RF field strength, verifying the observed robustness with respect to the pulse length. This set of simulations do not correspond well with the simulations performed in the absence of II couplings, suggesting a major influence of II couplings in the ^{1}H off-resonance behaviour of SW_f-TPPM

decoupling scheme. The set of simulations without II couplings suggests improved performance for SW_f-TPPM over TPPM.

The area of efficient decoupling for SW_{fp}-TPPM with II couplings is vertically elongated, suggesting the larger ^{1}H off-resonance bandwidth of the decoupling scheme. Many bands of large ^{1}H off-resonance range can be seen and another observation of significance is the optimum flip angle clearly well above 180°. According to the simulations, this sequence is sensitive to the flip angle. As it was found with SW_f-TPPM, the contours of SW_{fp}-TPPM in the presence and absence of II couplings do not match. In the absence of II couplings, the optimum performance of SW_{fp}-TPPM is comparable to that of SW_f-TPPM.

The experimental comparisons spanning a range of MAS frequencies are presented for RF field strengths of 100 and 130 kHz.

3.8.1 Experimental

Experimental performance of decoupling sequences was compared on a sample of glycine using a Bruker AV500 MHz spectrometer with a 3.2 mm CPMAS probe. The ^{13}C spectra were acquired with ramped cross-polarisation and ^{1}H spectrum was obtained with a 90° pulse. Histidine spectra were acquired on a 4 mm probe at an spectrometer of the same field.

3.8.2 Experimental performance of SW_{fp}-TPPM at low MAS frequency

Figure 3.23 shows the comparison of performance of various decoupling schemes at MAS frequency of 6 kHz and RF field strength of 100 kHz. Plot (A) shows the intensity of C_α peak of natural abundance glycine as a function of ^{1}H off-resonance ($\Delta\nu$ (^{1}H)) for TPPM, SPINAL-64, SW_f-TPPM, SW_{fp}-$TPPM_5$, and SW_{fp}-$TPPM_7$. All modulated TPPM sequences deliver efficient performance over TPPM in the range of ^{1}H offset and SW_f-TPPM is superior over others in the entire range. Performance of these sequences as a

function of pulse length is compared in plot (B), with the same set of legends as in plot (A). Modulated TPPM sequences in general, are less affected than TPPM by the variation of pulse length. SW_{fp}-TPPM sequences are the least affected by pulse length variation with optimum pulse length being significantly higher than 5 μs which translates to optimum flip angle of clearly higher than 180°.

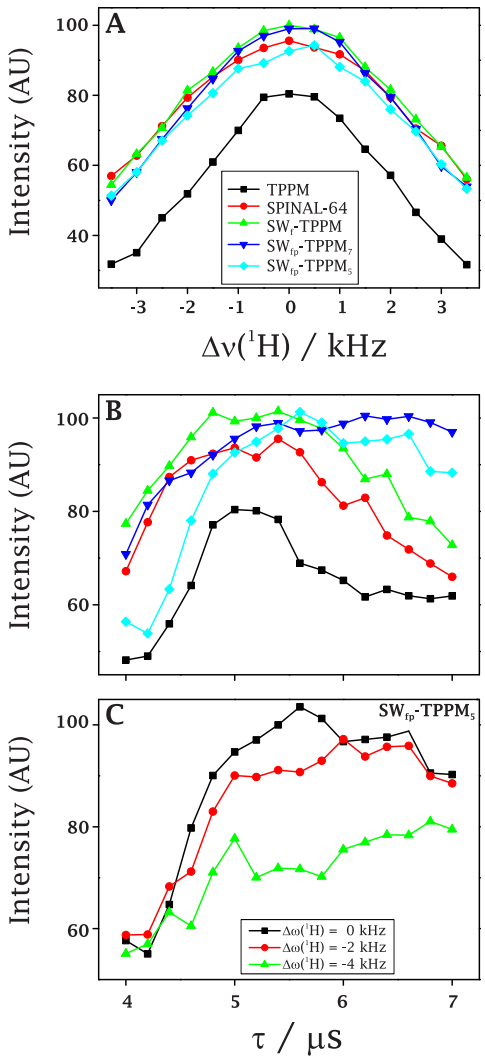

Figure 3.23: Intensity of CH_2 peak of glycine is plotted as a function of (A) ^{1}H off-resonance and (B) pulse length. Decoupling sequences investigated in (A) and (B) are TPPM, SPINAL-64, SW_f-TPPM, SW_{fp}-$TPPM_7$, and SW_{fp}-$TPPM_5$ and both the plots share the same set of legends. Plot (C) shows pulse length dependence of SW_{fp}-$TPPM_5$ for various ^{1}H off-resonance positions.

Discrete bands of enhanced ^{1}H off-resonance and sensitivity to RF field strength for SW_{fp}-TPPM sequences were found in simulations and experiments. Insensitivity towards

pulse length can be explained on the basis of enhanced robustness realised at low MAS frequencies. Maxima and minima in the variation of pulse length might separate at higher MAS frequencies. Pulse length variation was done for SW_{fp}-$TPPM_5$ at various ^1H offsets to detect the presence of bands of enhanced off-resonance, the results are presented in the (C) plot of Figure 3.23. It can be noticed that the optimum pulse length at on-resonance is sub-optimal for off-resonant decoupling. Comparing the on- and off-resonance behaviour, pulse lengths of 5.0 and 6.6 μs are more relevant for decoupling and off-resonance of SW_{fp}-TPPM sequences shown in top plot were done with the pulse length of 6.6 μs.

The band structure of ^1H off-resonance in the simulation of SW_{fp}-TPPM suggests the optimum pulse length to have the best off-resonance behaviour. Pulse duration for largest off-resonance bandwidth has to be optimised at large offset.

3.8.3 Experimental performance of SW_{fp}-TPPM at intermediate MAS frequencies

Figure 3.24 shows the performance comparison of SW_{fp}-TPPM sequences with TPPM, SPINAL-64, and SW_f-TPPM sequences at intermediate MAS frequencies of 14 to 22 kHz and at RF field strengths of 100 and 130 kHz. First (1A and 1B) and second row (2A and 2B) from the top show the comparison at MAS frequency of 14 and 20 kHz respectively keeping the RF field strength at 100 kHz, while third (3A and 3B) and fourth row (4A and 4B) show the comparison at MAS frequencies of 20 and 22 kHz respectively where the RF field strength was kept at 130 kHz. Performance of decoupling sequences as a function of pulse length and ^1H off-resonance is shown on the left and right column respectively. SW_{fp}-TPPM sequences of 5, 7, and 9 TPPM pairs were taken to monitor the relative effect of cycle time on the performance as a function of the MAS frequency. A shorter SW_f-TPPM analogue of 6 TPPM pairs, SW_f-$TPPM_6$ was also investigated. A guiding point that has to be considered in the ^1H off-resonance comparison is the better performance for

positive values than for the negative values. The root of this requirement is the general occurence of additional resonances in the ^{1}H spectrum with larger chemical shifts. Better performance in positive ^{1}H off-resonance is likely to result in enhanced spectrum. The convention of representing NMR spectrum, where frequency increases towards left hand side, is opposite to the general convention of number system and this aspect has to be considered while interpreting ^{1}H off-resonance behaviour.

The decoupling efficiency comparison at MAS frequency of 14 kHz and RF field strength of 100 kHz is shown in (1A) and (1B) of Figure 3.24 which displays the critical dependence of TPPM, SPINAL-64, and SW_f-$TPPM_6$ on the ^{1}H off-resonance. The shorter SW_f-$TPPM_6$ delivers enhanced bandwidth over the longer analogue which comes with an unwanted loss of efficiency. SW_{fp}-$TPPM_9$ performs comparable if not superior to SW_{fp}-$TPPM_7$ and both of them possess larger off-resonance bandwidth than other methods. Thus, enhanced robustness to ^{1}H off-resonance was delivered by SW_{fp}-TPPM sequences and another significant observation is the smaller relative drop in efficiency by off-resonant decoupling at MAS frequency of 14 kHz compared to that at 6 kHz, see Figure 3.23. This trend is also observed at higher MAS frequencies.

The variation in the decoupling efficiency of various sequences as a function of pulse length at MAS frequency of 14 kHz shows sensitivity of TPPM performance and robustness of modulated TPPM sequences. The local maxima for SW_{fp}-TPPM are more resolved than at 6 kHz.

A comparison of decoupling efficiency at MAS frequency of 20 kHz and RF field strength of 100 kHz was done with the inclusion of XiX which is shown in (2A) and (2B) of Figure 3.24. XiX is known to perform poorly in this region and its overall performance was matched by TPPM and easily surpassed by SPINAL-64. The shorter SW_f-TPPM analogue, SW_f-$TPPM_6$ performs clearly better than TPPM and SPINAL-64. The performance of SW_{fp}-TPPM sequences is comparable if not superior to that of SW_f-$TPPM_6$. The performance of all decoupling sequences becomes more sensitive to pulse

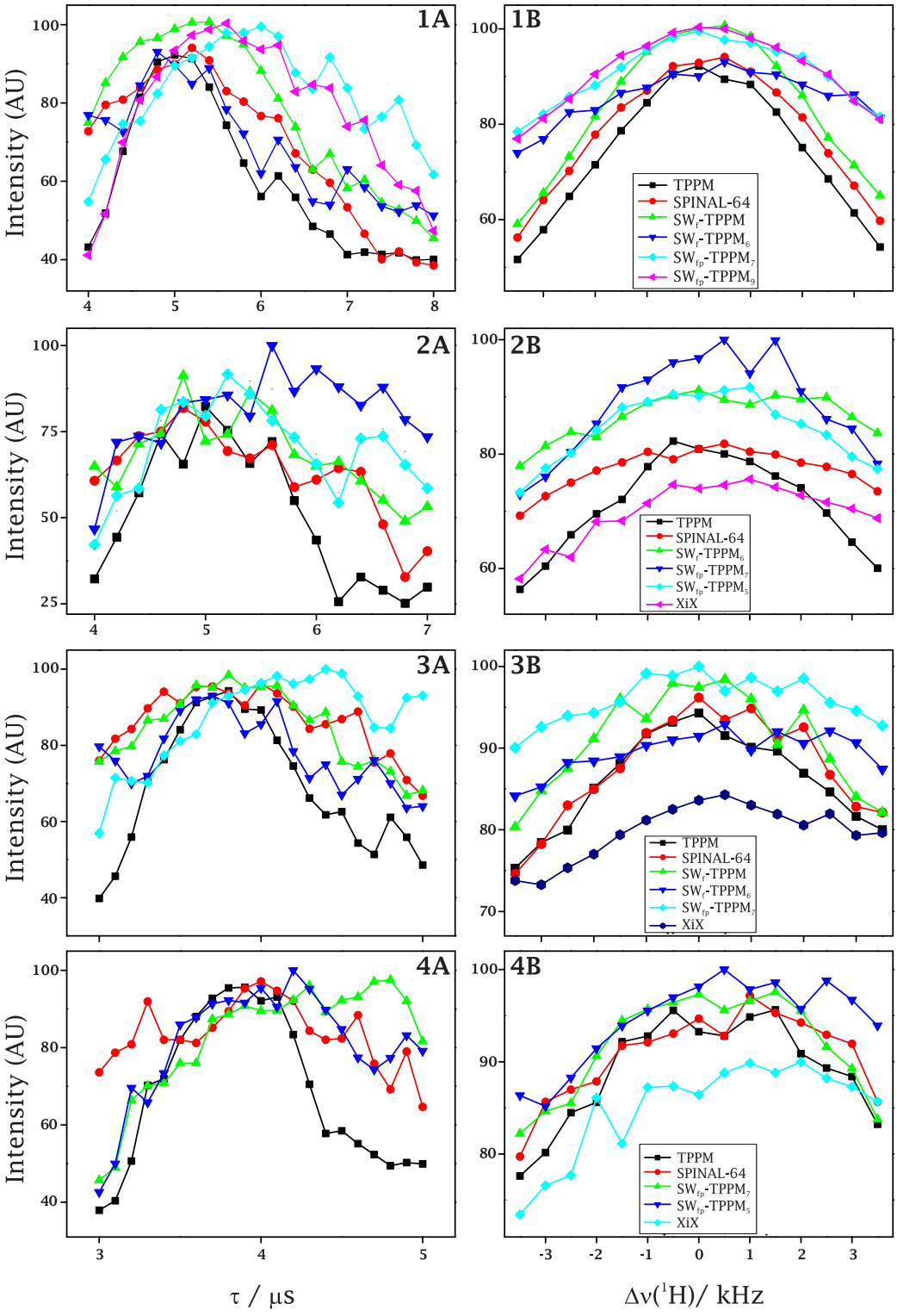

Figure 3.24: Intensity of CH_2 peak of glycine is plotted as a function of pulse length in left column (marked with 1A, 2A, 3A, and 4A) and and as a function of ^{1}H off-resonance in right column (marked with 1B, 2B, 3B, and 4B). 1A and 1B show these comparisons at MAS frequency of 14 kHz and RF field strength of 100 kHz. 2A and 2B show these comparisons at MAS frequency of 20 kHz and RF field strength of 100 kHz. 3A and 3B show these comparisons at MAS frequency of 20 kHz and RF field strength of 130 kHz. 4A and 4B show these comparisons at MAS frequency of 22 kHz and RF field strength of 130 kHz. Decoupling sequences investigated are TPPM, SPINAL-64, SW$_f$-TPPM, XiX and various SW$_{fp}$-TPPM analogues.

length and this variation was show less smooth at this combination of MAS frequency and RF field strength. This can arise from either RF field strength being an integer multiple (5 times) of MAS frequency, or a possible scaling of desired RF field strength with MAS frequency.

Another comparison of decoupling efficiency was done at higher RF field strength of 130 kHz keeping the MAS frequency at 20 kHz which is shown in (3A) and (3B) of Figure 3.24. XiX is again the least effective method over the entire range of ^{1}H offset, and the performance of SPINAL-64 becomes comparable to that of TPPM. The optimum peak intensity at ^{1}H on-resonance is delivered by the regular SW_f-TPPM but outperformed by the shorter analogue, SW_f-$TPPM_6$, at large offsets. SW_{fp}-$TPPM_7$ matches the best performance at ^{1}H on-resonance and its performance is the least affected by the variation of carrier frequency, making it a method of choice. The pulse length variation of various decoupling sequences are smoother than in lower RF field strength of 100 kHz at the same MAS frequency. Also, a smaller relative drop of intensity away from optimum value can be observed. The trend is more similar to that observed at MAS frequency of 14 kHz and RF field strength of 100 kHz, i.e. 1A and 1B.

The final comparison of decoupling efficiency was done at RF field strength of 130 kHz and MAS frequency of 22 kHz which is shown in (4A) and (4B) of Figure 3.24. XiX remains the least effective method over the range of ^{1}H offset. The performance of TPPM and SPINAL-64 matches near ^{1}H on-resonance but the later performs superior to TPPM at large off-resonance. SW_{fp}-$TPPM_7$ and SW_{fp}-$TPPM_5$ outperform other methods in this comparison, but the shorter analogue is clearly a better choice at large ^{1}H off-resonance.

3.8.4 Optimum SW_{fp}-TPPM profiles

The design of decoupling schemes involving adiabatic sweep can result in a multitude of combinations. Step size of pulse length and phase difference can be chosen with various starting and finishing values. Owing to these number of possibilities, a universally

applicable design is a desired method. It was shown earlier that smaller sequences are more effective at higher MAS frequencies, leading to MAS frequency specific designs. Comparison of few SW_{fp}-TPPM analogues are done to judge the good values of phase and pulse length and/or to select the optimum profile in regions of MAS frequencies.

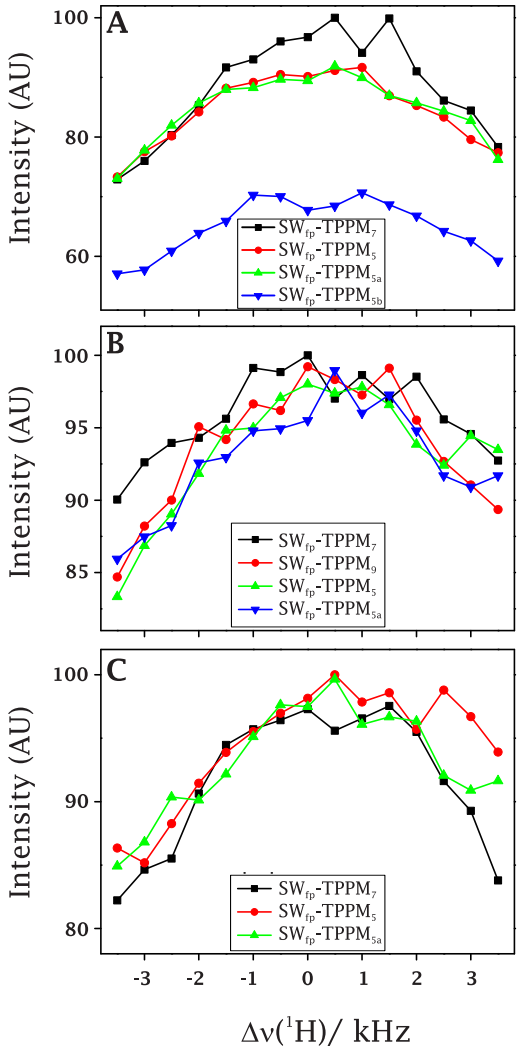

Figure 3.25: Intensity of CH_2 peak of glycine is plotted as a function of ^{1}H off-resonance for various SW_{fp}-TPPM sequences (mentioned in the figure) at various combinations of MAS frequency and RF field strengths. (A), (B), and (C) plots show the comparison at MAS frequencies (RF field strengths) of 20 kHz (100 kHz), 20 kHz (130 kHz), and 22 kHz (130 kHz).

Plot A of Figure 3.25 compares the ^{1}H off-resonance behaviour of the SW_{fp}-TPPM profiles at MAS frequency of 20 kHz and RF field strength of 100 kHz. This comparison suggests longer SW_{fp}-$TPPM_7$ to more effective over shorter SW_{fp}-$TPPM_5$ sequences.

Among SW_{fp}-$TPPM_5$ profiles the sequences with same central phase difference covering similar phase increments, SW_{fp}-$TPPM_5$ and SW_{fp}-$TPPM_{5a}$ performs comparably while the sequence with a larger central phase difference with the same phase steps is a less effective method at MAS frequency of 20 kHz and RF field strength of 100 kHz.

Plot B of Figure 3.25 shows the comparison of SW_{fp}-TPPM profiles at MAS frequency of 20 kHz and RF field strength of 130 kHz where SW_{fp}-$TPPM_7$ outperforms longer (SW_{fp}-$TPPM_9$) and shorter (SW_{fp}-$TPPM_5$ and SW_{fp}-$TPPM_{5a}$) methods, but the variation of intensity with ^{1}H off-resonance is not smooth. Among all methods SW_{fp}-$TPPM_5$ delivers smoothest variation of ^{1}H off-resonance.

The performance of SW_{fp}-$TPPM_7$, SW_{fp}-$TPPM_5$, and SW_{fp}-$TPPM_{5a}$ is compared at MAS frequency of 22 kHz and RF field strength of 130 kHz which is shown in the Plot C of Figure 3.25. At this combination of MAS frequency and RF field strength, SW_{fp}-$TPPM_5$ is better than the other methods.

3.8.5 Spectral enhancement with SW_{fp}-TPPM

The ^{1}H spectrum of glycine at MAS frequency of 22 kHz is shown in the top of Figure 3.26, the chemical shift is presented in frequency units and referenced with respect to ^{1}H on-resonance frequency of C_α. The frequency scale is chosen consistent with the convention to spectral representation in NMR. The ^{1}H on-resonance position of C_α resonance clearly lies towards aliphatic region, suggesting the isotropic chemical shift to be the on-resonance frequency for heteronuclear dipolar decoupling. This leads to separated ^{1}H on-resonance frequencies for different ^{13}C resonances, and thus, a distribution of ^{1}H chemical shifts can also lead to spectral broadening. A decoupling sequence with larger ^{1}H off-resonance bandwidth can result in intensity enhancement of ^{13}C resonances, specially in a sample with widely distributed chemical shifts. Intensity enhancement obtained with swept TPPM sequences over TPPM at lower MAS may be due to the averaging of linewidth contribution by distribution of the ^{1}H chemical shifts. An overall

enhanced spectral performance may be realised with enhanced off-resonance at higher MAS frequencies also.

A direct comparison of ^{1}H decoupling performance of TPPM and SW$_{fp}$-TPPM$_7$ is shown on ^{13}C spectrum of histidine. The ^{1}H carrier frequency was set on-resonant for C$_\alpha$ resonance and it was naturally off-resonant to other ^{13}C resonances in the molecule. A visible intensity enhancement for high-field resonances is obtained with the application of SW$_{fp}$-TPPM. More significant gains may be materialised on bigger molecules with large number of ^{1}H and ^{13}C resonances.

3.9 Conclusions

A method for heteronuclear dipolar decoupling, SW$_f$-TPPM, was designed by tangentially sweeping the modulation frequency of TPPM. The method was found to be comparable in efficiency to TPPM and SPINAL-64, but has the advantage of robustness with respect to the experimental parameters. The inherent adiabaticity of sweep is the source of robustness as suggested by theoretical analysis.

Various sweep profiles were tested for their efficiency and robustness in which adiabatic profiles were found to perform better than the others. A qualitative estimation of sweep width was also made in the study. A numerical study of the influence of II coupled bath on IS decoupling was made which suggested the assistance of the bath for heteronuclear decoupling under SW$_f$-TPPM scheme. The numerical study also highlighted the inefficient decoupling of SW$_f$-TPPM at higher MAS frequencies where variants with smaller number of TPPM pairs were designed to deliver improved performance. Study of starting phase and the increment step of SPINAL series suggested the sub-optimal performance of prescribed combination and indicated the need of optimisation at higher MAS frequencies.

The approach of adiabatic sweep was modified to design SW$_{fp}$-TPPM, a decoupling sequence with enhanced adiabaticity. Alongwith the tangential variation of modulation

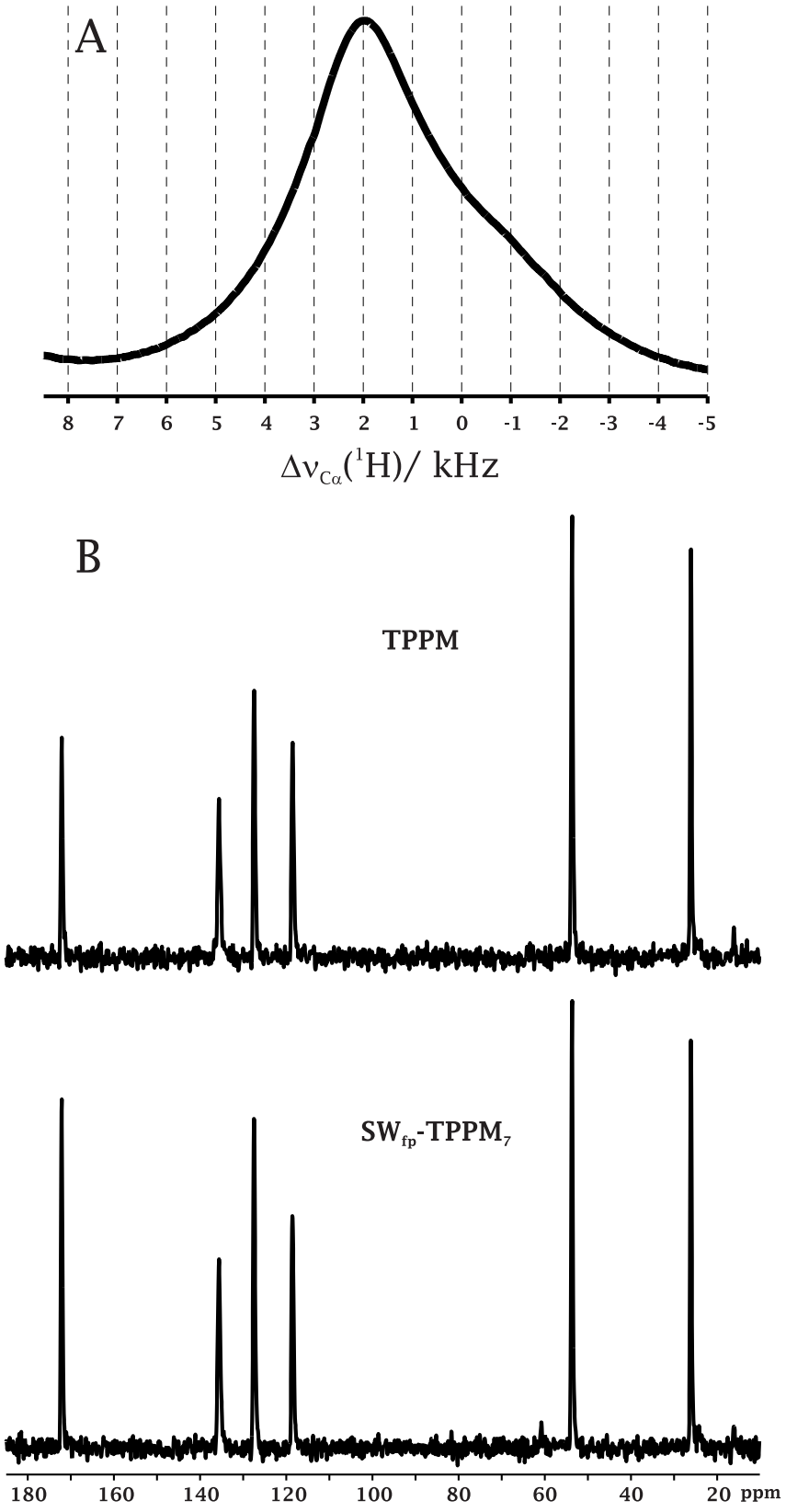

Figure 3.26: Plot A shows ^{1}H spectrum of glycine at a MAS frequency of 22 kHz, the chemical shift axis is referenced with respect to on-resonance frequency of C_α. Subsequent plots in (B) compares the ^{13}C spectrum of histidine acquired with TPPM (upper) and SW_{fp}-TPPM (lower) decoupling scheme with carrier frequency on-resonant to C_α. The sample was spinning at MAS frequency of 14 kHz and ^{1}H decoupling was applied with an RF field strength of 100 kHz.

frequency, as in SW_f-TPPM, the amplitude of phase modulation was also varied in the form of hyperbolic tangent. The choice of sweep width and phase variation was chosen from study of swept-TPPM and SPINAL series of sequences. SW_{fp}-TPPM demonstrated enhanced robustness to ^{1}H off-resonance and spectral enhancement in the study.

3.10 Future directions

Towards the end of this Chapter, improved methods were shown that resulted from enhanced adiabatic sweep. The method with enhanced adiabatic sweep, SW_{fp}-TPPM shows larger bandwidth for ^{1}H off-resonance over SW_f-TPPM, with the shortcoming of dependence of its performance on pulse length. The adiabatic sweep can be further enhanced to improve this aspect as well. Few adiabatic profiles were explored by Uğurbil et al. which are tolerant to variation of inhomogeneity as well as off-resonance of the applied RF field [73]. Uğurbil et al. also demonstrated adiabatic methods effective at lower values of RF field strength [74]. These approaches can be directly adapted for heteronuclear dipolar decoupling. Application of symmetry sequences for high MAS frequencies is also appealing.

A surprising observation of enhanced resolution was made by Paepe et al. [75], where longer dephasing time for ^{13}C coherence was obtained with a 180° pulse under ^{1}H decoupling. As 180° pulse refocusses the evolution of ^{13}C chemical shifts, collapsing the spectrum, this effect appears in experiments involving transfer of magnetisation during the indirect dimensions. The decoupling method, CM, which was developed and investigated by Paepe et al. is a numerically optimised solution and the application is involved [45]. The investigation of these effects under adiabatic decoupling methods can be made.

SW_f-TPPM scheme is also effective for J-decoupling and the study can be extended for SW_{fp}-TPPM scheme. These methods can be useful for J-decoupling and can also be effective for decoupling the residual dipolar coupling in macromolecules.

Chapter 4

Heteronuclear dipolar decoupling sequences in liquid crystal applications

Liquid crystals are one of the demanding systems in NMR for developing and testing methodologies. This phase also offers many model specific studies. Incomplete averaging of dipolar couplings in liquid crystals causes broadening of NMR spectrum. Sensitivity of this phase towards RF heating complicates the design of decoupling sequences. This Chapter describes the application of heteronuclear dipolar decoupling sequences, designed for spinning samples, for spectral enhancement in liquid crystals under static conditions. A systematic investigation of heteronuclear dipolar decoupling for a static sample is also presented, which uncovers the origin of resolution enhancement for liquid crystals with modulated TPPM methods and the criticality of pulse length for implementation of these methods.

4.1 Liquid crystals in NMR

The liquid crystal phase is characterised by partial or complete alignment of the molecules along a certain direction. This alignment is energetically favored over thermal tumbling motion by the molecular structure. A few liquid crystals suitable for NMR studies are

described here with their molecular structure in Figure 4.1. Numbering scheme of ^{13}C and ^{1}H resonances which are followed in literature are also mentioned in the diagram.

1. **MBBA** *N*-(*p'*-methoxybenzylidene)-*p*-*n*-butylaniline
2. **EBBA** *N*-(*p'*-ethoxybenzylidene)-*p*-*n*-butylaniline
3. **5-CB** 4-pentyl-4'cyanobiphenyl

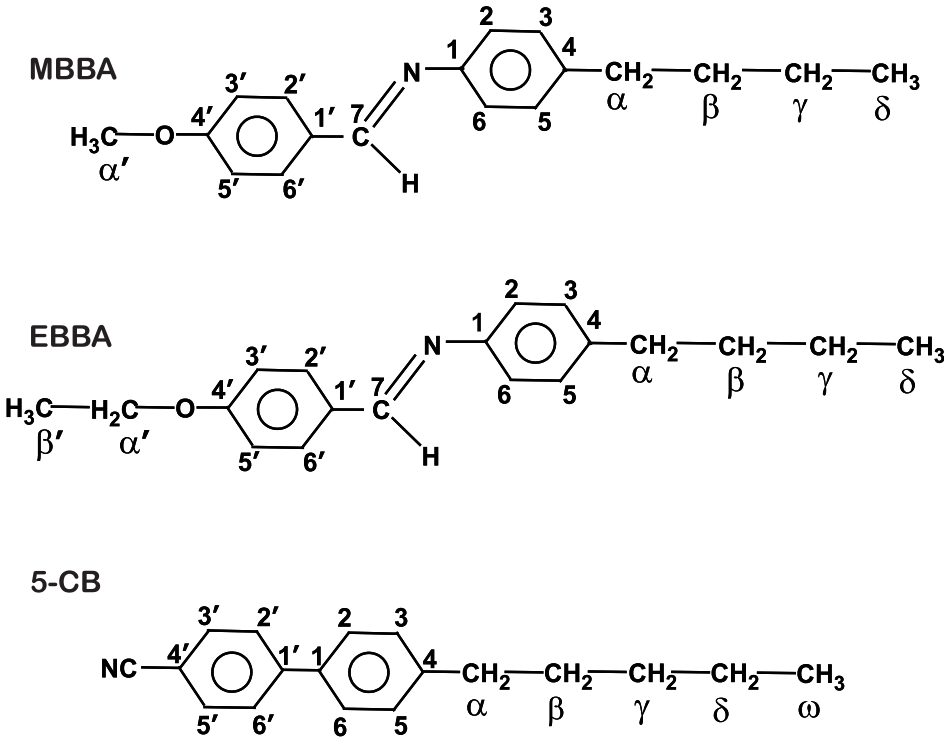

Figure 4.1: Structure of few liquid crystals popular for NMR studies. The nomenclature and numbering schemes of peaks are also shown.

Molecular structure of all these liquid crystals possess couple of aromatic benzene rings which favor stacking with an energy difference to overcome thermal tumbling. The liquid crystal molecules have preferential direction of motion allowed by their molecular alignment.

Such ordered structures mimic a large number of biologically important systems. For example, cell membranes, which are essentially lipid bilayers, are more similar to

liquid crystal phase than liquid or solid phase. Thus, membrane proteins residing in an aligned medium are modeled by liquid crystals. Membrane proteins, situated in plasma membrane, are known to play important roles in life processes, like transportation of hydophilic nutrient through hydrophobic cellwall [76]. Probing these structures along with their dynamics can unleash a great amount of novel information. However, such compounds have various levels of structural organisation with each level having its own relevance. NMR can be a candidate of choice for such studies as it can reveal various levels of hierarchy in structure associated with such systems, as in the case of proteins. However, being a partially aligned phase, resonances in the NMR spectrum are normally broad because of incomplete averaging of dipolar couplings. Incomplete averaging of homonuclear and heteronuclear dipolar couplings affects the observation of both ^{1}H and ^{13}C nuclear spins. Obtaining resolved ^{1}H spectra in liquid crystal is involved and unravelling information from ^{13}C spectra requires the need for efficient heteronuclear dipolar decoupling schemes at lower RF field strengths owing to deleterious effects of RF heating to such systems. Recent reviews cover the details of the use of NMR experiments to the study of liquid crystals with an emphasis on ^{13}C NMR [77, 78].

4.1.1 Heating effect of RF

An RF field of amplitude higher than the coupling strength is needed to effect heteronuclear dipolar decoupling. The application of RF decoupling produces heating effect, given by the universal laws of electromagnetism [79], is proportional to the square of RF field strength. Thus it is all the more important to use lower strength of RF field for sensitive samples. Owing to their rigidity, solids can tolerate large RF field strengths but liquid crystal phase stands upon a small stability over thermal energy. Thus liquid crystal is more sensitive to RF heating. Some liquid crystals are more tolerant to heating effect owing to their structure. MBBA is sensitive to RF heating, while EBBA and 5-CB are more tolerant to this effect. However, the presence of motion in this system makes

decoupling effective at lower RF field strengths.

The heating effect originates from the dissipation of RF field strength in the sample. In many biological samples, this process is assisted by the interaction of RF field with the ions in the salty sample and/or electric dipole moment of the molecules in the dielectric [80–83]. The heating effects increases with Zeeman field, owing to increased absorption of energy [84]. These effects can be controlled by the flow rate of the cooling gas [84]. At higher Zeeman field, enhanced dispersion of chemical shift demands higher RF field strength for effective decoupling of protons. Thus, it is important in the case of liquid crystals, to design decoupling methods which are effective at lower RF field strength.

4.2 Heteronuclear dipolar decoupling sequences for liquid crystals

Several heteronuclear dipolar decoupling sequences have been suggested for the study of liquid crystals. These include TPPM, SPARC, SPINAL, CM, and FLOPSY [33, 35, 36, 43, 85]. In fact, the SPINAL method orignally conceived for liquid crystals is universally adopted for MAS experiments in solids. Design principles and schematics of these decoupling sequences are described in Chapter 2.

The SPARC scheme designed by Fung et al. [35] was an improvement over TPPM [33] and SPINAL [36], again from the group of Fung, was a further improvement. Both SPARC and SPINAL rely on rapid phase cycling and phase increment was added in SPINAL. Such methods generate frequency modulations and an intuitive understanding of the efficiency of such sequences may be obtained on the basis of the Fourier picture of the corresponding RF schemes. Pulse duration of the basic TPPM scheme was tangentially swept to design SW_f-TPPM sequence. Tangential sweep of pulse length in SW_f-TPPM generated a normal distribution of Fourier components. Under MAS, SW_f-TPPM was found to be more robust with respect to various experimental parameters in

comparison with both TPPM and SPINAL. Subsequently, RF modulation schemes were designed on a variety of sweep profiles and found to be effective.

This Chapter presents the application of swept TPPM sequences, SW_f-TPPM, along with $SW_f^{tan_1}$-TPPM and SW_f^{inv}-TPPM for decoupling liquid crystal under static conditions. Among other variants, $SW_f^{tan_1}$-TPPM and SW_f^{inv}-TPPM were chosen for delivering better performance at lower MAS rates. A combined reference to SW_f-TPPM and analogues are made by swept TPPM sequences. The performance of these sequences is compared with SPINAL-64 and TPPM. A systematic optimisation of the initial phase on the static sample led to spectral enhancement under the SPINAL-64 scheme. The performance of swept TPPM sequences was studied as a function of phase difference (2ϕ) where higher values were found to perform better. Various ^{13}C resonances separated by large chemical shift were found to possess significantly separated on-resonance positions and this investigation suggested better ^1H off-resonance performance of swept TPPM sequence to result in spectral enhancement.

SPINAL-64 delivered a far superior performance than TPPM in the original report [36]. This observation was verified and the origin of enhanced performance of SPINAL-64 than TPPM was investigated. It was found that TPPM possess acute dependence on ^1H off-resonance under static conditions, and modulated TPPM sequences perform in a superior way owing to larger ^1H off-resonance bandwidth. Modulated TPPM methods refer to the set consisting of SPINAL-64 and swept TPPM sequences. The dependence of SPINAL-64 and swept TPPM sequences on ^1H off-resonance was found to be affected by the value of phase (ϕ) taken. A systematic study on the interplay of the ^1H off-resonance and phase are presented to corroborate this observation.

4.3 Improved decoupling sequences under static case

Decoupling efficiency comparison of SPINAL-64, SW_f-TPPM, SW_f^{inv}-TPPM, and $SW_f^{tan_1}$-TPPM will be presented in this Section. Value of phase (ϕ) and phase difference (2ϕ) is

denoted as subscripts for SPINAL-64 and swept TPPM sequences respectively.

4.3.1 Experimental

Experiments described in this Section were performed on a Bruker AV500 MHz spectrometer equipped with a double-resonance BBI probe. These experiments were performed on a liquid crystal sample of MBBA maintained at 22°C. Temperature was kept steady by appropriately regulating the gas flow (in excess of 11 l/min) and long recycle delays were given for cooling the sample. Recycle delays of 40 s were used for a decoupling RF field strength of 30 kHz and 30 s for RF field strength of 25 and 20 kHz. The acquisition time of 30 ms for RF field strength of 30 kHz and 40 ms for RF field strength of 25 and 20 kHz were chosen to avoid RF heating effects. These values of acquisition time and recycle delay were chosen following Fung's suggestion [77].

4.3.2 Off-resonance behavior of modulated TPPM sequences

Figure 4.2 shows intensity comparison of C_α, C_β, and C_7 resonances as a function of ^{1}H off-resonance, $\Delta\nu(^1\text{H})$, for SPINAL-64$_{\phi=10}$, SPINAL-64$_{\phi=15}$, SW$_f$-TPPM, SW$_f^{inv}$-TPPM, and SW$_f^{tan_1}$-TPPM. The relatively larger bandwidth for swept TPPM sequences is evident here with SW$_f^{inv}$-TPPM and SW$_f^{tan_1}$-TPPM being the least sensitive to ^{1}H off-resonance. After optimisation of initial phase (ϕ), SPINAL-64$_{\phi=15}$ was found to deliver larger bandwidth than the prescribed SPINAL-64$_{\phi=10}$. Initial phase of 15° was found to be the optimum in the study, which can be seen in Figure 4.12.

A more striking observation was the different ^{1}H on-resonance positions for different ^{13}C resonances. Optimum ^{1}H on-resonance frequency for C_7 resonance was found to be 3 kHz away (towards high-field side) from those of C_α and C_β peaks. C_α and C_β resonances possess the same ^{1}H on-resonance frequency within the resolution of investigation, 1.0 kHz. This difference of ^{1}H on-resonance frequencies corresponds to difference in ^{1}H chemical shift of resonances in corresponding environments. This explanation as-

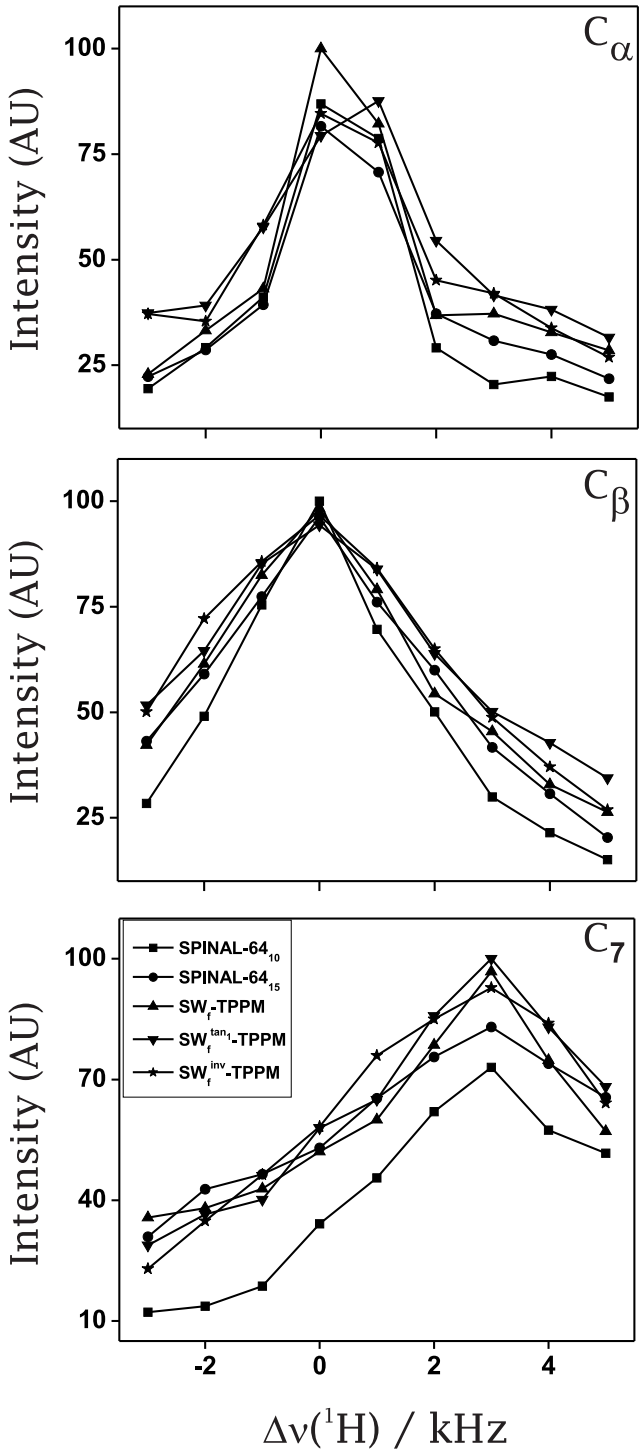

Figure 4.2: Comparison of spectral intensity as a function of ^{1}H offset ($\Delta\nu(^1\mathrm{H})$) of CH_2 (C_α, top plot), C_β (middle plot), and C_7 peaks (bottom plot) of MBBA obtained with various decoupling sequences, namely SPINAL-64_{10}, SPINAL-64_{15}, SW_f-TPPM, SW_f^{inv}-TPPM, and $SW_f^{tan_1}$-TPPM. The RF field strength was 25 kHz.

sumes isotropic chemical shift of ^{1}H resonances as on-resonance frequency for bonded ^{13}C resonances. This is surprising as ^{1}H spectra of anisotropic medium is broadened by homogeneous homonuclear dipolar coupling and this interaction is capable of spreading the effect of RF irradiation by the process of spin diffusion. The presence of individual ^{1}H off-resonance for various ^{13}C resonance will yield overall spectral enhancement under heteronuclear dipolar decoupling with large bandwidth.

The C_α, C_β, and C_7 resonances are chosen for study owing to their sensitiveness to decoupling. C_α (CH_2) resonance belongs to the aliphatic tail attached to benzene ring and dipolar interaction in this group is the least averaged by the wagging motion of aliphatic tail but the spatial interactions are relatively more averaged in the next CH_2 group (C_β). Aromatic ^{13}C resonances are also sensitive to decoupling as they belong to relatively immobile part of molecule. C_7 (CH_1) is a representative aromatic resonance, as it forms the bridge between two benzene rings.

4.3.3 Spectral performance of modulated TPPM sequences

Figure 4.3 shows the spectra of MBBA obtained with SPINAL-64_{10}, SPINAL-64_{15}, SW_f-TPPM, $SW_f^{tan_1}$-TPPM, and SW_f^{inv}-TPPM decoupling schemes applied on-resonance to C_α at an RF field strength of 25 kHz. The phase differences of swept TPPM sequences were 35°, 35°, and 45° for SW_f-TPPM, $SW_f^{tan_1}$-TPPM, and SW_f^{inv}-TPPM respectively. The intensity of C_α resonance stays the same with application of various decoupling sequences as the carrier frequency is on-resonant to it. The other peaks, especially aromatic resonances on the high field side of the spectrum show intensity enhancement with decoupling sequences of larger off-resonance bandwidth. In general, SPINAL-64_{15} and the swept-TPPM sequences perform well for all the the ^{13}C resonances. Considering the overall spectral appearance, $SW_f^{tan_1}$-TPPM and SW_f^{inv}-TPPM perform particularly better than the other sequences.

Figure 4.4 shows the comparison when ^{1}H carrier frequency was kept 1 kHz off-

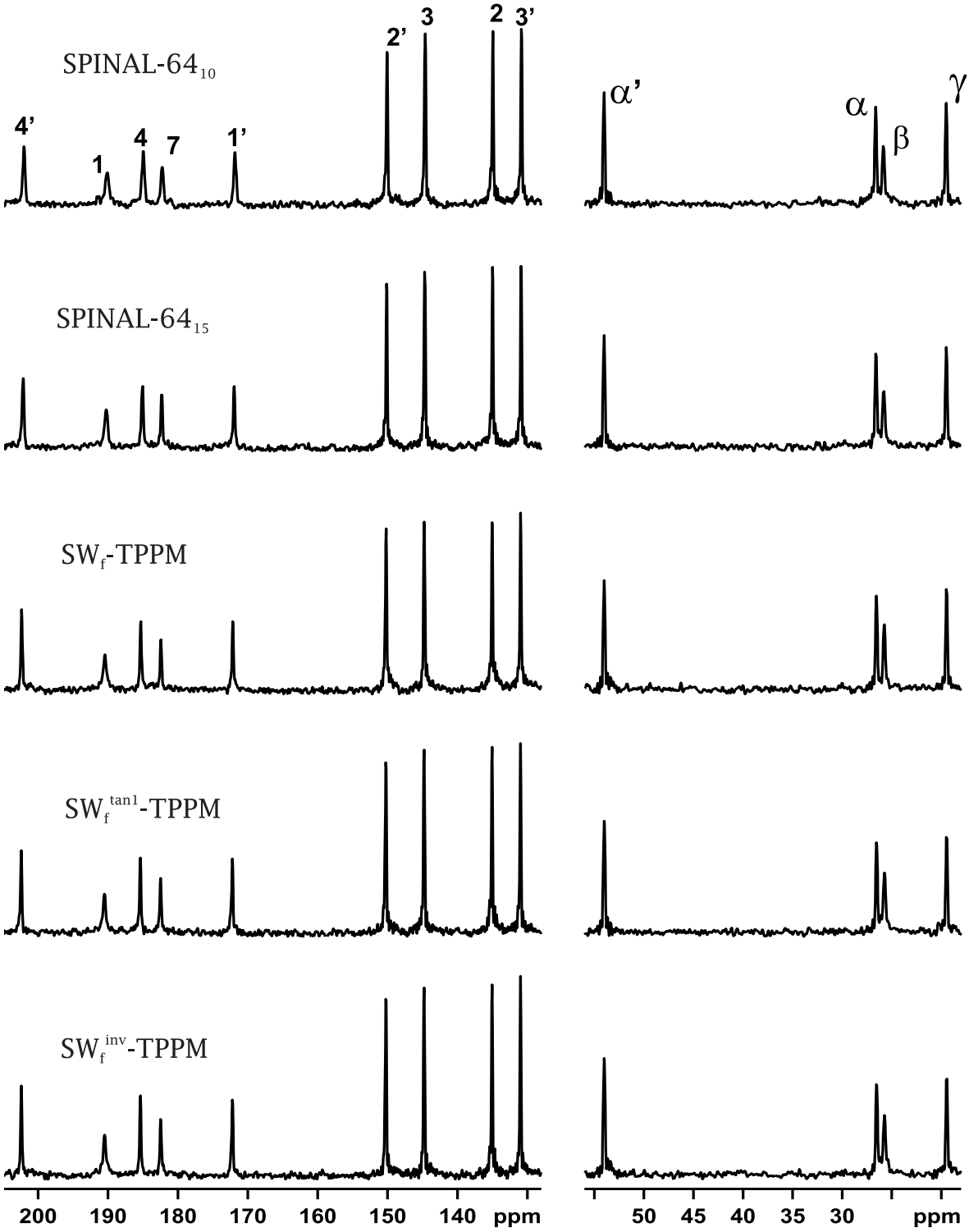

Figure 4.3: Static spectra of MBBA obtained with various decoupling sequences (mentioned on the figure itself) at an RF field strength of 25 kHz, the ^{1}H carrier-frequency was kept on-resonant to C_α (CH_2) peak.

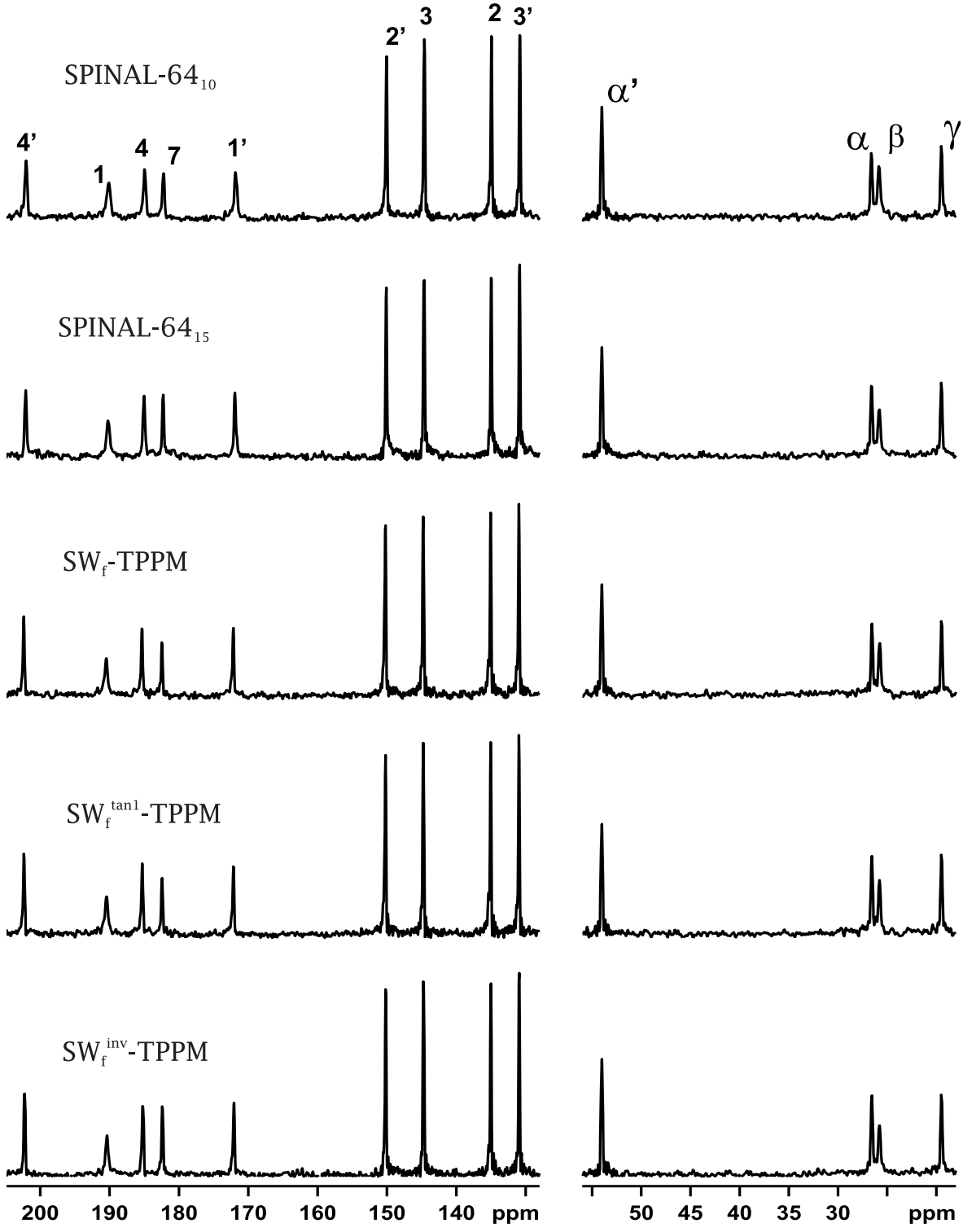

Figure 4.4: Static spectra of MBBA obtained with various decoupling sequences (mentioned on the figure itself) at an RF field strength of 25 kHz, the ^{1}H carrier-frequency was 1.0 kHz off-resonant to CH_2 (C_α) peak.

resonant (towards high field, in deshielding convention) to ^{1}H on-resonance of C_α peak. The other parameters were kept the same as in Figure 4.3. Now, it can be noticed that all peaks in the spectra recorded with swept TPPM sequences are more intense than those obtained with SPINAL-64_{10} scheme. Among the various methods, application of $SW_f^{tan_1}$-TPPM and SW_f^{inv}-TPPM decoupling sequences resulted in the best resolution. This feature is a manifestation of the larger ^{1}H off-resonance bandwidth of these sequences.

Comparing the performance of various decoupling sequences in Figure 4.3 and Figure 4.4, swept TPPM sequences especially $SW_f^{tan_1}$-TPPM and SW_f^{inv}-TPPM are recommended for heteronuclear dipolar decoupling in liquid-crystal NMR applications.

4.3.4 Performance of swept-TPPM sequences as a function of phase

Robustness of $SW_f^{tan_1}$-TPPM and SW_f^{inv}-TPPM sequences towards the phase difference (2ϕ) will be examined in this Section. The intensity of C_α and C_7 peaks of MBBA as a function of 2ϕ at three RF field strengths of 20, 25, and 30 kHz is shown in Figure 4.5. Both the sequences are fairly insensitive to a phase variation from 35° to 45°. This feature is a clear advantage over SPINAL-64 where efficiency was critically dependent on the initial phase.

To determine the phase for optimum performance and for comparing the spectral enhancement of various decoupling schemes, intensity of the sensitive C_7 peak of MBBA is monitored in Figure 4.6. The specrum obtained (C_7 peak) with TPPM, $SPINAL_{10}$, $SPINAL_{15}$, SW_f-TPPM, $SW_f^{tan_1}$-TPPM, and SW_f^{inv}-TPPM is plotted from left to right in each trace. The left, middle, and right columns correspond to decoupling RF field strengths of 20, 25, and 30 kHz, respectively. Decoupling with independently optimised phase for each sequences is shown in top row. The phase values corresponding to spectra shown in Figure 4.6 are shown in Table 4.1. SPINAL-64_{15} is more efficient than the originally reported SPINAL-64_{10} at all RF field strengths. The performance of SW_f-TPPM, $SW_f^{tan_1}$-TPPM, and SW_f^{inv}-TPPM schemes are nearly the same with SW_f^{inv}-TPPM having an edge

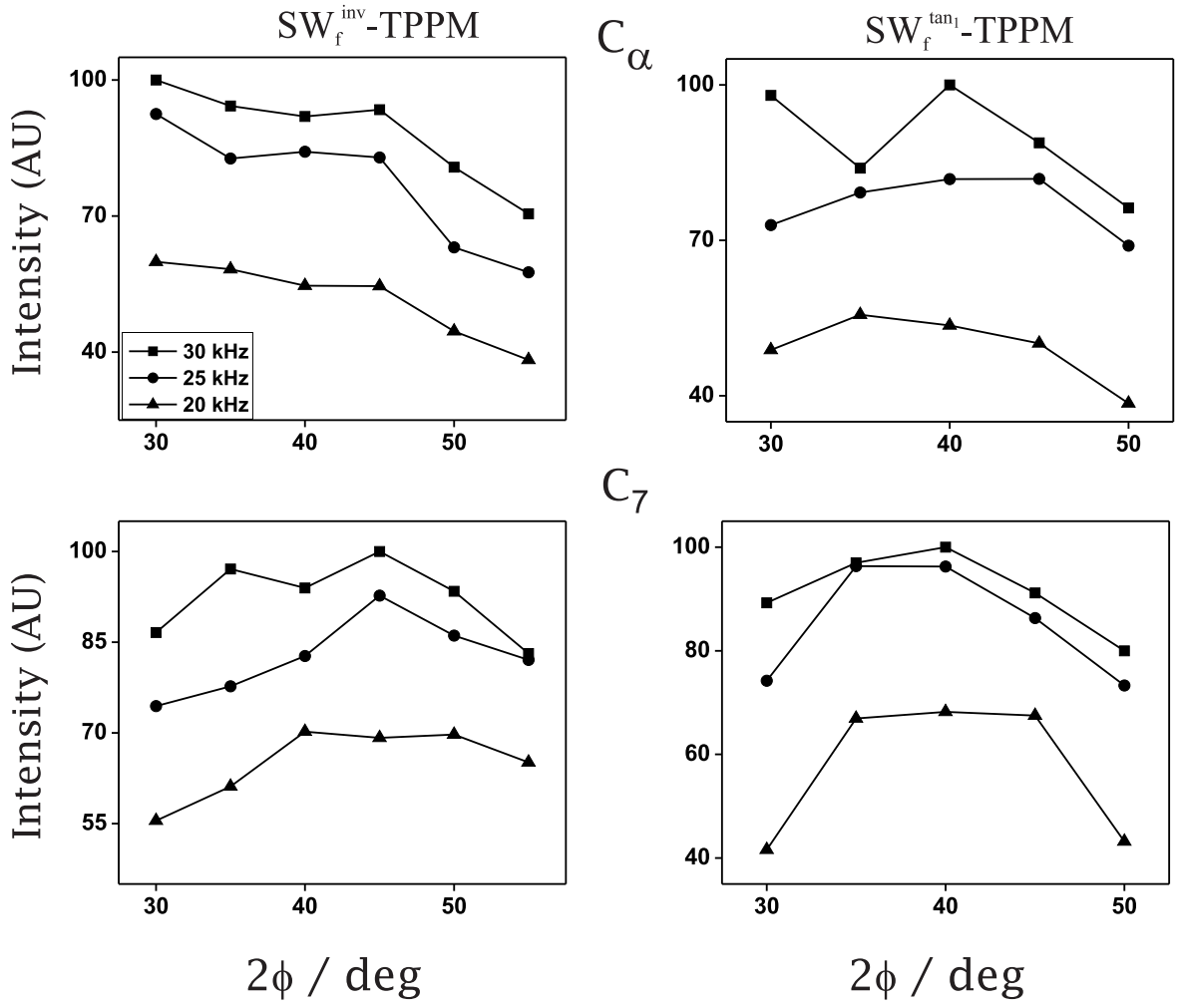

Figure 4.5: The intensity of the C_α (top row) and C_7 (bottom row) peaks of MBBA plotted as a function of the phase difference (2ϕ) obtained with SW_f^{inv}-TPPM (left column) and $SW_f^{tan_1}$-TPPM (right column) sequences for decoupler RF field strength, ν_1, of 20, 25, and 30 kHz.

over the others which becomes pronounced at higher RF field strengths.

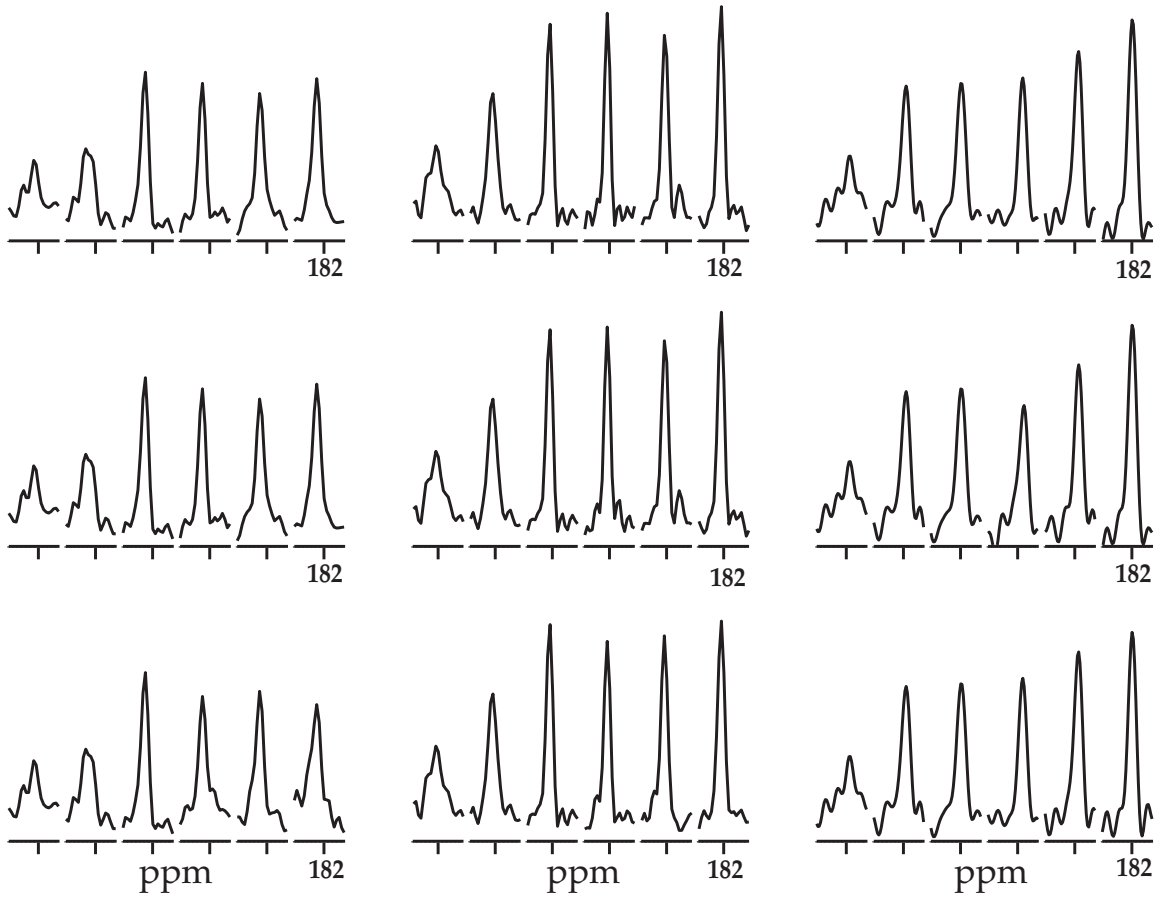

Figure 4.6: Spectral intensity comparison of the C_7 resonance of MBBA (at ≈182 ppm) for the decoupling sequences, TPPM, $SPINAL_{10}$, $SPINAL_{15}$, SW_f-TPPM, $SW_f^{tan_1}$-TPPM, and SW_f^{inv}-TPPM from left to right, in each trace. The left, middle, and right columns correspond to decoupling RF field strengths of 20 kHz, 25 kHz, and 30 kHz respectively. The top, middle, and bottom rows correspond to decoupling with optimised phases for each sequence at each RF field strength, with compromise phase values that are different for each of the swept TPPM sequences but the same for all RF field strengths, and compromise phase values that are same for all the swept TPPM sequences for all RF field strengths, respectively. The phase values for each of the decoupling sequences are mentioned in Table 4.1.

It is evident from Table 4.1 that for various RF field strengths, the optimal phase values differ for the swept TPPM sequences with the spectral comparison shown in the top row of Figure 4.6. Hence, a compromise has to be made between the conflicting demands of optimum efficiency and optimisation of the method.

In the first level of compromise, the same phase values at all RF field strengths were used for each sequence but different phase for different sequences were taken. The comparison is shown in the middle row of Figure 4.6 and the phase values are given in Table 4.1. Comparison of top and middle row shows the lack of perceivable change, especially at higher RF field strengths.

In the second, even grosser level of trade-off, all the swept TPPM sequences were applied with same phase value at all RF field strengths. The results are displayed in bottom row of Figure 4.6 and phase values can be found in Table 4.1. The compromise phase values were chosen so that efficiency drop should not exceed 15% of the optimum values. Comparison with the top row shows a small intensity reduction at lowest RF field strength of 20 kHz. The phase values for each of the decoupling sequences are mentioned in Table 4.1 arranged in the order in which spectra were displayed.

Table 4.1: Phase difference, 2ϕ, for the various decoupling sequences corresponding to the spectra shown in Fig. 4.6.

		2ϕ		
Decoupling Sequence		20 kHz	25 kHz	30 kHz
TPPM		25°	30°	25°
SPINAL-64_{10}		20°	20°	20°
SPINAL-64_{15}		30°	30°	30°
SW_f-TPPM	Top row	35°	30°	40°
	Middle row	35°	35°	35°
	Bottom row	40°	40°	40°
$SW_f^{tan_1}$-TPPM	Top row	40°	35°	35°
	Middle row	35°	35°	35°
	Bottom row	40°	40°	40°
SW_f^{inv}-TPPM	Top row	45°	45°	45°
	Middle row	45°	45°	45°
	Bottom row	40°	40°	40°

4.3.5 Conclusions

Heteronuclear dipolar decoupling in the NMR of liquid crystals was revisited. For the sample (MBBA) studied, SPINAL-64_{15} was found to be better than the commonly used SPINAL-64_{10} for a range of RF field strengths. The application of swept TPPM sequences designed for decoupling under MAS, namely, SW_f-TPPM, $SW_f^{tan_1}$-TPPM, and SW_f^{inv}-TPPM to the study of liquid crystals under static conditions at low RF field strengths of 20-30 kHz was investigated. These sequences were chosen according to their superior performance at lower MAS rates.

Heteronuclear dipolar decoupling sequences, besides providing enhanced intensity for the resonances, should also be robust with respect to the experimental parameters such as ^{1}H off-resonance, pulse duration, and phase difference. The scheme should also be routinely implementable on any spectrometer. Swept TPPM sequences satisfy these requirements, except the criteria of insensitivity to pulse duration. The performance of decoupling sequences with variation of pulse duration is presented in the next Section.

All the swept TPPM sequences delivered decoupling efficiency superior or comparable to SPINAL-64_{15} with $SW_f^{tan_1}$-TPPM and SW_f^{inv}-TPPM often having the edge over the others. The phase of modulated TPPM sequences, including SPINAL-64, needs to be optimised for performance. The swept TPPM sequences have a larger bandwidth and a common phase of 40° could be selected with minimal compromise on the efficiency of decoupling. For heteronuclear dipolar decoupling in liquid crystals, SW_f^{inv}-TPPM with a phase of 40° can be a method of choice.

4.4 Investigation of decoupling efficiency on liquid crystals

Various aspects of heteronuclear dipolar decoupling for NMR applications on liquid crystals are presented in this Section. It includes investigation of superior spectral perfor-

mance of modulated TPPM sequences over TPPM.

4.4.1 Experimental

All experiments were performed on a Bruker AV500 MHz spectrometer with a 4 mm triple-resonance CPMAS probe. 5-CB was used as liquid crystal sample and room temperature (27°C) was maintained with moderate air-flow of 4.8 l/min. Spectra were acquired with ramped cross-polarisation technique and heteronuclear dipolar decoupling schemes were applied for 30 ms with an RF field strength of 30 kHz.

4.4.2 Unraveling the origin of resolution enhancement

An experimental investigation of decoupling sequences was done to understand the mechanism of decoupling in liquid crystals under static conditions.

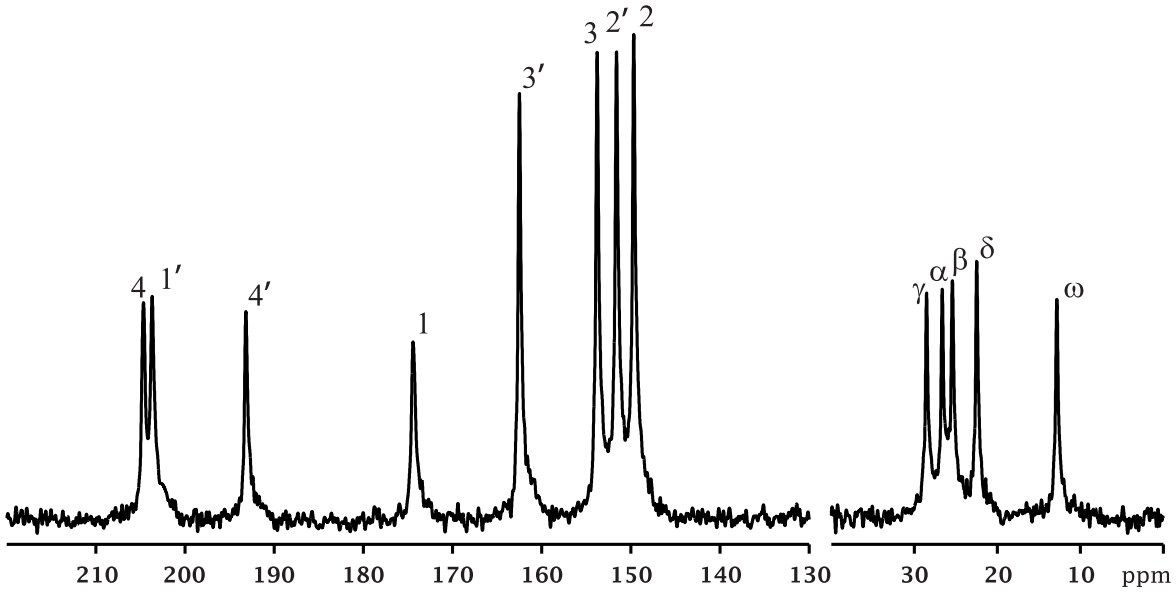

Figure 4.7: A representative spectrum of 5-CB acquired with SW_f-$TPPM_{35}$ decoupling scheme. Numbering scheme is according to the structure shown in Figure 4.1. Other experimental parameters are mentioned in the text.

Figure 4.7 shows a representative spectrum of 5-CB obtained with SW_f-$TPPM_{35}$ decoupling scheme. The resonances are marked with their chemical sites displayed in

Figure 4.1. C_α and C_γ are taken for investigation of heteronuclear dipolar decoupling.

Figure 4.8 shows intensity of C_α (right) and C_γ (left) resonances of 5-CB as a function of pulse length for SPINAL-64_{15}, SW_f-$TPPM_{35}$, $SW_f^{tan_1}$-$TPPM_{35}$, and SW_f^{inv}-$TPPM_{35}$. The carrier was kept on resonance to C_α in both comparisons. The sensitivity of decoupling efficiency on pulse length can be clearly seen in both the comparisons. This is against the observations under MAS, where modulated TPPM sequences were robust with pulse length. The optimum pulse length for all decoupling sequences is around 16.3 μs for both resonances, which corresponds to a flip angle of 180°.

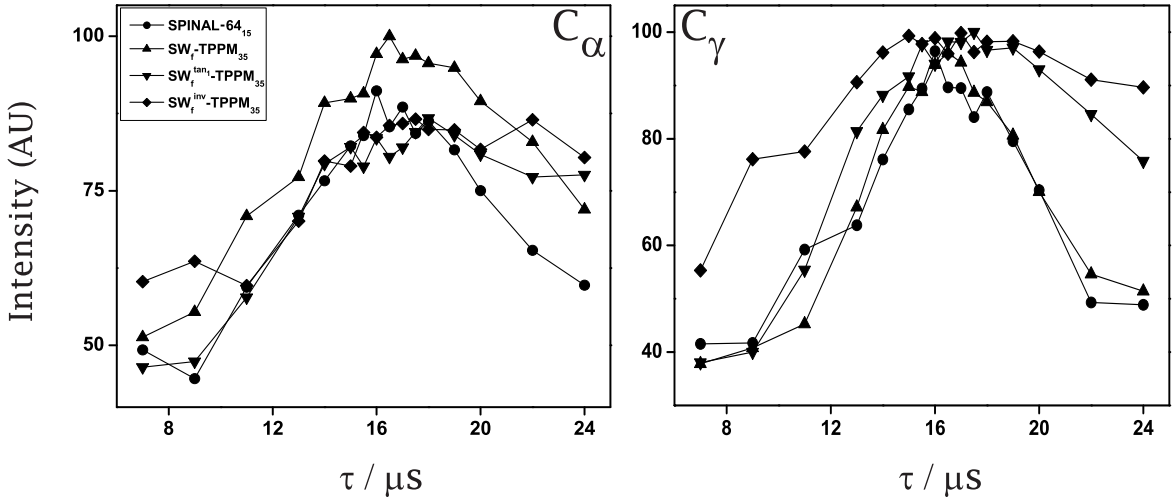

Figure 4.8: Intensity of C_α (CH_2, on left) and C_γ (CH_2, on right) resonances as a function of pulse length for SPINAL-64_{15}, SW_f-$TPPM_{35}$, $SW_f^{tan_1}$-$TPPM_{35}$, and SW_f^{inv}-$TPPM_{35}$. Other parameters are mentioned in the text.

A direct comparison of efficiency of various decoupling schemes can be seen in the Figure 4.9. Top row of Figure 4.9 shows aliphatic region of 5-CB spectra acquired with CW (marked with 1), $TPPM_{15}$ (2), SPINAL-64_{10} (3), $SW_f^{tan_1}$-$TPPM_{25}$ (4), SW_f-$TPPM_{25}$ (5), and SW_f^{inv}-$TPPM_{25}$ (6) at an RF field strength of 30 kHz, keeping the carrier at on-resonance to C_α. Aliphatic regions of 5-CB spectrum is sufficient for current purpose. CW is not able to resolve C_α peak but this peak is clearly resolved with the application of TPPM. The modulated TPPM methods do not offer visible intensity enhancement on C_α peak over TPPM but other resonances are significantly improved.

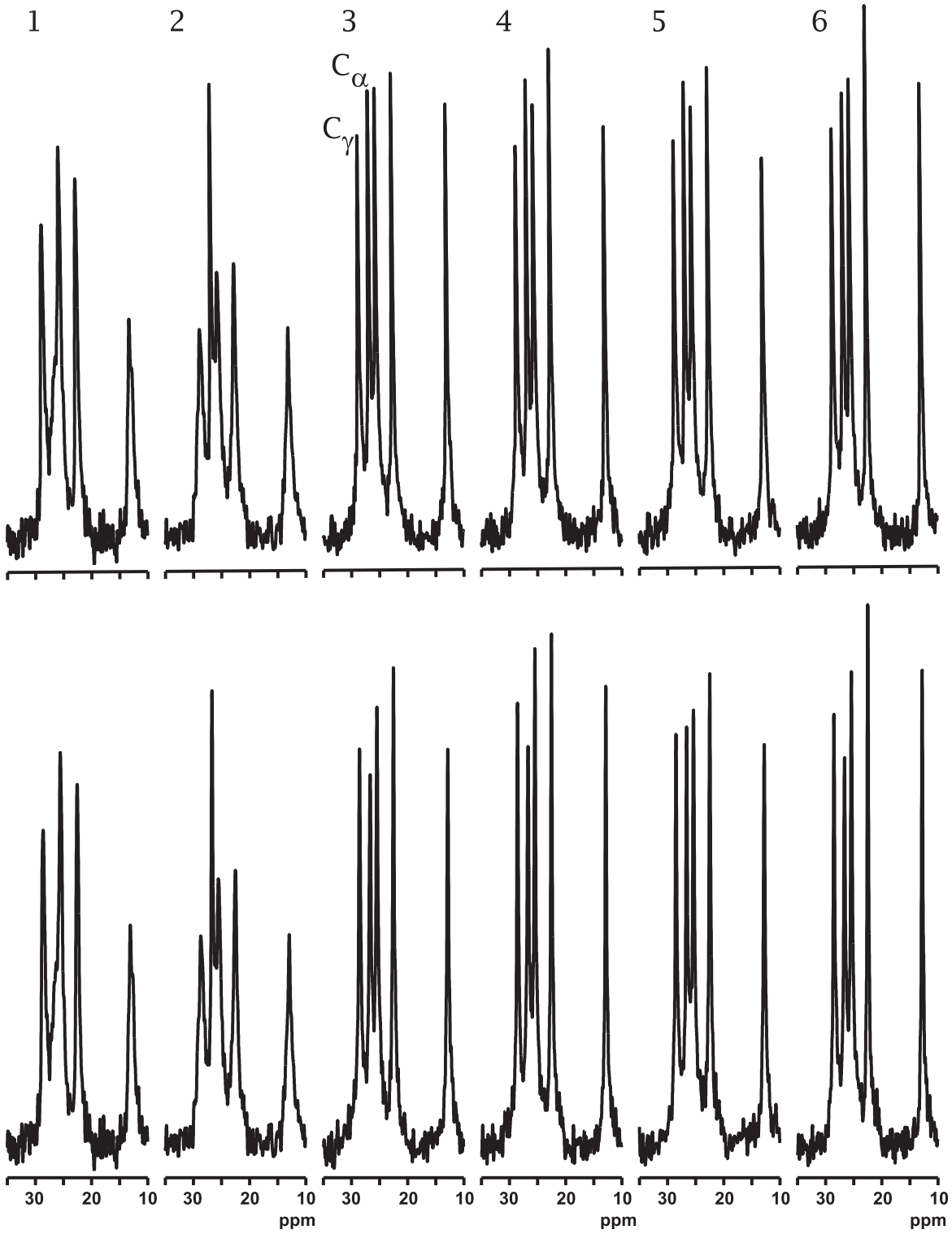

Figure 4.9: Aliphatic region of 5-CB spectra acquired with CW (marked with 1), $TPPM_{15}$ (2), SPINAL-64_{10} (3), $SW_f^{tan_1}$-$TPPM_{25}$ (4), SW_f-$TPPM_{25}$ (5), and SW_f^{inv}-$TPPM_{25}$ (6) are shown in top panel, keeping the carrier frequency on-resonance to C_α. The bottom panel shows the same comparison with higher phase for modulated TPPM sequences, i.e. CW, TPPM, SPINAL-64_{15}, $SW_f^{tan_1}$-$TPPM_{35}$, SW_f-$TPPM_{35}$, and SW_f^{inv}-$TPPM_{35}$.

Another set of spectral comparison with higher phases for modulated TPPM sequences was done keeping other parameters same as in upper row. Lower row of Figure 4.9 shows spectra acquired with CW, $TPPM_{15}$, SPINAL-64_{10}, $SW_f^{tan_1}$-$TPPM_{35}$, SW_f-$TPPM_{35}$, and SW_f^{inv}-$TPPM_{35}$. Intensity of C_α peak is reduced slightly in this comparison but other peaks in the vicinity show visible enhancement owing to better ^1H off-resonance characteristics. This aspect will be explored towards the end of this Section.

It was observed in the study on MBBA that better ^1H off-resonance leads to an overall improvement in the spectrum, a possible critical ^1H off-resonance behavior of TPPM can explain limited effectiveness to only C_α resonance. ^1H off-resonance behavior of TPPM was compared with modulated TPPM methods. Left panel in Figure 4.10 shows intensity of C_α resonance as a function of ^1H off-resonance with application of $TPPM_{15}$, $TPPM_{25}$, SPINAL-64_{10}, $SW_f^{tan_1}$-$TPPM_{35}$, SW_f-$TPPM_{35}$, and SW_f^{inv}-$TPPM_{35}$ decoupling schemes. Right panel shows an inset of left panel, where the same comparison is shown for a smaller range of carrier frequency. A critical dependence of TPPM performance on ^1H off-resonance can be noticed while modulated TPPM methods display significantly larger bandwidth for ^1H off-resonance.

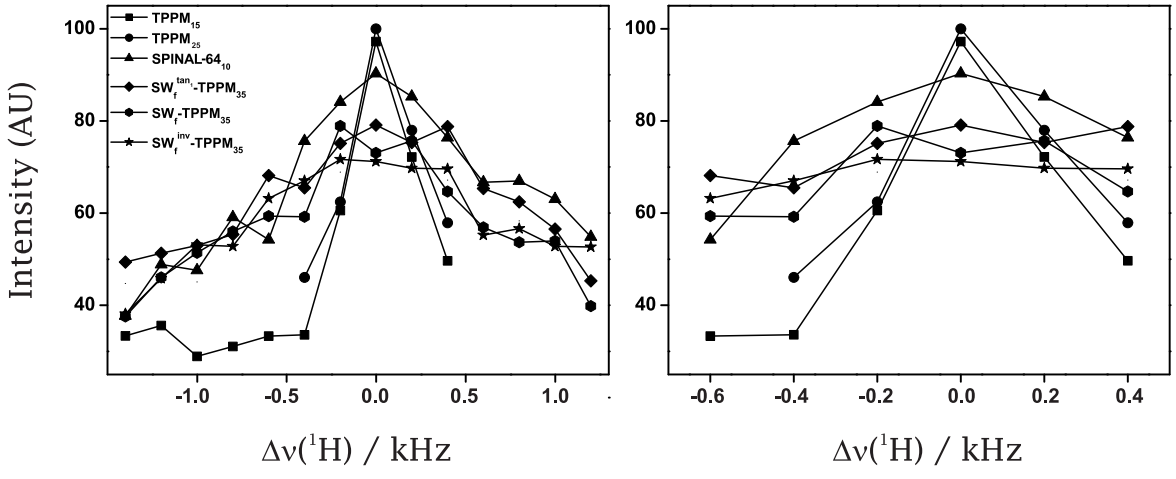

Figure 4.10: Intensity of C_α (CH_2) peak as a function of ^1H off-resonance ($\Delta\nu$ (^1H)) for $TPPM_{15}$, $TPPM_{25}$, SPINAL-64_{10}, $SW_f^{tan_1}$-$TPPM_{35}$, SW_f-$TPPM_{35}$, and SW_f^{inv}-$TPPM_{35}$. Left plot shows the comparison for a larger bandwidth and smaller bandwidth is shown on right for enhanced clarity. Other parameters are mentioned in the text.

Figure 4.11 shows the aliphatic region of 5-CB with TPPM decoupling with ^{1}H off-resonance varied in a region of 1 kHz. The top row shows the spectra obtained with TPPM with phase difference of 25°, as a function of ^{1}H off-resonance. The carrier frequency is varied in absolute sense which is opposite to high-field convention adopted to state chemical shift. The spectrum obtained with carrier frequency on-resonant to C_α is the third from right with C_α and C_γ resonances marked on it. The bottom row compares the performance of SPINAL-64_{15} in the same set of paramters. Following the intensity variation of C_α resonance, critical ^{1}H off-resonance behavior of TPPM can be noticed and different ^{1}H off-resonance positions for C_α and C_γ resonances can be clearly noticed in TPPM comparison. This set of comparisons highlights lack of sufficient bandwidth in TPPM for decoupling in liquid crystals.

4.4.3 Interplay of off-resonance and phase

Modulated TPPM sequences give resolution enhancement over TPPM in liquid crystal spectrum. SPINAL-64_{15} displayed larger ^{1}H off-resonance bandwidth over originally reported SPINAL-64_{10}. The optimum phase-difference for SW_f-TPPM sequences for spinning samples was around 25° but enhanced specral resolution for liquid crystal was realised for higher phase difference values of around 40°. The ^{1}H off-resonance bandwidth was found to depend upon the value of phase difference, 2ϕ.

A systematic study on the interplay of the phase and ^{1}H off-resonance bandwidth was done, which is shown in Figure 4.12. The intensity of C_α peak of 5-CB was monitored as a measure of decoupling efficiency. Figure 4.12A shows the off-resonance behavior of SPINAL-64_{10}, SPINAL-64_{15}, SW_f-$TPPM_{25}$, SW_f^{inv}-$TPPM_{25}$, SW_f^{inv}-$TPPM_{40}$, $SW_f^{tan_1}$-$TPPM_{25}$, and $SW_f^{tan_1}$-$TPPM_{40}$. This comparison indicates improved ^{1}H off-resonance bandwidth for higher values of phase while the lower values are more efficient at on-resonance. The reverse was also attempted, determination of optimum value of the phase difference (2ϕ) for various off-resonance positions. The comparison of decou-

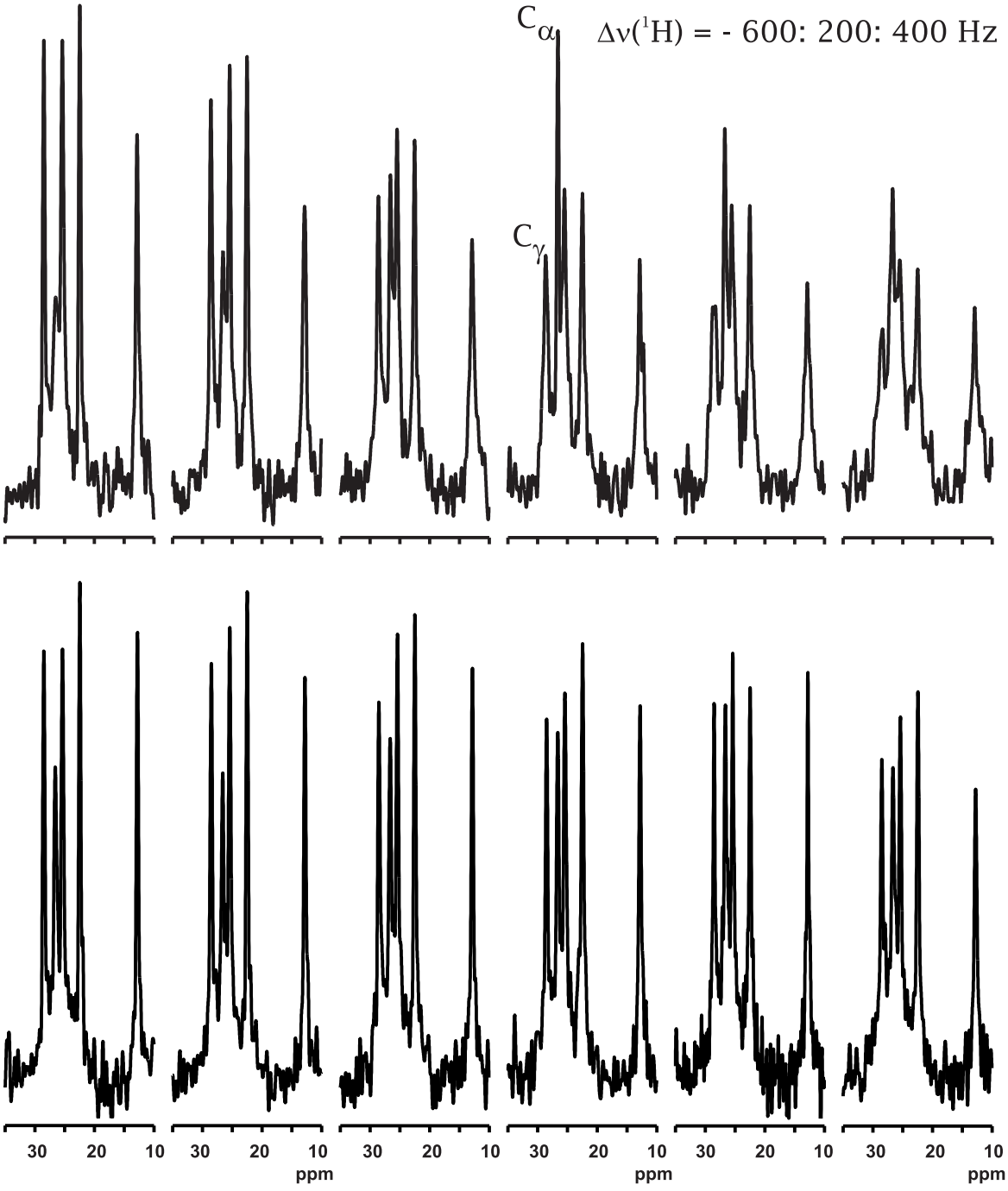

Figure 4.11: Spectral comparison (of aliphatic region of 5-CB) as a function of ^{1}H off-resonance ($\Delta\nu(^1H)$) for $TPPM_{25}$ and $SPINAL\text{-}64_{15}$. ^{1}H off-resonance is mentioned on the figure in absolute sense, which is opposite to high field convention adopted in NMR. C_α and C_γ resonances are marked in the spectrum where carrier is on-resonant to C_α. Other parameters are mentioned in the text.

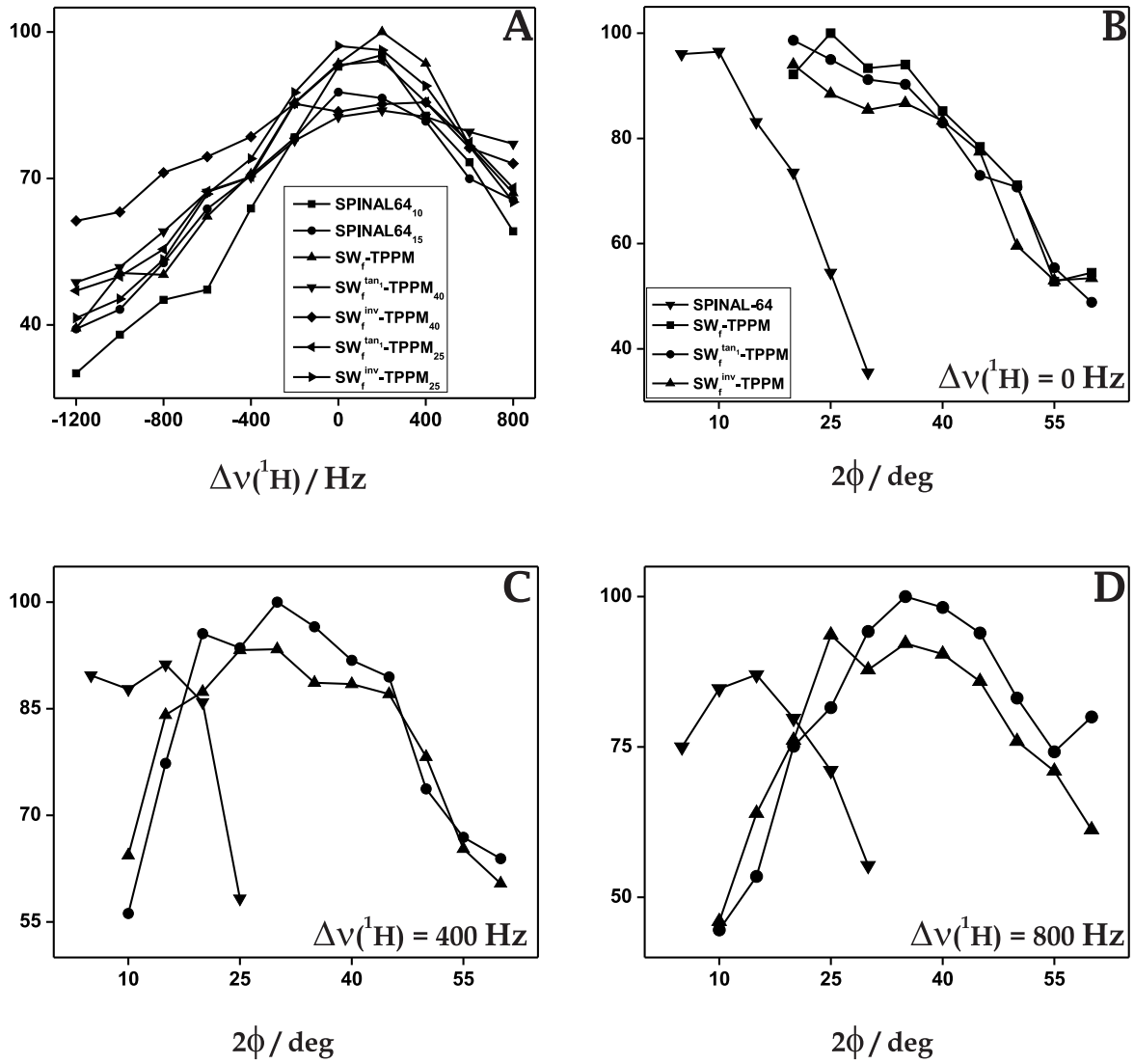

Figure 4.12: Intensity of the C_α peak of 5-CB obtained with various decoupling sequence. Plot (A) compares the off-resonance behavior of SPINAL-64_{10}, SPINAL-64_{15}, SW$_f$-TPPM$_{25}$, SW$_f^{inv}$-TPPM$_{25}$, SW$_f^{inv}$-TPPM$_{40}$, SW$_f^{tan_1}$-TPPM$_{25}$, and SW$_f^{tan_1}$-TPPM$_{40}$. Plot (B) shows the efficiency of decoupling as a function of phase for SPINAL-64, SW$_f$-TPPM, SW$_f^{inv}$-TPPM, and SW$_f^{tan_1}$-TPPM under on-resonance condition. (C and D) The comparison of decoupling efficiency at off-resonance values of 400 and 800 Hz, respectively as a function of phase for SPINAL-64, SW$_f^{inv}$-TPPM, and SW$_f^{tan_1}$-TPPM. (B-D) share the same set of legends for sequences where SPINAL-64, SW$_f$-TPPM, SW$_f^{inv}$-TPPM, and SW$_f^{tan_1}$-TPPM are denoted by inverted triangle (▼), square (■), triangle (▲) and circle (•), respectively.

pling efficiency of various sequences as a function of the phase difference (phase for SPINAL-64) for on-resonance decoupling is shown in Figure 4.12B. Smaller phase values are more efficient in this situation. Figures 4.12C and 4.12D show the same comparison at off-resonance of 400 and 800 Hz respectively and combining with Figure 4.12B the optimum value of phase can be seen to move towards higher side with increase in ^{1}H off-resonance.

It may be noticed that SPINAL-64_{10} performs much better than SPINAL-64_{15} at on-resonance while the latter possesses larger ^{1}H off-resonance bandwidth. Similar behavior is observed with swept TPPM sequences e.g. SW_f-$TPPM_{40}$ possesses significantly larger ^{1}H off-resonance bandwidth than SW_f-$TPPM_{25}$, albeit with slightly lower intensity at on-resonance. It can be noticed that SW_f-TPPM sequences are more immune to this trend than SPINAL-64. The insensitivity to off-resonance is important as any system can have more than one ^{13}C resonances which are sensitive to decoupling of ^{1}H nuclei. Larger ^{1}H off-resonance bandwidth of swept TPPM sequences ensures an overall improvement in sensitivity and resolution of the spectra.

4.4.4 Conclusions

The investigation of heteronuclear dipolar decoupling in liquid crystal sample of 5-CB under static condition suggested insufficiency of TPPM scheme owing to its acute dependence on ^{1}H off-resonance. Modulated TPPM sequences possess a significantly larger bandwidth compared to TPPM leading to overall enhanced spectral resolution.

The ^{1}H off-resonance bandwidth of modulated TPPM methods depends upon the phase of the modulation offering larger bandwidth at higher phase with loss of resolution invoking for a compromise. Optimisation of pulse length for modulated TPPM sequences was found to be crucial and a flip angle of 180° is recommended.

For heteronuclear dipolar decoupling applications in liquid-crystal NMR, SW_f^{inv}-TPPM and $SW_f^{tan_1}$-TPPM sequences are recommended with a phase difference of 30°-40°.

4.5 Future directions

The modulated TPPM methods are shown to be more efficient on liquid crystal samples than the TPPM scheme. These schemes consist of TPPM blocks and they owe their efficiency due to sweep of the phase modulation frequency. SW_f-TPPM was designed by incorporating the adiabatic frequency sweep. The enhanced adiabatic method, SW_{fp}-TPPM, was shown to be more effective on spinning solids. SW_{fp}-TPPM might be more effective on liquid crystals, and its superior performance is likely to be realised at lower RF field strengths. Effective schemes at lower RF field strengths are needed as spectrometer field for solid-state NMR applications are being pushed towards higher values by their manufacturers.

The designs and principles of SW_f-TPPM and SW_{fp}-TPPM schemes are explained in Chapter 2. For implementation of SW_{fp}-TPPM on static samples, the phase differences might be set to higher values.

Chapter 5

Resolution enhancement of half-integer spin quadrupolar nuclei by heteronuclear dipolar decoupling

Nuclei having spin angular momentum larger than $\frac{1}{2}$ are termed quadrupolar and they constitute a large fraction of NMR active nuclei. These nuclei are important in the study of inorganic materials which include minerals, catalysts, and zeolites as representative examples. High-resolution spectrum is achievable in half-integer spin quadrupolar nuclei by echoing 2^{nd} order quadrupolar interaction by Multiple Quantum MAS (MQMAS) scheme [86]. Heteronuclear dipolar decoupling schemes can be applied then to further enhance the resolution. This Chapter deals with the application of SW_f-TPPM and SPINAL-64 on quadrupolar nuclei.

5.1 Quadrupolar interaction

Quadrupolar interaction is the strongest interaction for nuclei having spin angular momentum, $I > \frac{1}{2}$. These nuclei are non-spherical and their resulting electric quadrupole moment interacts with electric field gradient of surrounding electric field. Main contri-

bution of electric field surrounding the nucleus in an atom or molecule is the electronic charge distribution. A symmetric charge distribution can lead to diminished quadrupolar coupling of a nuclei. Electric origin of quadrupolar interaction makes it orders of magnitude stronger than other internal interactions which are magnetic in origin. Often quadrupolar interaction is even larger than amplitude of RF field strength, and thus, quadrupolar transitions are normally not inverted by RF pulses.

Energy levels of a nucleus with spin I splits into $2I+1$ components under the influence of magnetic field, the m quantum number of these levels being $-I, -I+1, \cdots, I-1, I$. The influence of quadrupolar interaction is decided by the m quantum number of these levels. Symmetry of Zeeman levels in the nucleus of half-integer spin leads to simplified treatment of quadrupoles. It is exemplified in the absence of first-order quadrupolar interaction for symmetric transitions as explained in Chapter 1. Symmetry in the energy levels of half integer spins allows refocussing of second-order quadrupolar interaction under simultaneous action of RF and MAS, the details of which will be explained in Section 5.1.2. An easily implementable technique MQMAS, which is explained in the next Section, exploits this scenario to achieve high-resolution spectra of quadrupolar nuclei with half integer spin [86, 87].

Second-order quadrupolar couplings are averaged to zero under MQMAS scheme, and contribution of other internal interactions dominates the linewidth of the spectrum. Dipolar coupling of quadrupolar nuclei with an abundant nuclus becomes the major contributor in the linewidth if the molecular composition allows this situation. The application of heteronuclear dipolar decoupling schemes, like CW and TPPM, on the abundant nuclei had shown promising resolution enhancement [96, 97]. The application of more sophisticated schemes, like SPINAL-64 and SW_f-TPPM, is presented in this Chapter.

5.1.1 The MQMAS scheme

The technique of MQMAS relies upon the absence of 1^{st} order quadrupolar couplings in symmetric transitions ($m \longleftrightarrow -m$) for half-integral spins and 2^{nd} order couplings are averaged by a combination of MAS and RF pulses. Thus, the spectrum obtained with MQMAS scheme is free from quadrupolar broadening and is called isotropic spectrum. MQMAS involves evolution and refocussing of multiple-quantum coherences arising from symmetric transition under MAS. The coherence order involved in an MQMAS scheme decides the name of the variant, e.g. 3QMAS and 5QMAS. Many MQMAS variants for a nuclei can exist as the largest coherence order is decided by the spin angular momentum of the nuclei.

The basic scheme of MQMAS [86] is a two-pulse experiment, where the first pulse creates coherence of all possible orders which evolves for an specific amount of time and then the second pulse converts the coherences into observable single-quantum coherence. The desired coherence is selected by appropriate phase cycling. The 2^{nd} order quadrupolar echo is obtained at a fractional multiple of evolution time and this multiplicative fraction is decided by the coherence order involved. Thus, position of echo is a function of evolution period echo keeps getting shifted with the evolution of multiple-quantum coherence, demanding for special methods of data processing.

5.1.2 The principle of MQMAS scheme

The form of first- and second-order quadrupolar coupling is given in Chapter 1 where the absence of first-order quadrupolar coupling for symmteric transitions is explained. Under MAS, the spatial part of second-rank quadrupolar term contains Legendre polynomials with rank 0, 2, and 4. Thus, MAS is ineffective for second-order quadrupolar broadening. Under special condition of the symmteric transitions, a simple expression is obtained,

$$\nu_Q^2(m,-m) = \sum_{l=0,2,4} \nu_Q^l(\alpha,\beta,\gamma) C_l(I,m) P_l(\cos\theta_{MA}) \tag{5.1}$$

where $P_l(\cos\theta)$ is the Legendre polynomial of rank l, and $C_l(I,m)$ are the corresponding coefficients. Their explicit forms are produced here:

$$C_0(I,m) = 2m[I(I+1) - 3m^2]$$

$$C_2(I,m) = 2m[8I(I+1) - 12m^2 - 3]$$

$$C_4(I,m) = 2m[18I(I+1) - 34m^2 - 5] \tag{5.2}$$

The evolution undergone by a $m \longleftrightarrow -m$ spin coherence can be expressed in terms of the phase accumulation, which is given by

$$\phi = \nu^{CS} 2mt + \nu_Q^0 C_0(I,m)t + \nu_Q^2(\alpha,\beta) C_2(I,m) P_2(\cos\theta)t + \nu_Q^4(\alpha,\beta) C_4(I,m) P_4(\cos\theta)t \tag{5.3}$$

where θ is the angle of rotation axis with respect to the static magnetic field, B_0. Isotropic chemical shift of the spin is denoted by ν^{CS}, and C coefficients which are functions of spin quantum number I and the order of excited coherence, $M = 2m$ are described above. The phase accumulation (ϕ) is a function of orientation (α and β) and this equation describes the scenario for a single crystal. For a powdered sample, distribution of ϕ denotes the dephasing of quadrupolar coherence. This equation also shows $2m$-fold evolution of chemical shift under MQ evolution, thus CSA and heteronuclear dipolar coupling will also evolve $2m$-fold under MQMAS scheme, as pointed out by Duer [92].

In a 2D experiment in which an MQ coherence order evolves during t_1 and another MQ coherence order evolves during t_2, a spectrum free of anisotropic broadening is achieved if phase accumulation is set to zero. Thus, an echo will be obtained in this experiment when the following two conditions are satisfied.

$$\nu_Q^2(\alpha,\beta) C_2(I,m_1) P_2(\cos\theta)t_1 + \nu_Q^2(\alpha,\beta) C_2(I,m_2) P_2(\cos\theta)t_2 = 0 \tag{5.4}$$

$$\nu_Q^4(\alpha,\beta)C_4(I,m_1)P_4(\cos\theta)t_1 + \nu_Q^4(\alpha,\beta)C_4(I,m_2)P_4(\cos\theta)t_2 = 0 \tag{5.5}$$

Any order of MQ coherences can be used in an MQMAS experiment, however central transition is routinely chosen during t_2, this being an observable coherence. This fixes m_2 to 1 and refocussing condition for a nucleus of spin I where MQ of order m is correlated with SQ, is given by

$$t_2 = \left| \frac{C_4(I,m_1)}{C_4(I,\frac{1}{2})} \right| t_1 \tag{5.6}$$

To conclude, an echo is formed at time t_2, refocussing second-order quadrupolar terms. As t_2 is not equal to t_1, the position of echo is a function of t_1. Shifting of echo yields sheared peaks in the spectrum. Time proportional phase correction is employed to obtain pure phase spectrum.

5.1.3 Improving the MQMAS scheme

Few modifications have been devised to obtain MQMAS spectrum free from phase distortion [88, 89]. These methods essentially work by reconstruction of data either by acquisition method (called isotropic-reconstruction) [88] or by modifying the pulse-sequence (called split-t_1 or whole-echo) [89]. The details of the MQMAS and related developments are summarised in recent reviews [90, 91].

5.1.4 Enhancing the sensitivity of MQMAS scheme

The MQMAS scheme suffers from lack of sensitivity due to inefficient excitation of multiple-quantum coherences and the subsequent conversion to observable single-quantum coherence. Another reason for lack of sensitivity is the limited bandwidth of pulses to excite energy levels broadened by strong quadrupolar interaction.

Many attempts were made to enhance sensitivity of MQMAS scheme by replacing non-modulated pulses of the basic scheme by modulated pulses of various kinds. Modu-

lated pulses possess better excitation profiles and significant sensitivity enhancement has been reported by the application of Fast Amplitude Modulation [93], Double Frequency Sweep [94], and Hyperbolic Secant [95] pulses.

5.1.5 Enhancing the resolution of MQMAS scheme

Quadrupolar nuclei are part of inorganic materials, and MQMAS is naturally suited to the study of minerals. The spin half nuclei with large gyromagnetic ratios, ^{1}H and ^{19}F are often part of molecular structure of inorganic materials and use of heteronuclear dipolar decoupling methods were found to enhance resolution of MQMAS spectrum of quadupolar systems.

Hanaya and Harris reported intensity enhancement with CW decoupling [96]. Thereafter subsequent linewidth reduction with application of TPPM decoupling was demonstrated by Lacassagne et al. [97]. In addition, *m*-fold dephasing by heteronuclear dipolar coupling during *m*-quantum evolution in MQMAS scheme was suggested by Duer [92], hence, it becomes even more important to use improved decoupling sequences. Although SPINAL-64 demonstrated improved performance over TPPM, it was surprisingly not attempted for MQMAS scheme. A detailed account of decoupling sequences has been covered in Chapter 2. This Chapter deals with the study of SPINAL-64 and SW$_f$-TPPM decoupling schemes in MQMAS experiments.

5.2 Experimental

The experiments were performed on a Bruker AV500 MHz spectrometer equipped with a triple-channel 4 mm probe. Gibbsite, A mineral of composition Al(OH)$_3$ (basic aluminum trihydroxide) was chosen to demonstrate the performance of the various decoupling sequences. The molecular and crystal symmetry of gibbsite is monoclinic and C21/c respectively [98]. Two crystallographically inequivalent aluminium sites are present

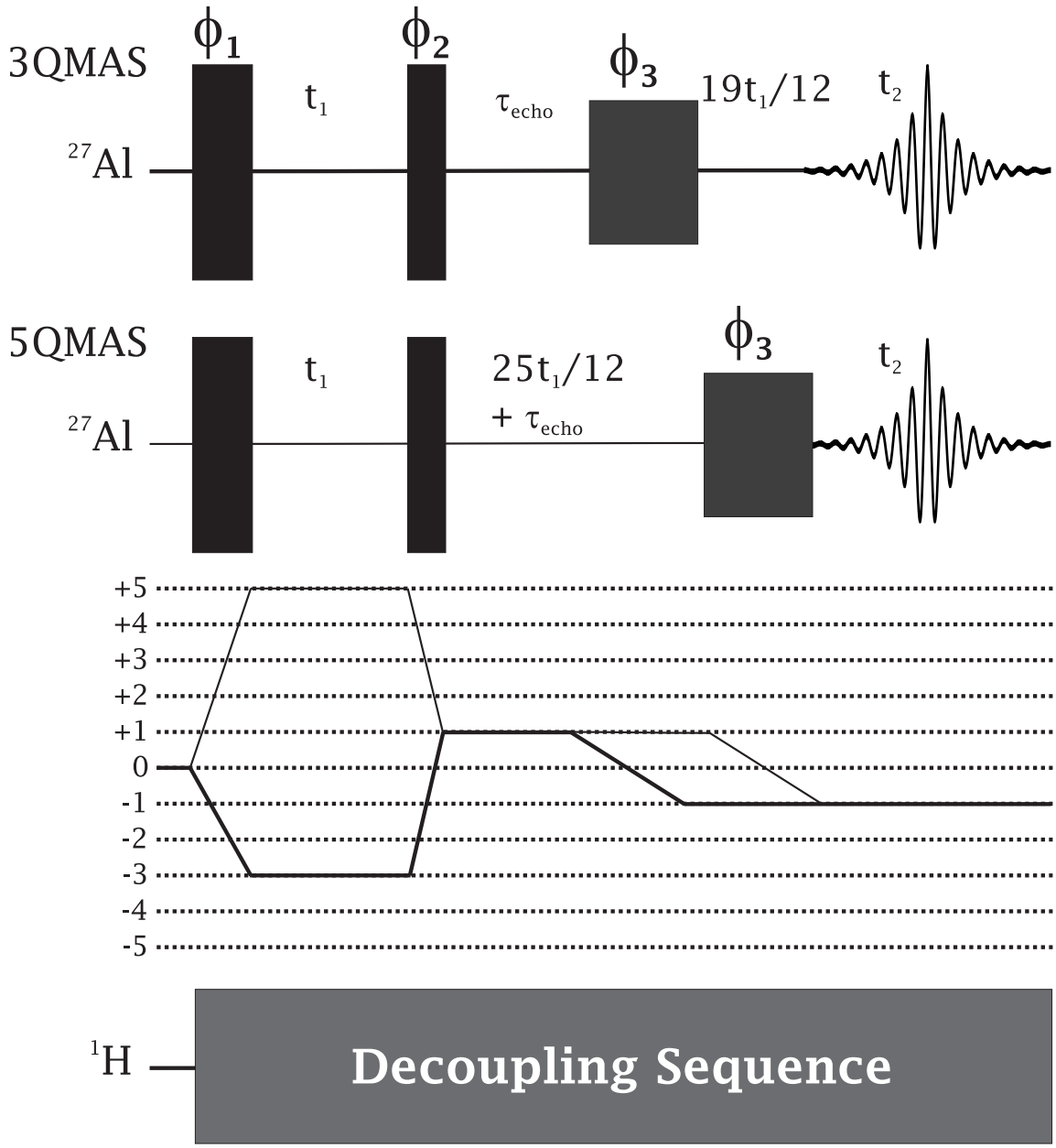

Figure 5.1: Schematic of 3QMAS and 5QMAS scheme on ^{27}Al nuclei with ^{1}H decoupling. Suitable phase cycling of ϕ_1 and ϕ_2 is needed to choose the desired coherence order during t_1 evolution. A 180° pulse of phase is applied (on central transition, denoted by ϕ_3) to shift the position of echo by τ_{echo}, 2.5 ms in the study presented. Split-t_1 with whole-echo acquisition was adopted for spectral acquisition, which distinguishes between positive and negative coherence orders and this aspect is shown in the coherence selection pathway. In a nuclei of spin $\frac{5}{2}$, this scheme selects $+5$ and -3 quantum coherences, pathways for these are drawn in thin and thick lines respectively. ^{1}H decoupling was applied from the first pulse of the MQMAS scheme.

(denoted by A and B) which form layers of edge-sharing $Al(OH)_6$ octahedra to produce the stacked layer sequence AB BA AB BA $\cdots$. The hydroxyl groups of the adjacent layers are situated directly opposite to each other creating a large bath of protons which are strongly dipolar coupled among themselves and with the Al nuclei in the structure. The structural distinction, quantification, and unambiguous assignment of the structure building octahedral aluminium environments of gibbsite have been made through MAS and 3QMAS NMR and ab initio quantum-chemical calculations [99]. They have lead to the characterisation of the two octahedral Al sites in terms of the chemical shielding and quadrupole interaction parameters.

Split-t_1-shifted echo [89] method was used to obtain ^{27}Al MQMAS (3QMAS and 5QMAS) spectra of gibbsite at 10 kHz of MAS. The excitation and conversion pulses were applied at a central-transition nutation frequency of 60 kHz whilst the central-transition selective 180^o pulse to shift the echo was applied at a central-transition nutation frequency of 6 kHz. 10 ms of acquisition time was taken along the direct dimension. The t_1 increment was 20 μs for both 3QMAS and 5QMAS with 80 and 60 t_1 increments respectively. Optimal durations of excitation and conversion pulses for 3QMAS were 3.8 and 1.7 μs respectively whereas they were 3.2 and 2.1 μs for 5QMAS experiments. The 3QMAS and 5QMAS experiments respectively had 48 and 80 transients for each t_1 increment and the decoupling was applied from the first pulse of the MQMAS scheme. All the experiments were performed at MAS frequency of 10 kHz. The RF field strength of ^{1}H channel was calibrated by nutation experiment on adamantane. A pictorial schematic of the implementation of decoupling in MQMAS is shown in Figure 5.1.

5.3 Results and discussion

In 3QMAS and 5QMAS spectra acquired without application of ^{1}H decoupling, considerably weak intensities for unresolved ^{27}Al sites were obtained. Two distinctly separate ^{27}Al sites were obtained with ^{1}H decoupling.

Upper row of Figure 5.2 is a comparison of the isotropic projection of the 3QMAS spectra of gibbsite with the decoupling sequences being (from left to right) CW, TPPM, SPINAL-64, and SW_f-TPPM. The peak intensity increases by approximately two-fold from CW to TPPM. With SPINAL-64 or SW_f-TPPM decoupling, further intensity enhancement of 20% is achieved over TPPM. Lower row of Figure 5.2 shows the same comparison for 5QMAS spectra of gibbsite. The separation between two ^{27}Al sites is larger here than in the 3QMAS spectrum, owing to isotropic shift contribution from second-order quadrupolar interaction. An additional peak (marked with asterisk) is the spinning sideband of the more intense peak. For the low field chemical site, the intensity enhancement for SW_f-TPPM over TPPM is around 8%, whereas SPINAL-64 offers lesser advantage. An improved shape with larger intensity is obtained for resonance with higher chemical shift.

The duration of 180° pulse for RF field strength of 90 kHz is 5.505 μs and optimum pulse length for ^{1}H decoupling at 90 kHz of RF field strength came out to be 5.5, 6.1, and 6.1 μs for TPPM, SPINAL-64, and SW_f-TPPM, respectively. The optimum flip angle for modulated TPPM sequences is significantly higher than 180°. This can be explained by the loss of B_1 intensity owing to the ionic nature of gibbsite.

Figure 5.3 shows the efficiency comparison of decoupling sequences applied at RF field strengths of 80 and 100 kHz for 3QMAS spectra of gibbsite. Intensity enhancements of 15% and 22% over TPPM with the application of SW_f-TPPM and SPINAL-64 are achieved at RF field strengths of 80 and 100 kHz respectively. Pulse length of decoupling sequences was optimised while optimum values of phase and offset were taken from earlier investigation. The optimum pulse length for TPPM, SPINAL-64, and SW_f-TPPM came out to be 6.8, 7.4, and 7.4 μs respectively for 80 kHz and 5.1, 5.5, and 5.5 μs for 100 kHz of RF field strength. These values are again the signature of ionic character of gibbsite.

Robustness of the decoupling schemes on 3QMAS scheme at RF field strength of 90

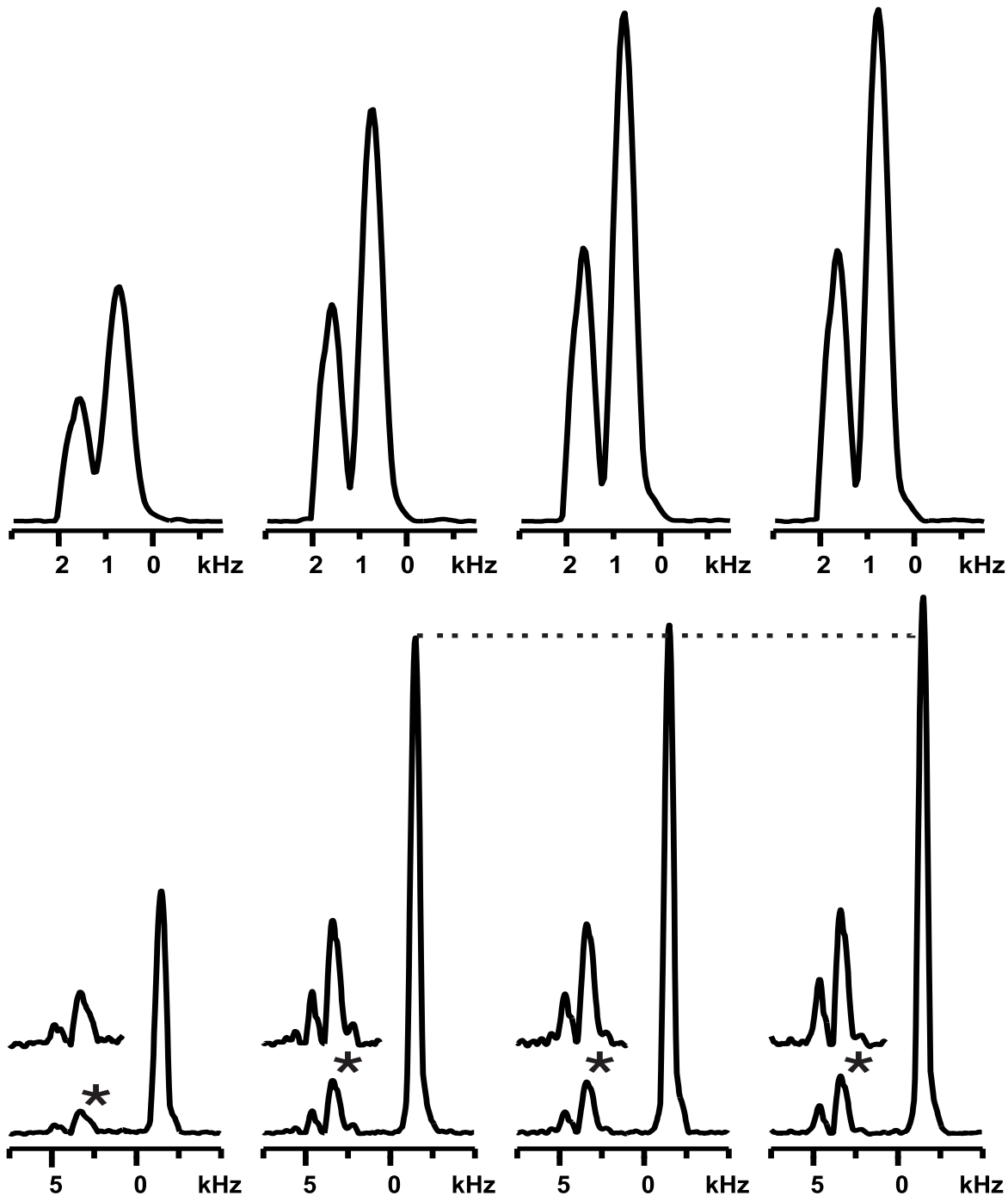

Figure 5.2: Isotropic projections of the ^{27}Al 3QMAS (upper row) and 5QMAS (lower row) spectrum of gibbsite obtained with CW, TPPM, SPINAL-64, and SW$_f$-TPPM are shown from left to right. The decoupling RF field was applied on ^{1}H spins with an strength of 90 kHz. The optimal values of τ for TPPM, SPINAL-64, and SW$_f$-TPPM were 5.5, 6.1 and 6.1 μs, respectively, while 2ϕ was 15^o, 10^o and 25^o, respectively, with the phase increment in SPINAL being 5^o.

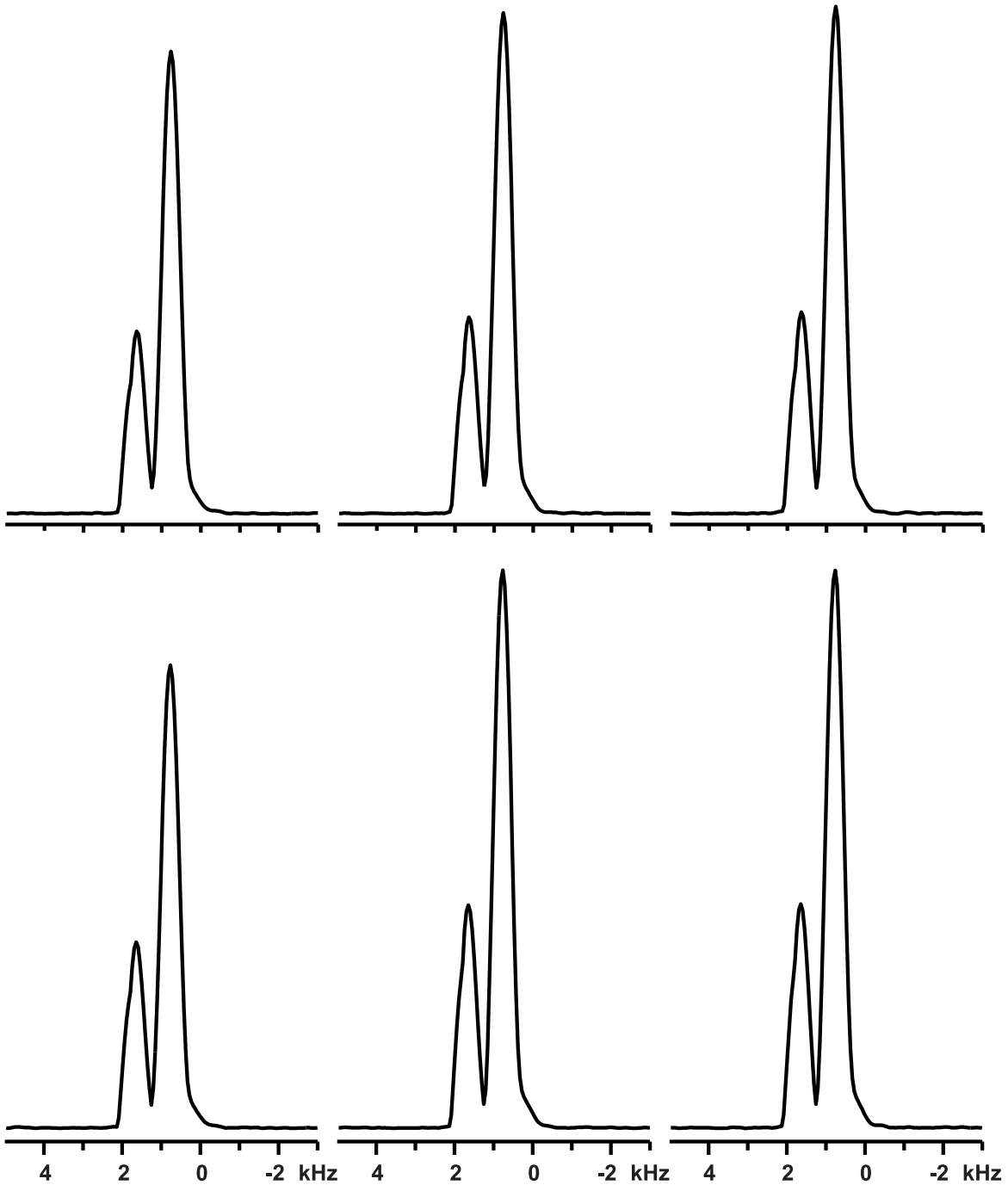

Figure 5.3: Isotropic projections of the ^{27}Al 3QMAS spectrum of gibbsite obtained with TPPM, SPINAL-64, and SW$_f$-TPPM are shown from left to right with an RF field strength of 80 kHz on upper row of spectra and 100 kHz on the lower row of spectra.

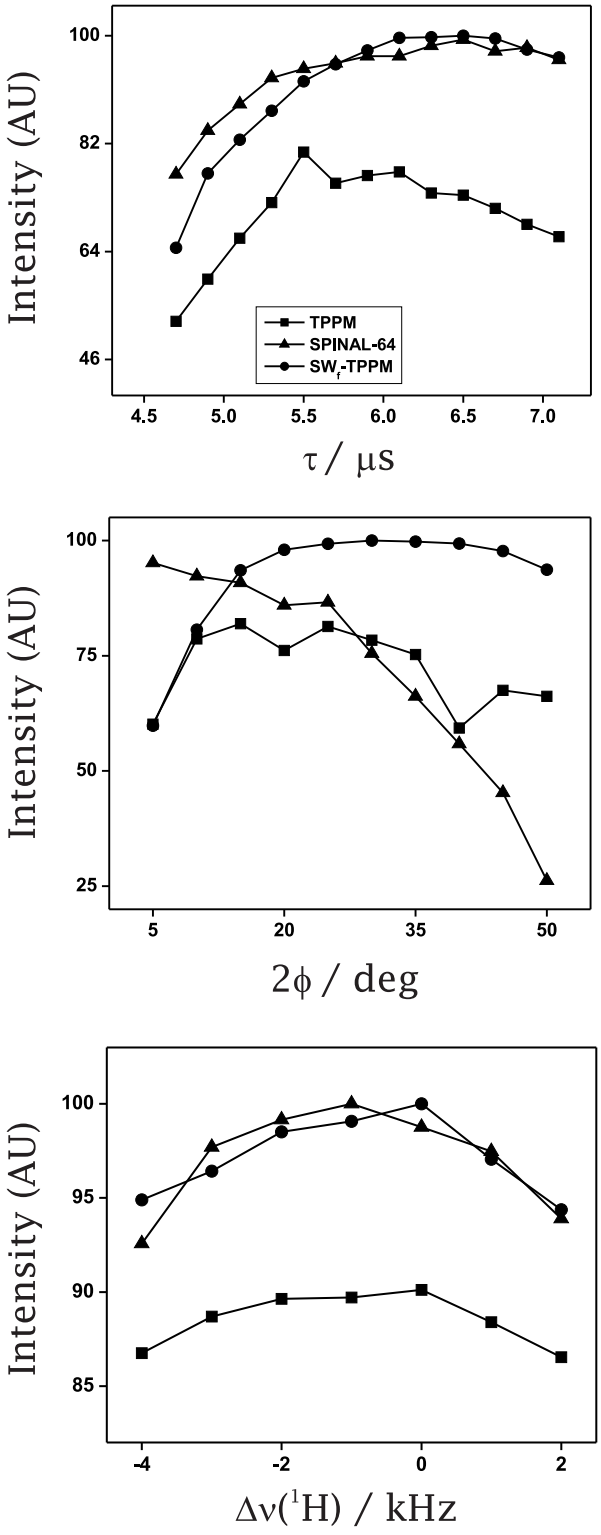

Figure 5.4: Robustness comparison of various decoupling sequences for ^{27}Al 3QMAS spectra of gibbsite. The intensity of isotropic projection of 3QMAS spectra (more intense peak) of gibbsite is plotted as a function of misset of parameters for TPPM, SPINAL-64 and SW$_f$-TPPM. The top, middle, and bottom plots compare the robustness with respect to pulse length (τ), phase difference (2ϕ), and ^{1}H off-resonance ($\Delta\nu(^1\text{H})$) respectively. The decoupling RF field was applied on ^{1}H spins with an strength of 90 kHz.

kHz was also studied. Peak height of the more intense peak in the 3QMAS isotropic projection was monitored when various experimental parameters were changed from their optimal values. Figure 5.4 shows the intensity plotted as a function of the pulse length (τ), the phase difference (2ϕ), and the ^{1}H off-resonance ($\Delta\nu(^1\mathrm{H})$) for various decoupling schemes. Relatively minor changes in the intensity of the monitored peak with the variation of experimental parameters suggest SW$_f$-TPPM to be more robust than the other decoupling schemes.This observation is consistent with observations under MAS for spin $\frac{1}{2}$ nuclei.

5.4 Conclusions

Experimental investigation shows that heteronuclear dipolar decoupling may be essential in certain half-integer spin quadrupolar systems. In such circumstances, the use of sophisticated decoupling schemes will be of great help and SW$_f$-TPPM sequence outperforms the commonly used decoupling sequences in terms of both efficiency and robustness.

Chapter 6

Study of heteronuclear dipolar decoupling for HRMAS experiments

Soft condensed matter is a category of solids which are neither rigid nor aligned. Its NMR behavior stands between rigid solid and liquid crystal. A separate class of NMR experiments, High-Resolution Magic Angle Spinning (HRMAS), has emerged for the study of soft condensed matter.

This Chapter covers the study of decoupling sequences for HRMAS experiments, which is gaining in popularity as it is applicable to a wide class of soft condensed matter ranging from tissues on the one hand to synthetic polymers on the other. These materials are spun at low spinning frequencies ($\sim$ 5 kHz) and do not tolerate high RF field strengths. Especially in systems with intrinsic motion, decoupling of the ^{1}H spins is achieved at smaller RF field strengths compared to the case in rigid samples. This scenario is similar to the case of liquid crystals where both SW$_f$-TPPM and SPINAL-64 have been shown to be effective in Chapter 4. The presence of motion in the system makes cross polarisation an inefficient process.

6.1 Study on regular rubber band

Naturally found rubber is a polymer of isoprene, with molecular weight in the range of 100-1000 kDa. Regular rubber band is prepared by adding some additives to modify the characteristics. It is a known sample for HRMAS experiments.

6.1.1 Experimental

The rubber band was packed tightly in a 4 mm rotor in order to spin the sample. The sample was spun at 2 kHz and heteronuclear dipolar decoupling schemes were applied with 50 kHz of RF field strength. The spectra were acquired on a Bruker AV500 MHz spectrometer using a triple-resonance 4 mm probe. Signal from a 90° pulse was acquired with ^{1}H decoupling.

6.1.2 Results and discussion

Figure 6.1 shows the ^{13}C NMR spectrum of rubber which consists of five lines. Spectrum shown on the top is obtained without ^{1}H decoupling and the bottom spectrum is obtained with SW$_f$-TPPM decoupling scheme. All lines are significantly broad (typical broad lines as in powder) in the spectrum without ^{1}H decoupling and considerable narrowing takes place with SW$_f$-TPPM decoupling scheme.

Resonances of ^{13}C spectrum are assigned assuming it to be an isoprene polymer. Molecular structure of the isoprene unit is also shown in Figure 6.1. ^{13}C resonance with the smallest chemical shift normally belongs to CH_3 group which possesses methyl rotation leading to averaging of anisotropic interactions and are unaffected by heteronuclear decoupling. The decoupling efficiency on regular rubber band was made on C_5 resonance. Figure 6.2 shows the intensity variation of C_5 peak with phase difference (left plot) and pulse length (right plot) for TPPM, SPINAL-64, and SW$_f$-TPPM. A random variation of intensity with these parameters for decoupling sequences is against the

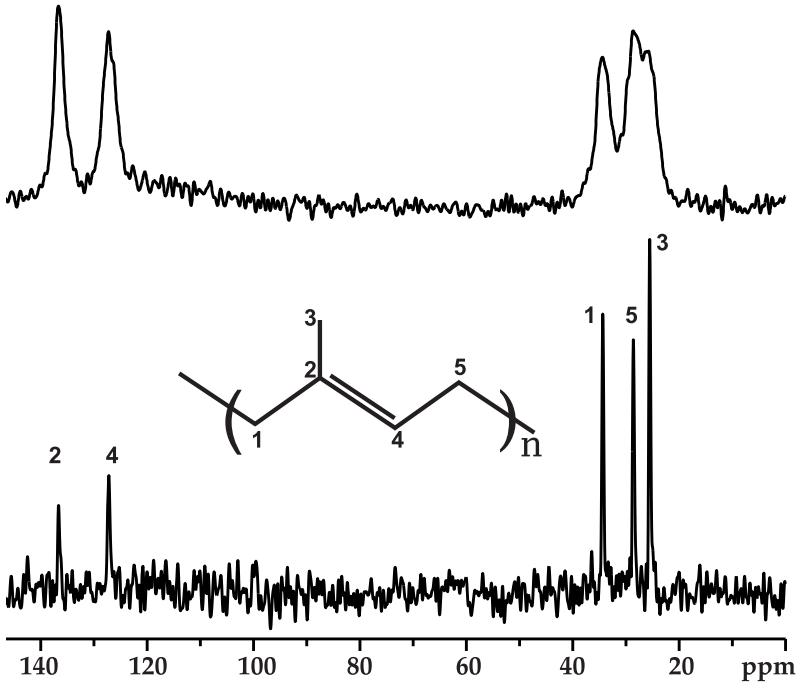

Figure 6.1: ^{13}C spectrum of regular rubber band obtained without ^{1}H decoupling shown on top while the bottom spectrum is obtained with SW_f-TPPM decoupling applied on abundant nuclei. Broad spectra was acquired with larger number of scans and processed with smaller number of data points to improve the appearance. Width of peaks are unaffected by processing.

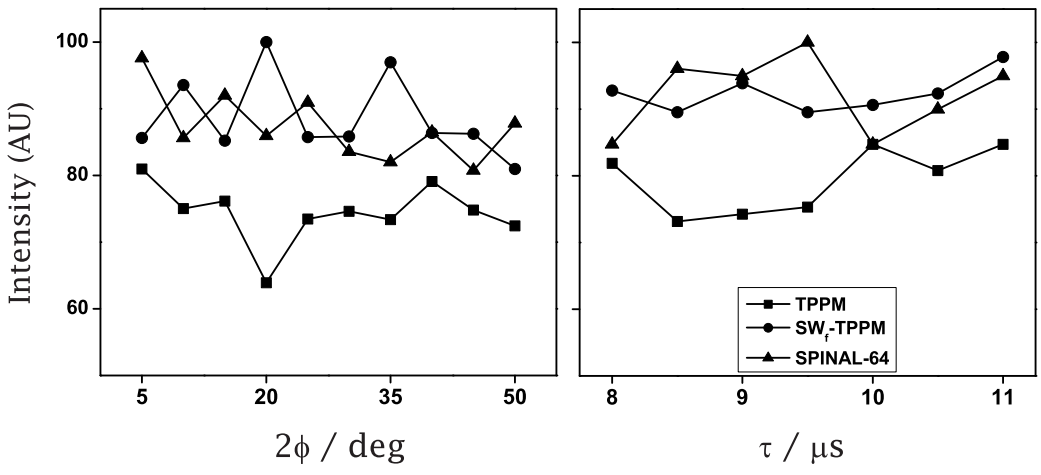

Figure 6.2: Comparison of various decoupling sequences on rubber band. The variation in the intensity of the peak labeled 5 in the spectra of rubber-band (Figure 6.1) obtained with TPPM (■), SPINAL-64(▲), and SW_f-TPPM(●) decoupling is plotted as a function of the phase difference (2ϕ) on the left and pulse length (τ) in the right.

observations on spinning rigid samples and static liquid crystals. Unlike in the case of rigid solid and liquid crystal, performance of phase modulated sequences are unaffected with pulse duration and ^{1}H off-resonance. The mechanism of decoupling with phase modulated methods suggests a clear maxima with smooth rise and fall of intensity on either side of it. The random efficiency variation of TPPM based sequences with pulse length indicates the ineffectiveness of phase modulated decoupling.

The investigation of heteronuclear dipolar decoupling on regular rubber band suggested the need of decoupling for HRMAS experiments. However, the mechanism of phase modulation seems to be ineffective. Further investigation of heteronuclear dipolar decoupling is done on a synthetic polymer sample.

6.2 Study on a synthetic polymer

Another investigation of heteronuclear dipolar decoupling for HRMAS experiments was done on a synthetic polymer sample. A block-copolymer named F-127 was used to study heteronuclear dipolar decoupling for HRMAS studies. It is a mixed polymer of Ethylene-Oxide (EtO) and Propylene-Oxide (PrO) with the composition $(EtO)_{100}$-$(PrO)_{65}$-$(EtO)_{100}$ and has the molecular weight of 12,600 daltons.

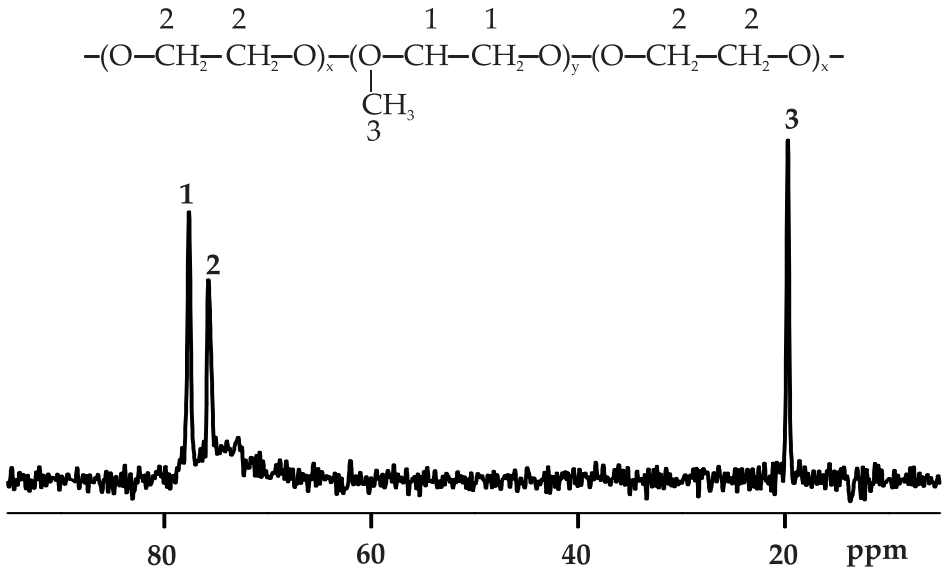

Figure 6.3: The structure and a representative ^{13}C spectrum of F-127. SW_f-TPPM decoupling scheme was applied on ^{1}H spins.

6.2.1 Experimental

The sample was spun at 4 kHz and an RF field strength of 20 kHz was applied to effect heteronuclear dipolar decoupling. A 90° pulse was applied on the ^{13}C channel, the signal of which was acquired with ^{1}H decoupling. The experiments were performed on a Bruker AV500 MHz spectrometer using a triple-resonance 4 mm probe.

6.2.2 Results and discussion

The structure and ^{13}C NMR spectrum of F-127 consisting of three lines is shown in Figure 6.3 along with the resonance assignment. As found earlier with regular rubber band, all lines were significantly broad (typical broad lines as in powder) when not decoupled. Decoupling with sophisticated schemes (TPPM, SPINAL-64, and SW$_f$-TPPM) lead to no pronounced resolution enhancement over simple CW scheme. The intensities of the spectral lines when the pulse duration, τ_p, and the decoupler offset, $\Delta\nu(^1\mathrm{H})$, were varied is shown in Figure 6.4. It again indicates ineffectiveness of decoupling mechanism of phase modulation.

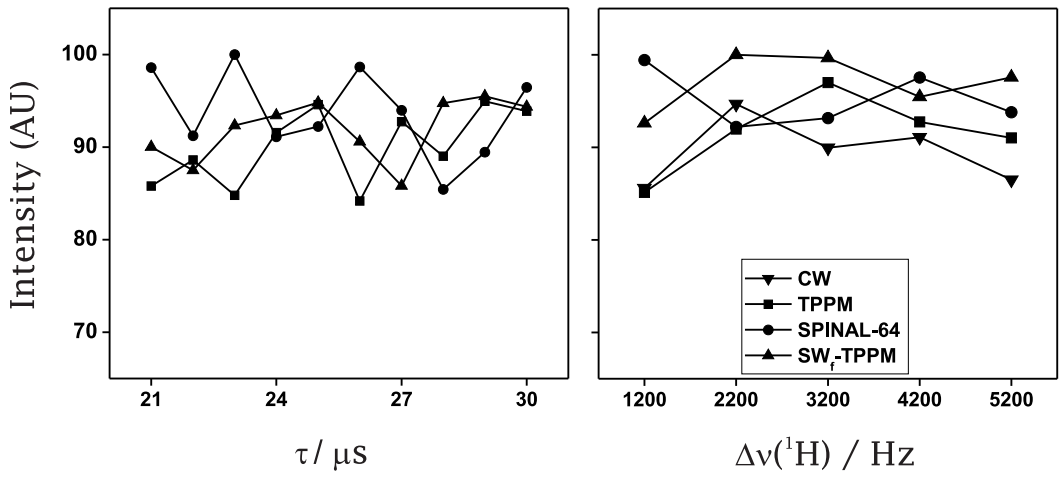

Figure 6.4: Comparison of various decoupling sequences on F-127. The variation in the intensity of the peak labeled 2 in the spectra of F-127 (Figure 6.3) obtained with TPPM (■), SPINAL-64(●), SW$_f$-TPPM(▲) and CW (▼; only on the right panel) decoupling is plotted as a function of the pulse length (τ) in the left plot, and the ^{1}H off-resonance ($\Delta\nu(^1\mathrm{H})$) in the right plot.

There are no marked intensity differences amongst the various sequences and the observed maximum deviation in intensity in these plots is of the order of 15% indicating that the use of sophisticated decoupling schemes is not mandatory for such samples.

6.3 Conclusions

Study on regular rubber band and F-127 suggested the ineffectiveness of phase modulation for heteronuclear dipolar decoupling. Thus, sophisticated heteronuclear dipolar decoupling schemes are not needed for HRMAS experiments and simple CW scheme can be used without significant loss in sensitivity. The small loss in resolution is more than compensated by the time saved for optimisation of sophisticated decoupling sequences.

These observations can be attributed to the partial averaging of the anisotropic interactions due to the motion present in the system. It is also true that at low spinning frequencies the interference of the sample spinning on the RF pulse schemes used for decoupling is rather limited. To conclude, at the low spinning speeds under consideration for HRMAS experiments, CW decoupling competes favourably with the other schemes which have more complicated modulation profiles.

Bibliography

[1] E. M. Purcell, H. C. Torrey, and R. V. Pound, Phys. Rev. **69**, 37 (1946).

[2] F. Bloch, W. W. Hansen, and M. Packard, Phys. Rev. **69**, 127 (1946).

[3] M. H. Levitt, *Spin Dynamics: Basics of Nuclear Magnetic Resonance* (Wiley, 2001).

[4] A. Abragam, *The Principles of Nuclear Magnetism* (Oxford Press, Oxford, 1961).

[5] M. Mehring, *High Resolution NMR Spectroscopy in Solids* (Springer-Verlag, Germany, 1976).

[6] M. Mehring, *Encyclopedia of NMR*, edited by D. M. Grant and R. K. Harris (Wiley, Chichester, 1996), Vol. 4, p. 2585.

[7] U. Haeberlen, *High Resolution NMR in Solids - Selective Averaging* (Academic Press, New York, 1976).

[8] M. Duer (ed.), *Introduction to Solid-State NMR Spectroscopy: Principles and Applications* (Blackwell Sciences, U.K., 2002).

[9] M. Duer, *Introduction to Solid-State NMR* (Blackwell Sciences, U.K., 2002).

[10] D. D. Laws, H. M. L. Bitter, and A. Jerschow, Angew. Chem. Int. Ed. **41**, 3096 (2002).

[11] R. R. Ernst and W. A. Anderson, Rev. Sci. Instrum. **37**, 93 (1966).

[12] M. H. Levitt, *Encyclopedia of NMR*, edited by D. M. Grant and R. K. Harris (Wiley, Chichester, 1996), Vol. 9, p. 165.

[13] A. J. Shaka, *Encyclopedia of NMR*, edited by D. M. Grant and R. K. Harris (Wiley, Chichester, 1996), Vol 3, p. 1558.

[14] A. E. Bennett, R. G. Griffin, and S. Vega, *NMR Basic Principles and Progress* (1994), Vol. 33, p. 1.

[15] P. W. Atkins and R. S. Friedman, *Molecular Quantum Mechanics* (Oxford Press, Oxford, 1997).

[16] D. G. Cory, A. F. Fahmy, and T. F. Havel, Proc. Nat. Am. Soc. **94**, 1634 (1997).

[17] N. A. Gershenfeld and I. L. Chuang, Science **275**, 350 (1997).

[18] T. Reiss, N. Khaneja, and S. J. Glaser, J. Mag. Res. **154**, 192 (2002).

[19] C. T. Kehlet , A. C. Sivertsen, M. Bjerring, T. O. Reiss, N. Khaneja, S. J. Glaser, and N. C. Nielsen, J. Am. Chem. Soc. **126**, 10202 (2004).

[20] E. R. Andrew, A. Bradbury, and R. G. Eades, Nature **182**, 1659 (1958).

[21] I. J. Lowe, Phys. Rev. Lett. **2**, 285 (1958).

[22] J. Schaefer and E. O. Stejskal, J. Am. Chem. Soc. **98**, 1031 (1976).

[23] M. M. Maricq and J. S. Waugh, J. Chem. Phys. **70**, 3300 (1979).

[24] S. R. Hartmann and E. L. Hahn, Phys. Rev. **128**, 2042 (1962).

[25] A. Pines, M. G. Gibby, J. Schaefer, and J. S. Waugh, J. Chem. Phys. **59**, 569 (1973).

[26] E. O. Stejskal, J. Schaefer, and J. S. Waugh, J. Magn. Reson. **28**, 105 (1977).

[27] G. Metz, X. Wu, and S. O. Smith, J. Magn. Reson. **110**, 219 (1994).

[28] A. L. Bloom and J. N. Shoolery, Phy. Rev. **97**, 1261 (1955).

[29] L. Müller, A. Kumar, T. Baumann, and R. Ernst, Phy. Rev. Lett. **34**, 1402 (1974).

[30] R. K. Hester, J. L. Ackerman, B. L. Neff, and J. S. Waugh, Phys. Rev. Lett. **36**, 1081 (1976).

[31] E. F. Rybaczewski, B. L. Neff, J. S. Waugh, J. S. Sherfinski, J. Chem. Phys. **67**, 1231 (1977).

[32] M. Ernst, H. Zimmermann, and B. H. Meier, Chem. Phys. Lett. **317**, 581 (2000).

[33] A. E. Bennett, C. M. Rienstra, M. Auger, K. V. Lakshmi, and R. G. Griffin, J. Chem. Phys. **103**, 6951 (1995).

[34] Z. Gan and R. R. Ernst, Solid State Nucl. Magn. Reson. **8**, 153 (1997).

[35] Y. Yu and B. M. Fung, J. Magn. Reson. **130**, 317 (1998).

[36] B. M. Fung, A. K. Khitrin, and K. Ermolaev, J. Magn. Reson. **142**, 97 (2000).

[37] R. S. Thakur, N. D. Kurur, and P. K. Madhu, Chem. Phys. Lett. **426**, 459 (2006).

[38] R. S. Thakur, N. D. Kurur, and P. K. Madhu, J. Magn. Reson. **185**, 264 (2007).

[39] R. S. Thakur, N. D. Kurur, and P. K. Madhu, J. Magn. Reson. **193**, 77 (2008).

[40] R. S. Thakur, N. D. Kurur, and P. K. Madhu, Magn. Reson. Chem. **46**, 166 (2008).

[41] R. S. Thakur, N. D. Kurur, and P. K. Madhu, Manuscript in preparation.

[42] M. H. Levitt, R. Freeman, and T. Frenkiel, Adv. Magn. Reson. **11**, 47 (1983).

[43] G. De Paëpe, D. Sakellariou, P. Hodgkinson, S. Hediger, and L. Emsley, Chem. Phys. Lett. **368**, 511 (2003).

[44] G. D. Paëpe, A. Lesage, P. Hodgkinson, and L. Emsley, Chem. Phys. Lett. **376**, 259 (2003).

[45] G. D. Paëpe, A. Lesage, and L. Emsley, J. Chem. Phys. **119**, 4833 (2003).

[46] G. D. Paëpe, B. Elèna, and L. Emsley, J. Chem. Phys. **121**, 3165 (2004).

[47] G. Gerbaud, F. Ziarelli, and S. Caldarelli, Chem. Phys. Lett. **377**, 1 (2003).

[48] A. Khitrin and B. M. Fung, J. Chem. Phys. **112**, 2392 (2000).

[49] M. Edèn and M. H. Levitt, J. Chem. Phys. **111**, 1511 (1999).

[50] K. Riedel, J. Leppert, O. Ohlenschläger, M. Görlach, and R. Ramachandran, Chem. Phys. Lett. **395**, 356 (2004).

[51] K. Riedel, C. Herbst, J. Leppert, O. Ohlenschläger, M. Görlach, and R. Ramachandran, Chem. Phys. Lett. **429**, 590 (2006).

[52] A. Detken, E. H. Hardy, M. Ernst, and B. H. Meier, Chem. Phys. Lett. **356**, 298 (2002).

[53] P. Tekely, P. Palmas, and D. Canet, J. Magn. Reson. A **107**, 129 (1994).

[54] M. Ernst, A. Samoson, and B. H. Meier, J. Chem. Phys. **123**, 064102 (2005).

[55] M. Leskes, R. S. Thakur, P. K. Madhu, N. D. Kurur, and S. Vega, J. Chem. Phys. **127**, 024501 (2007).

[56] M. Ernst, H. Geen, and B. H. Meier, Solid State Nucl. Magn. Reson. **29** 2 (2006).

[57] N. C. Nielsen, H. Bildsøe, and H. J. Jakobsen, J. Chem. Phys. **101**, 1805 (1994).

[58] T. G. Oas, R. G. Griffin, and M. H. Levitt, J. Chem. Phys. **89**, 692 (1988).

[59] M. Ernst, J. Magn. Reson. **162**, 1 (2003).

[60] P. Hodgkinson, Prog. Nucl. Magn. Reson. Spectrosc. **46**, 159 (2005).

[61] R. Verel, M. Ernst, and B. H. Meier, J. Magn. Reson. **150**, 81 (2001).

[62] R. N. Bracewell, *The Fourier Transform and its Applications* (McGraw-Hill, New York, 2000).

[63] J. S. Waugh, *Encyclopedia of NMR*, edited by D. M. Grant and R. K. Harris (Wiley, Chichester, 1996), Vol. 1, p. 849.

[64] S. Vega, *Encyclopedia of NMR*, edited by D. M. Grant and R. K. Harris (Wiley, Chichester, 1996), Vol. 3, p. 2011.

[65] E. Vinogradov, P. K. Madhu, S. Vega, *Topics in Current Chemistry* (Springer-Verlag, Berlin, 2005), Vol 246, p. 33.

[66] M. Baldus, T. O. Levante, and B. H. Meier, Z. Naturforsch., A: Phys. Sci. **49**,84 (1994).

[67] T. O. Levante, M. Baldus, B. H. Meier, and R. R. Ernst, Mol. Phy. **86**, 1195 (1995).

[68] I. Scholz, B. H. Meier, and M. Ernst, J. Chem. Phys. **127**, 204504 (2007).

[69] M. Veshtort and R. G. Griffin, J. Magn. Reson. **178**, 248 (2006).

[70] T. Bräuniger, G. Hempel, and P. K. Madhu, J. Magn. Reson. **181**, 68 (2006).

[71] A. Schiff, *Quantum Mechanics* (McGraw Hill, New York, 1955).

[72] E. Kupče and R. Freemann, J. Magn. Reson. A **117**, 246 (1995).

[73] K. Uğurbil, M. Garwood, A. R. Rath, and M. R. Bendall, J. Magn. Reson. **78**, 472 (1998).

[74] K. Uğurbil, M. Garwood, and A. R. Rath, J. Magn. Reson. **80**, 448 (1998).

[75] G. De Paëpe, N. Giraud, A. Lesage, P. Hodgkinson, A. Böckmann, and L. Emsley, J. Am. Chem. Soc. **125**, 13938 (2003).

[76] D. J. Voet and J. G. Voet, *Biochemistry* (Wiley, USA, 2004).

[77] B. M. Fung, Prog. Nucl. Magn. Reson. Spectrosc. **41**, 171 (2002).

[78] S. V. Dvinskikh, D. Sandström, H. Zimmermann, and A. Maliniak, Prog. Nucl. Magn. Reson. Spectrosc. **48**, 85 (2006).

[79] D. J. Griffiths, *Introduction to Electrodynamics* (Prentice Hall, New Jersey, 1991).

[80] A. E. Kelly, H. D. Ou, R. Withers, and V. Dotsch, J. Am. Chem. Soc. **124**, 12013 (2002).

[81] C. G. Li, Y. M. Mo, J. Hu, E. Chekmenev, C. L. Tian, F. P. Gao, R. Q. Fu, P. Gorkov, W. Brey, and T. A. Cross, J. Mag. Reson. **180**, 51 (2006).

[82] D. K. Lee, K. A. H. Wildman, and A. Ramamoorthy, J. Am. Chem. Soc. **126**, 2318 (2004).

[83] R. W. Martin and K. W. Zilm, J. Mag. Reson. **168**, 51 (2004).

[84] J. J. Led and S. B. Petersen, J. Mag. Reson. **32**, 1 (1978).

[85] S. V. Dvinskikh, K. Yamamoto, U. H. N. Dürr, and A. Ramamoorthy, J. Magn. Reson. **184**, 240 (2007).

[86] L. Frydman and J. S. Harwood, J. Am. Chem. Soc. **117**, 5367 (1995).

[87] A. Medek, J. S. Harwood, and L. Frydman, J. Am. Chem. Soc. **117**, 12779 (1995).

[88] D. Massiot, B. Touzo, D. Tremeau, J. P. Coutures, J. Virlet, P. Florian, and J. P. Grandinetti, Solid State Nucl. Magn. Reson. **6**, 73 (1996).

[89] S. P. Brown and S. Wimperis, J. Mag. Reson. **124**, 279 (1997).

[90] A. Goldbourt and P. K. Madhu, Monatshefte fűr Chemie **133**, 1497 (2002).

[91] A. Goldbourt and P. K. Madhu, Ann. Rep. NMR Spect. **54**, 81 (2004).

[92] M. J. Duer, Chem. Phys. Lett. **277**, 167 (1997).

[93] A. Goldbourt, P. K. Madhu, L. Frydman and S. Vega, Chem. Phys. Lett. **307**, 41 (1999).

[94] A. P. M. Kentgens and R. Verhagen, Chem. Phys. Lett. **300**, 435 (1999).

[95] R. Siegel, T. T. Nakashima, and R. E. Wasylishen, Chem. Phys. Lett. **388**, 441 (2004).

[96] M. Hanaya and R. K. Harris, Solid State Nucl. Magn. Reson. **8**, 147 (1997).

[97] V. Lacassagne, P. Florian, V. Montouillout, C. Gervais, F. Babonneau, and D. Masssiot, Magn. Reson. Chem. **36**, 956 (1998).

[98] H. Saalfeld and M. Wedde, Z. Kristallogr. **139**, 129 (1974).

[99] K. Damodaran, P. R. Rajamohanan, D. Chakrabarty, U. S. Racherla, V. Manohar, C. Fernandez, J. P. Amoureux, and S. Ganapathy, J. Am. Chem. Soc. **124**, 3200 (2002).